Spring 1-1-2016

Investigating the Emission Sources of Air Pollutants Using an Atmospheric Chemical Transport Model and Its Adjoint

Hyung-Min Lee
University of Colorado at Boulder, hyungmin.lee@colorado.edu

Investigating the emission sources of air pollutants using an atmospheric chemical transport model and its adjoint

by

Hyung-Min Lee

B.S., Ewha Womans University, 2008

M.S., Ewha Womans University, 2010

A thesis submitted to the

Faculty of the Graduate School of the

University of Colorado in partial fulfillment

of the requirements for the degree of

Doctor of Philosophy

Department of Civil, Environmental, and Architectural Engineering

2016

This thesis entitled:
Investigating the emission sources of air pollutants using an atmospheric chemical transport model and its adjoint
written by Hyung-Min Lee
has been approved for the Department of Civil, Environmental, and Architectural Engineering

_____

Prof. Daven K. Henze

_____

Prof. Lupita D. Montoya

Date _____

The final copy of this thesis has been examined by the signatories, and we find that both the content and the form meet acceptable presentation standards of scholarly work in the above mentioned discipline.

Lee, Hyung-Min (Ph.D., Environmental Engineering)

Investigating the emission sources of air pollutants using an atmospheric chemical transport model and its adjoint

Thesis directed by Prof. Daven K. Henze

Quantifying the origin of air pollutants that have detrimental impacts on human health and ecosystems is a necessary but challenging aspect of studying and mitigating our impact on the environment. Using a 3-dimensional atmospheric chemical transport model, GEOS-Chem, and its adjoint we investigate emission sources and transport mechanisms of air pollutants. Adjoint-based source attribution enables quantification of the percent contribution of each emission source and gas-phase chemical reaction to the air pollutants of interest. This thesis is a collection of three studies conducted at different regional and temporal scales: 1) monthly average surface level nitrate in Antarctica, 2) seasonality of nitrogen deposition in federal Class I areas in the US, and 3) daily $PM_{2.5}$ concentrations in Seoul metropolitan area, Korea.

The results of these studies highlight the various roles of gas and aerosol emissions in impacting different aspects of the environment. Our results suggest that background levels of total nitrate at the surface level in Antarctic in austral winter are sensitive to NO_x emissions from mid-latitudes, which is transported to Antarctica as total nitrate formed above continental source regions in the free troposphere. In other seasons, more NO_x is transported as a reservoir species (e.g., peroxyacetyl nitrate, PAN) through the free troposphere, transforming into total nitrate within a cone of influence that extends to 35°S and above 4 km altitude. From the second project, we find that while it is effective to control emissions in the western US to reduce the area of regions in critical loads (CL) exceedance, it can be more effective to control emissions in the eastern US to reduce the magnitude of Nr deposition above the CL. In our final project, we find that average contributions to the high $PM_{2.5}$ episodes occurred in Seoul in May from 2009 to 2013 simulated by the model are 39% from the Shandong region, 16% from the Shanghai region, 14% from the Beijing region, and

15% from South Korea. Anthropogenic SO_2 emissions from South Korea are negligible with 90% of the total contribution originating from China.

Findings from this study may guide 1) interpretation of nitrate records from Antarctic ice cores, 2) setting protection plans for Class I areas, and 3) strategizing to meet $PM_{2.5}$ air quality standards for the Seoul metropolitan area.

Dedication

This thesis is dedicated to my devoted parents, G.M. Jeong-Mi Choi and Dr. Sang-Leem Lee.

Acknowledgements

I couldn't think of words that sufficiently describe my gratitude to my advisor Professor Daven Henze for his bottomless support and patience. Academically and personally, I would like to express my greatest respect to him. My sincere thanks also goes to Professor Rokjin Park, who supports me to continue my research in Korea by providing me an opportunity to join his group and project. I cannot start my story in this field without Professor Yong-Pyo Kim, my master's advisor. Among many fields of study in Environmental Science and Engineering, I decided to study air pollution because he was the best professor in my undergraduate life. Also, Professor Daniel Jacob, who opened my eyes to the atmospheric chemical transport modeling world. I appreciate that he accepted me as an visiting undergraduate intern when I was finding things to do in Boston.

Special thanks goes to Suehyun K. Cho who filled my life in Boulder with tremendous beautiful memories including eating Lark Burgers. I also thank my colleagues Kateryna, Nicolas, and Alex, who were always there during the days and nights in dungeon. I was able to endure long time of debugging because at least one of them was always there.

I am grateful to my brother, Choong, for plenty of wise advice and his wife, Sun, for always cheering me up. Thank you Sungwoo, Yuan, and Yuhyun, for motivating me to complete the Ph.D and making my life so dramatic. I became stronger and humble. Also my appreciation goes to my family in law for enabling me to earn a degree in Environmental Engineering.

Contents

Chapter

1 Introduction **1**

1.1 Research questions 1

1.2 Methods 4

1.2.1 Adjoint modeling 5

2 Investigating the sensitivity of surface-level nitrate seasonality in Antarctica to primary sources using a global model **6**

2.1 Introduction 6

2.2 Model description 8

2.3 Results 11

2.3.1 Seasonal variations of total nitrate 11

2.3.2 Source attribution of total nitrate (TNIT) 14

2.4 Summary and conclusions 31

3 Sources of nitrogen deposition in Federal Class I areas in the US **33**

3.1 Introduction 33

3.2 Methods 36

3.2.1 Measurement data 36

3.2.2 GEOS-Chem model description 37

3.2.3 Nr deposition metrics in Federal Class I areas 40

3.2.4 GEOS-Chem adjoint model 41
3.3 Results 42
3.3.1 Evaluation of simulated Nr deposition 42
3.3.2 Source attribution using GEOS-Chem adjoint 48
3.3.3 Uncertainty caused by NH_3 emissions 52
3.4 Discussion and conclusions 53

4 $PM_{2.5}$ source attribution for Seoul in May from 2009 to 2013 using GEOS-Chem and its adjoint model **62**
4.1 Introduction 62
4.2 Methods 64
4.2.1 Measurement data 64
4.2.2 GEOS-Chem model 64
4.2.3 Anthropogenic emission inventories 65
4.2.4 GEOS-Chem adjoint model and cost function 67
4.3 Results 68
4.3.1 Total and speciated $PM_{2.5}$ measurements 68
4.3.2 Forward model evaluation 70
4.3.3 Source attribution of high $PM_{2.5}$ episodes 70
4.4 Discussion and conclusions 72

5 Conclusions **76**

Bibliography **78**

Tables

Table

2.1 Surface air nitrate measurements from previous studies 13

2.2 Global contributions of emissions and stratospheric tracers to J_{TNIT} 16

2.3 Global total contribution of major reactions forming HNO_3 to J_{TNIT} 19

3.1 NADP and CASTNET sites used for Nr deposition measurements. 38

3.2 NO_x and NH_3 emissions in the contiguous US in 2010. 39

Figures

Figure

1.1 Schematic of major pathways of NO_x oxidation in the atmosphere. 2

2.1 Monthly NO_x emissions for 15°S - 90°S from March 2006 to February 2007. 10

2.2 Modeled TNIT concentration from March 2006 to February 2007 with measurements in symbols. The solid black line is the hourly TNIT concentration averaged over Antarctica (60°S - 90°S, see text for details) and shadings indicate first and third quartiles. Two measurements are indicated with values as they are too high to show on the same y-axis. NO_3^- measurements are converted to TNIT concentrations based on the partitioning in Jourdain et al.[98]. 12

2.3 Monthly average (a) surface level concentration of TNIT estimated by GEOS-Chem and (b) boundary layer top pressure (62°S - 90°S). 15

2.4 Spatial distribution of source contributions to J_{TNIT} (15°S - 90°S). 17

2.5 Spatial distribution of J_{TNIT} sensitivities to reactions producing HNO_3 (15°S - 90°S). 21

2.6 Vertical distribution of J_{TNIT} sensitivities to reactions producing HNO_3 (15°S - 90°S). 22

2.7 Horizontal and vertical distribution of J_{TNIT} sensitivities to (a) dry deposition and (b),(c) reaction of NO with O_3. 23

2.8 Vertical distribution of J_{TNIT} sensitivities to the formation and decomposition of PAN (15°S - 90°S). (a) PAN formation, (b) thermal decomposition, (c) photolysis. . 24

2.9 Same as Fig. 2.8 but for horizontal distribution. 25

2.10 Monthly HNO_3 vertical profiles averaged over Antarctica (70°S - 90°S). (a) GEOS-Chem, (b) GMI, (c) Modified GEOS-Chem. 27

2.11 Same as Fig. 2.2 but showing impacts of enforced HNO_3 enhancement in lower stratosphere in GEOS-Chem. From June to November 2006. Blue dash line is the mean and blue solid lines are first and third quartiles of surface level TNIT concentrations calculated by modified GEOS-Chem. 28

2.12 Annual variation of sensitivities of J_{TNIT} to the PAN formation and decompositions. 30

3.1 Composition of vegetation types of select Class I areas used in this study based on Olson et al.[165]. 35

3.2 GEOS-Chem modeled Nr deposition in 2010. Select Class I areas for case studies are indicated by initials. Inset number is the annual contiguous US total Nr deposition. 43

3.3 Seasonal variation of Nr deposition in select Class I areas. Model values (open red diamond) correspond to only those species that are measured (closed black circle). Cost function values (J_p, open blue diamond) also include dry deposition of NH_3, NO_2, PANs, alkyl nitrate, and N_2O_5. Bars indicate standard deviation of monthly averages in the season. R^2 is squared correlation coefficient for measured and modeled seasonal deposition. Dotted lines are for annual CLs divided by twelve in each site. MAM: March April May, JJA: June July August, SON: September October November, DJF: December January February. 46

3.4 Stacked bar of modeled seasonal Nr deposition showing speciation. Others includes dry deposition of NO_2, PANs, alkyl nitrate, and N_2O_5. Blueish: oxidized N, reddish: reduced N, dark: wet deposition, light: dry deposition. 47

3.5 Annual-averaged monthly footprint (χ) of Nr deposition in each Class I area and pie chart of fractional contribution from emission sectors. ls: livestock, fe: fertilizer, na: natural, sf: surface inventory, eg: electric generating units, ne: non-eg industrial stacks, ac: aircraft, li: lightning, so: soil. Inset numbers are cost function (J_p), annual Nr deposition in each Class I area. Site locations are shown with open circles. Footprint values are scaled for visibility with numbers in parenthesis. 49

3.6 Annual averaged monthly cumulative contribution as a function of distance from the site. Vertical lines are for 50% (blue) and 90% (red) of total Nr deposition. Note that the change in scale of the y-axis for SM and SD. 57

3.7 Same as Fig. 3.5 but for oxidized and reduce Nr deposition in RM. Units for the pie charts and colorbar are kg N/ha/yr. The sum of the oxidized and reduced Nr deposition is smaller than the inset number in Fig. 3.5 because the number here excludes Nr from "other species." 57

3.8 Efficiencies of impacts on Nr deposition showing cost function (J_p) change per kg N or kg S emission for the tracer and season indicated in the plot. (a) Joshua Tree (b) Rocky Mountain (c) Shenandoah national parks. Wind-roses for each site show fraction of wind frequencies based on daily surface winds during the season. 58

3.9 CL exceedance in Class I areas; color indicates magnitude of exceedance. The size of Class I areas are not reflected. Grid cells containing Class I areas are shown as colored regardless of the fraction of Class I areas. Bold line divides Western and Eastern US. 59

3.10 Same figure as Fig. 3.5 but with different cost functions. (a) J_a, the sum of Nr deposition in all Class I areas in CL exceedance, (b) J_c, the sum of square of the difference of annual Nr deposition and CL in all Class I areas in CL exceedance. Sensitivities of (a) are scaled by $\times 2$ to share the colorbar with (b). 59

3.11 Sum of NH_3 emissions from anthropogenic, natural, biomass burning, and biofuel sources. Inset numbers are contiguous US total NH_3 emissions in each month. 60

3.12 Map of sensitivities of J_p to NH_3 emissions for 3 selected Class I areas (VY, SD, and RM) for two different NH_3 emission inventories (optimized NEI2005 and default NEI2008) in each month. 61

4.1 Monthly emissions in May used in modeling. (a) Default inventory and (b) KU-CREATE inventory. See text for details. 66

4.2 Daily averaged concentrations of $PM_{2.5}$ in May during 2009 - 2013 measured by BAM and TrcSum. See text for details. 69

4.3 Monthly average concentrations of $PM_{2.5}$ and components in May from 2009 to 2013 in Seoul. Green is the measured $PM_{2.5}$ using β-ray absorption method, black is the sum of measured SO_4^{2-}, NO_3^-, NH_4^+, BC, and 1.8×OC, blue is the corresponding model estimates using default emissions, and red is the model values using NIER/KU-CREATE emissions including diurnal variation of NH_3 emissions. Inset numbers are correlation coefficient between the measurements and each model result, with NMB(%) in the parenthesis. 71

4.4 Daily $PM_{2.5}$ concentration ($\mu g/m^3$) in Seoul from 2009 to 2013. Red line indicates 24-h $PM_{2.5}$ air quality standard for Seoul (50 $\mu g/m^3$). R is correlation coefficient. Shadings indicate high $PM_{2.5}$ episode. See text for details. 73

4.5 Averaged sensitivities (normalized gradient) with respect to emissions sectors for high $PM_{2.5}$ episodes that exceed the Korean daily air quality standard (50 $\mu g/m^3$) shown in Fig. 4.4. 74

Chapter 1

Introduction

1.1 Research questions

Air pollution encompasses a broad range of scales in terms of both spatial and temporal resolutions. From large scale problems such as inter-continental transport of air pollutants and interactions of trace gases in the troposphere with constituents from the stratosphere, to small scale problems such as living organisms' exposure to toxic air pollutants in daily life. In this thesis, we investigate emission sources and transport mechanisms for a wide array of air pollution problems. Here we provide an introduction to the research questions and modeling tools used in three separate studies, the first two of which are published [121, 119] and the last of which is currently undergoing final revisions prior to submission to Environmental Pollution.

Nitrogen cycle in the environment plays important roles in changing nitrogen's form in various ways. In the biosphere, nitrogen is an essential constituent of proteins, and it is a key nutrient in the hydrosphere and geosphere. The atmosphere is 78% elemental nitrogen (N_2) by volume and comprises an inexhaustible reservoir of this essential element [134]. However, what receives our attention by altering the atmospheric environment and causing health problems is not this bulky inert species but the trace amounts of NO, NO_2, and HNO_3 in the atmosphere. As shown in Fig. 1.1, NO_x is closely coupled with ozone (O_3) chemistry, contributing to formation or depletion of O_3 depending on the atmospheric chemical composition. NO_x is primarily removed from the atmosphere after it is transformed into total nitrate (i.e., gas phase HNO_3 and particulate NO_3^-) followed by wet and dry deposition. Nitrate makes up a substantial fraction of aerosols (suspended

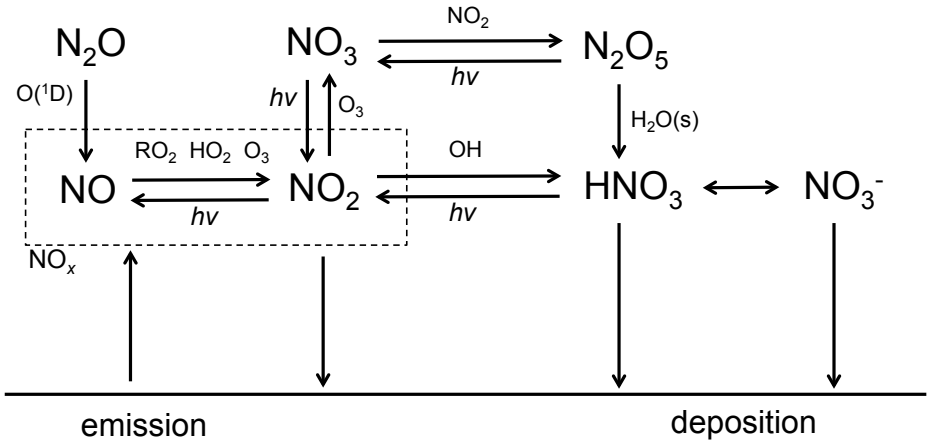

Figure 1.1: Schematic of major pathways of NO_x oxidation in the atmosphere.

solid or liquid particle in the atmosphere), which are associated with environmental issues such as visibility reduction, human health effects, and climate change.

One of the challenges in understanding large scale, long term impacts of climate change and anthropogenic activity on atmospheric chemistry is explaining factors that drive trends in records of nitrate, a terminal form of NO_x oxidation. Ice core records from poles are often investigated to provide insight about such trends. Sources of tropospheric NO_x include anthropogenic emissions, natural emissions such as soil and lightening, transport from the stratosphere, and re-emissions from snow by photolysis. Also, there are several pathways of NO_x oxidation (Fig. 1.1). Those various sources and pathways complicate the source attribution of nitrate records from ice cores. The annual variability of the flux of nitrate at the surface is observed to have minimum levels during the austral winter, a first peak in August, and a second, larger, peak in the austral summer. The mechanisms and sources driving these patterns are not well known, and had yet to be evaluated with 3-dimensional atmospheric chemical transport models. Quantifying the sources contributing to this observed variability is thus needed.

In addition to being a proxy for broader trends in atmospheric chemistry, nitrogen deposition is itself a concern due to its cascading impact on the environment [65]. It is directly linked to the supply of nutrition to the hydrosphere and geosphere [23, 64, 12]. When a receptor ecosystem is

exposed to nitrogen deposition exceeding its critical loads (CLs), significant harmful effects may manifest [162]. Many parts of the world are currently subject to excessive reactive nitrogen (Nr) deposition [189, 65, 61, 202, 51, 39], and this problem may continue to grow as anthropogenic emissions of NH_3 increase even though NO_x emissions may be decreasing [54]. In the US, Nr deposition currently exceeds CLs in many Class I areas and changes in ecosystems due to Nr exceedances are evident [60, 21]. Consequently, the US Environmental Protection Agency (EPA) is currently reviewing secondary national ambient air quality standards (welfare-based) for NO_2 (and SO_2, due to their inextricable relationship) to mitigate Nr deposition. Quantifying source contribution of various emission sectors and sources of Nr deposition will help inform the process of reviewing and possibly even setting such standards.

Another concern related to reactive nitrogen and other anthropogenically emitted atmospheric constituents is their impact on air quality, particularly in mega-cities (having more than 10 millions of population) concentrated in East Asia. The Seoul metropolitan area (SMA) of South Korea is one of the most densely populated mega-cites in the world. With the rapid economic and industrial development in China, there is increasing attention on the degradation of air quality in Korea. The Korean Ministry of Environment devised a Special Act legislation for improving air quality in the SMA in 2003 (enacted in 2005). In the second master plan, formulated for the period of 2015 - 2024, $PM_{2.5}$ and O_3 were added to the regulations. Both emission sources contained in the SMA and long-range transport from China have been suggested as sources of air pollutants in SMA; however, quantitative analysis of the relative contribution of local versus distant sources to $PM_{2.5}$ in Seoul are still limited. In order to investigate sources and mechanisms of high concentrations of air pollutants in the SMA, there was an intensive ground-based and airborne measurement campaign (KORUS-AQ) in May to June 2016. Prior to analyzing data obtained from the campaign, it is valuable to have insights on trends and source distributions of $PM_{2.5}$ in the region for this season.

Atmospheric chemical transport models (e.g., [16, 72]) provide a useful means of investigating this broad range of research questions, from depositional trends in Antarctica to air pollution sources in the SMA. Given emissions inventories, these models utilize assimilated or forecast me-

teorology to simulate transport and detailed chemical and physical air pollution transformations. This is the main use of forward modeling. However, quantifying the contribution to air pollutant concentrations from specific individual sources, sectors, and processes entails developing and using sophisticated source attribution and sensitivity models of air quality. In this thesis, we use a 3-dimensional atmospheric chemical transport model, GEOS-Chem, and its adjoint to investigate three aforementioned research questions: 1) monthly average surface level nitrate in Antarctica, 2) seasonality of nitrogen deposition in federal Class I areas in the US, and 3) daily $PM_{2.5}$ concentrations in Seoul metropolitan area, Korea. The adjoint-based source attribution method using the GEOS-Chem model is described in the following section.

1.2 Methods

GEOS-Chem [16] and its adjoint [80] are utilized to estimate the contribution of different sources to simulated values of deposition and air pollution. GEOS-Chem, a forward model, enables calculation of the state of air pollutants (e.g., concentration, flux, deposition amount, etc.) by solving Equation 1.1,

$$\frac{\partial c_i}{\partial t} + \underbrace{\nabla \cdot (\mathbf{u} c_i)}_{advection} = \underbrace{(\nabla \cdot \mathbf{K} \nabla) c_i}_{turbulent\ diffusion} + \underbrace{R_i(c_1, c_2, ..., c_k)}_{reactions} + \underbrace{E_i(x, y, z, t)}_{emission} - \underbrace{S_i(x, y, z, t)}_{sink} \tag{1.1}$$

Here c_i is the concentration of species i, $\mathbf{u}$ is the velocity vector, and $\mathbf{K}$ is the corresponding eddy diffusivities. Model calculations are performed at a horizontal resolution of $2^\circ \times 2.5^\circ$ or $0.5^\circ \times 0.667^\circ$ and 47 vertical layers up to 0.01 hPa using GEOS-5 (The Goddard Earth Observing System Model, Version 5) meteorological fields. In Equation 1.1, the tropospheric chemical mechanism (R_i) comprises 87 species and 307 reactions, and simple production and loss rates are applied for 24 species at the tropopause to account for stratospheric chemistry. The emissions (E_i) consists of anthropogenic, biofuel, biogenic, biomass burning, lightning, ship, and aircraft emissions using regional (Canada, Europe, US, Mexico, South East Asia, and North America) inventories as well as global (EDGAR) inventories. The sink term (S_i) includes wet and dry deposition. Model specification and modifications for each study are described more in each Chapter.

1.2.1 Adjoint modeling

The adjoint method is a tool for efficiently calculating the gradient (λ_p) of a cost function (J) with respect to numerous model parameters (p) with minimal computational expense.

$$\lambda_p = \frac{\partial J(c_i)}{\partial p} \cdot p \tag{1.2}$$

An adjoint model has two main applications: data assimilation and sensitivity analysis. These applications differ in terms of how the cost function is defined, and how the gradients are used. For data assimilation, the cost function measures the discrepancy between a dataset and the model estimate, and the gradients from the adjoint are used to iteratively minimize the cost function. For sensitivity analysis, the cost function is defined as a set of forward model estimates and the gradient is found by running the forward and adjoint models only once. Considering the number of grid cells and emission sources and sectors, this receptor-based sensitivity analysis using the adjoint model is $\sim 10^6$ times faster than source-based sensitivity analysis using a forward model.

This method was introduced in the early 1970s to solve inverse problems and for sensitivity analysis across a variety of disciplines. In meteorology, adjoint modeling has been actively adopted in many studies since the 1980s [55]. The first adjoint model of a 3-dimensional Eulerian chemical transport model to include chemistry was presented by Elbern and Schmit in 1999 [53] followed by several subsequent and applications (e.g., [219, 154, 76]). Still, these studies were limited to gas-phase species or regional domains. The first adjoint of global chemical transport model equipped with dynamics, full chemistry, aerosol thermodynamics, and heterogeneous chemistry was developed in 2007 by Henze et al.[80]. This is the prototype of the model we use throughout this thesis with additional updates. The study on annual variability of surface level nitrate flux in Antarctica is the first study using adjoint sensitivity calculations with respect to climatological representation of stratospheric production and loss rates of gaseous tracers. Cost functions quantifying total (wet and dry) deposition of Nr species are first introduced in the study on Nr deposition in Class I areas in the US. For the study of daily $PM_{2.5}$ in the SMA, we implement an up-to-date emissions inventory for East Asia. More about the use of the adjoint is described in each Chapter in detail.

Chapter 2

Investigating the sensitivity of surface-level nitrate seasonality in Antarctica to primary sources using a global model

2.1 Introduction

TNIT ($\equiv NO_3^- + HNO_3$) is an oxidation product of nitrogen oxides ($NO_x \equiv NO + NO_2$) in the atmosphere associated with important environmental issues such as aerosol concentrations and the oxidative capacity of the atmosphere. A significant fraction of NO_x is sequestered as TNIT and then removed from the atmosphere by wet and dry deposition, providing nitrogen to the surface where it serves as a key ecosystem nutrient. Given its environmental importance, there are interests in understanding past variability of atmospheric NO_x. Numerous studies have reported seasonal and historical variations in TNIT concentrations in Antarctica, yet the mechanisms and sources driving these variations are still not well quantified.

As a proxy for historical variability of atmospheric NO_x, ice cores from polar regions provide chronologically preserved records of TNIT [237, 127, 141, 125, 90, 96, 238]. Greenland ice core NO_3^- records show that the Northern Hemispheric NO_3^- burden has doubled since the mid twentieth century due to anthropogenic emissions [139]. In contrast, impacts of human activity on NO_3^- are not as prominent in Antarctic ice cores [141]. Aerosol measurements at the surface are also used to constrain recent trends and seasonal variability of nitrate [193, 223, 231, 192, 97]. Antarctic measurements consistently show minimum levels of TNIT in April – June, a small peak in August, and a steady increase afterward until maximum levels are reached in November – January [193, 192, 96, 233].

To interpret the significance of Antarctic ice-core and aerosol measurements, three important types of processes that influence Antarctic surface-level TNIT must be considered. First, variations in TNIT burden are impacted by long-range tropospheric transport of species emitted outside Antarctica. Emissions of NO_x include surface sources (fossil fuel, biofuel, soil exhalation, biomass burning), lightning, and aircraft emissions. TNIT may be transported directly, as NO_x or aerosol nitrate, or as reservoir species such as peroxyacetyl nitrate (PAN). PAN is produced by chemical reactions between hydrocarbons and NO_x and has a highly temperature dependent lifetime (1 hr at 298 K, 5 months at 250 K). Once it ascends to the free troposphere, it can be transported to the polar regions and then decomposed upon descent into NO_x by thermal decomposition or photolysis [147, 90, 96].

Second, stratospheric influences in Antarctic TNIT include sedimentation of polar stratospheric clouds (PSCs) and HNO_3-rich airmass mixing across the tropopause. One of the major components of PSCs is HNO_3 [29, 176]. The polar vortex provides a favorable environment for PSCs to form and grow; subsequent sedimentation of PSCs is responsible for removal of gas-phase HNO_3 in winter from the Antarctic stratosphere, i.e., denitrification [58, 28]. Also, an enhanced polar vortex can result in disappearance of the tropopause above Antarctica [188] leading to more active airmass mixing between the stratosphere and troposphere [193, 223, 231].

Lastly, TNIT deposited on snow can recycle several times by re-emission to the atmosphere by HNO_3 evaporation or photochemical reduction into NO_x [232, 192, 97]. This process, so called post-depositional processing, has been suggested to cause observed TNIT maximum concentrations in late spring and early summer [192, 97, 233].

The variety and complexity of these sources and mechanisms make it challenging to relate observed Antarctic TNIT to atmospheric NO_x [249, 185, 192, 239]. While local meteorology and post-depositional processing influence the high TNIT concentrations in summer by active photochemistry within Antarctica, the original source of TNIT for this recycling remains to be quantified [239]. Specifically, it is of interest to determine the contribution of continental emissions versus stratospheric input, the role of different types of natural versus anthropogenic emissions, and the

chemical mechanisms by which TNIT is processed and transported to Antarctica in the troposphere.

Atmospheric chemical transport models provide a means of investigating the importance of possible sources of Antarctic TNIT. Although there have been modeling studies investigating atmospheric transport towards Antarctica [108, 203], most have been limited to non-reactive tracers (e.g., black carbon, radon) and thus focused on transport of airmass and decay of tracers. A more comprehensive modeling study, considering critical processes for reactive tracers such as chemical reactions, emissions, and dry deposition, has been conducted for Antarctic CO [217]. However, due to the complicated characteristics of NO_x chemistry and transport, there has not to our knowledge been a comprehensive modeling attempt at analyzing sources of Antarctic TNIT until now.

In this study, we use the global 3-D chemical transport model GEOS-Chem and its adjoint to quantify sensitivities of surface level Antarctic TNIT to its precursor processes. These include emissions, and production and loss of tracers resulting from tropospheric and stratospheric chemistry. In doing so, we evaluate the model by comparing the modeled seasonality with measurements from previous studies, although we expect the model to underestimate austral summer observations due to a lack of post-depositional processing in the model.

2.2 Model description

We use GEOS-Chem [16] version 8-02-04 with updates described below to estimate the TNIT concentrations over Antarctica. GEOS-Chem is a global 3-D atmospheric chemical transport model driven by meteorological input from the Goddard Earth Observing System (GEOS) of the NASA Global Modeling and Assimilation Office (www.geos-chem.org). The version of the model employed in this study uses GEOS-5 meteorological fields at 2° latitude × 2.5° longitude horizontal resolution, with 47 vertical layers up to 0.01 hPa. The model's tropospheric chemical mechanism consists of more than 290 reactions and 90 gas and aerosol species. Aerosols are assumed to be externally mixed. SO_4^{2-}-NO_3^--NH_4^+ thermodynamic equilibrium is calculated using RPMARES [170], which is based on the MARS-A routine of [17]. More comprehensive aerosol treatment including sea-salt (Na^+ and Cl^-) and crustal ions (K^+, Ca^{2+}, and Mg^{2+}) is available using another thermodynamic

scheme in the model, i.e., ISORROPIA, however, we use RPMARES due to the lack of an adjoint of ISORROPIA until very recently [27]. Carbonaceous and size-resolved dust aerosols are based on [36], [169], and [59]. Wet deposition includes sub-grid scavenging in convective updrafts, large scale in-cloud rainout and below-cloud washout [128]. Dry deposition is calculated using a resistance-in-series model [234, 227].

A new stratospheric chemistry scheme is implemented for this study. The standard version 8-02-04 of GEOS-Chem applies zonal mean production and loss rates to 23 gaseous species, as archived from earlier 2-D models [16]. The new linearized stratospheric chemistry [156], updated in the adjoint model as well for this study, uses monthly climatological 3-D production and loss rates from the GMI (Global Modeling Initiative) Combo model (http://gmi.gsfc.nasa.gov) for 24 gaseous tracers above the tropopause, including CO, O_3, NO_x, and HNO_3. These production and loss rates only reflect gas-phase chemistry. Stratospheric O_3 chemistry is treated using the Linoz scheme [145, 129].

Figure 2.1 shows the monthly variation of NO_x emissions summed over 15°S – 90°S from the following emission inventories. EDGAR 3.2-FT2000 is used for fossil fuel combustion [164] and GFED2 for biomass burning emissions [216]. Biofuel sources are based on Yevich et al.[242], lightning is based on Murray et al.[156], and soil and aircraft emissions are described in Sauvage et al.[191]. Fossil fuel combustion is fixed throughout the year, and the magnitude of biofuel and aircraft emissions in this latitude range are negligibly small. Biomass burning has a maximum in late winter and early spring (August and September). Lightning and soil emissions are higher from spring to summer and lower from fall to winter.

We use the GEOS-Chem adjoint model [80] to evaluate the sensitivity of TNIT reaching the surface level of Antarctica to precursor emissions and stratospheric production and loss rates. The GEOS-Chem adjoint model has been used previously for source attribution [105, 225, 173, 172] and data assimilation using remote sensing or in-situ observations [81, 104, 94, 230]. The adjoint, a receptor-based sensitivity model, is a very efficient tool for quantifying the sensitivity of a scalar

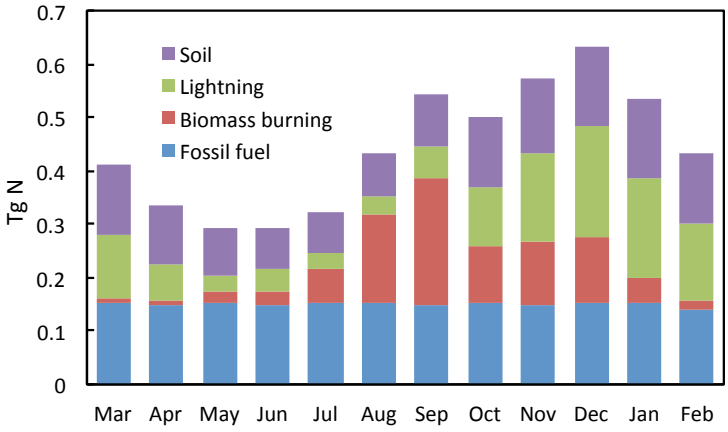

Figure 2.1: Monthly NO_x emissions for 15°S - 90°S from March 2006 to February 2007.

forward model estimate to numerous model parameters. The normalized sensitivity is defined as

$$\lambda_p \equiv \frac{\partial J(c_i)}{\partial p} \cdot \frac{p}{J(c_i)} \tag{2.1}$$

where $\frac{\partial J(c_i)}{\partial p}$ is found from solution of the adjoint model. Here c_i is the concentration of species i and $J(c_i)$ is a scalar function of forward model estimates. In this study, $J(c_i)$ is defined as the weekly average TNIT concentration evaluated in flux units over Antarctica at the surface level, i.e., J_{TNIT}. The flux unit here is the total mass of TNIT in the first level of the model per surface area per hour. Considering that the surface area of Antarctica varies during the course of a year as sea ice expands and melts [203], we determine Antarctica as the land or ice south of 60°S according to the GEOS-5 land-water indices. λ_p is the sensitivity of $J(c_i)$ with respect to the model parameters (p). p in this study consists of emissions of all tracers from various sectors (e.g., fossil fuel, lightning NO_x, natural NH_3, etc.), and stratospheric production and loss rates. In addition, sensitivities with respect to reaction rates (i.e., kinetic reaction rates, deposition rates, photolysis rates, and hydrolysis rates) are also calculated. We performed adjoint simulations for each month from March 2006 to February 2007. J_{TNIT} is evaluated over the final week of each month and percent contributions are summed globally throughout the month.

2.3 Results

2.3.1 Seasonal variations of total nitrate

We first compare seasonal variations of surface level TNIT concentrations estimated from GEOS-Chem with measurement studies in Fig. 2.2, with additional details on the measurements provided in Table 2.1. From each of the yearly measurement studies, we extract and plot data relevant to three key observed features: the fall minimum, the August peak, and the maximum [193, 192, 96, 233]. Symbols are placed in the middle of the period that they represent. Given the differences in the locations of these measurements, the species measured (NO_3^-, HNO_3, or TNIT), and the area these measurements represent compared to the size of the model grid cell, we primarily make qualitative comparisons between them and the model estimates.

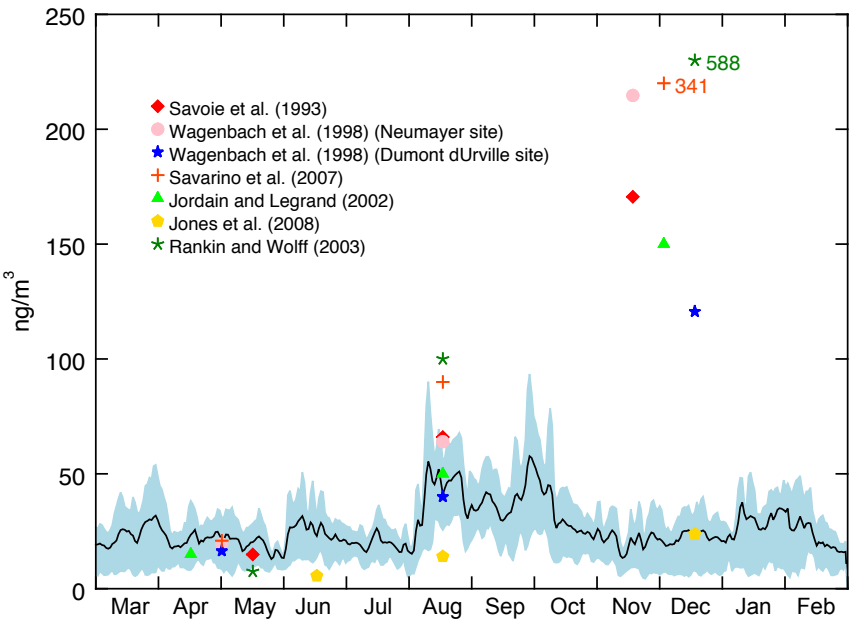

Figure 2.2: Modeled TNIT concentration from March 2006 to February 2007 with measurements in symbols. The solid black line is the hourly TNIT concentration averaged over Antarctica (60°S - 90°S, see text for details) and shadings indicate first and third quartiles. Two measurements are indicated with values as they are too high to show on the same y-axis. NO_3^- measurements are converted to TNIT concentrations based on the partitioning in Jourdain et al.[98].

Table 2.1: Surface air nitrate measurements from previous studies

Site (tracer)	Minimum	August peak	Maximum	Time
Mawson [1] (NO_3^-)	May (10 ng/m^3)	33 ng/m^3	Nov (58 ng/m^3)	1987 - 1991
Neumayer [2] (NO_3^-)	Apr - May (13 ng/m^3)	32 ng/m^3	Nov (73 ng/m^3)	1983 - 1996
Dumont d'Urville [2] (NO_3^-)	Apr - May (11 ng/m^3)	20 ng/m^3	Nov - Jan (41 ng/m^3)	1991 - 1995
Dumont d'Urville [3] (NO_3^-)	Mar - Jun (14 ng/m^3)	45 ng/m^3	Nov - Dec (116 ng/m^3)	2001
Dumont d'Urville [4] (NO_3^-)	Apr (12 ng/m^3)	25 ng/m^3	Nov - Dec (55 ng/m^3)	2000 - 2001
Dumont d'Urville [4] (HNO_3)	Apr (5 ng/m^3)	25 ng/m^3	Dec (95 ng/m^3)	2000 - 2001
Halley [5] (TNIT)	Jun (2 pptv)	5 pptv	Dec (8.5 pptv)	2004
Halley [6] (NO_3^-)	May ($\sim$5 ng/m^3)	50 ng/m^3	Dec (200 ng/m^3)	2001

[1] Savoie et al.[193], [2] Wagenbach et al.[223], [3] Savarino et al.[192]
[4]Jourdain et al. [98], [5] Jones et al.[97], [6] Rankin et al.[180]

Measured concentrations show large variations from study to study. It is possible that differences are owing to variations in local conditions (e.g., meteorology, topography, post-depositional processes) and measurement methods. We focus our analysis on TNIT rather than NO_3^- and HNO_3 separately, as thermodynamic partitioning between NO_3^- and HNO_3 in the model may be biased, underestimating NO_3^- due to lack of sea-salt and crustal ions. Considering a dataset that includes both separately [98], NO_3^- constitutes 67% of the minimum TNIT, 50% of the August TNIT peak, and 34% of the maximum TNIT. Based on this observed partitioning we convert NO_3^- measurements to TNIT concentrations for the other studies shown in Fig. 2.2. Measured minima and August peaks lie within the modeled first and third quartiles of simulated values over Antarctica. As expected, the model considerably underestimates the maximum in November to January that is thought to be due to post-depositional processing [192, 97, 233]. The model reasonably represents the magnitude of the August peak even though GEOS-Chem has no scheme describing PSC formation and sedimentation. PSC sedimentation has been suggested as a source of the August peak or the spring maximum [141, 223, 192]. It is still ambiguous from these results whether PSC sedimentation has a small effect on the August peak or its impact on surface level TNIT appears in spring not in August. This issue is considered further in Sec. 2.3.2.2.

The spatial distributions of modeled TNIT at the surface level are shown in Fig. 2.3. For all seasons, East Antarctica has a higher mixing ratio than West Antarctica, and the mixing ratio in the Northeast is higher than in the Southwest. As shown in Fig. 2.3, the spatial distribution of

TNIT is similar to the boundary layer top pressure distribution which corresponds to topography (lower pressure to higher topography). The effects of topography will cause spatial variations in accumulation rate, which is expected to impact TNIT concentrations via post-depositional processing [183, 6].

2.3.2 Source attribution of total nitrate (TNIT)

To better understand the factors governing the abundance of TNIT, we comprehensively diagnose the sensitivity of J_{TNIT} to sources using the GEOS-Chem adjoint. Table 2.2 shows the three sources with the largest percent contribution ($\lambda_p \times 100\%$) to J_{TNIT} in each month, and Fig. 2.4 shows the spatial distribution of sources to which J_{TNIT} is sensitive. For example, in the final week of March, the average TNIT flux to the Antarctic surface, i.e., J_{TNIT}, is 3.7 μg/m^2 hr. Over the course of the entire month, NO_x emissions from fossil fuel combustion contribute the most to J_{TNIT}, responsible for a 5.3% increase, and stratospheric loss of HNO_3 is responsible for a 4.4% decrease of J_{TNIT}.

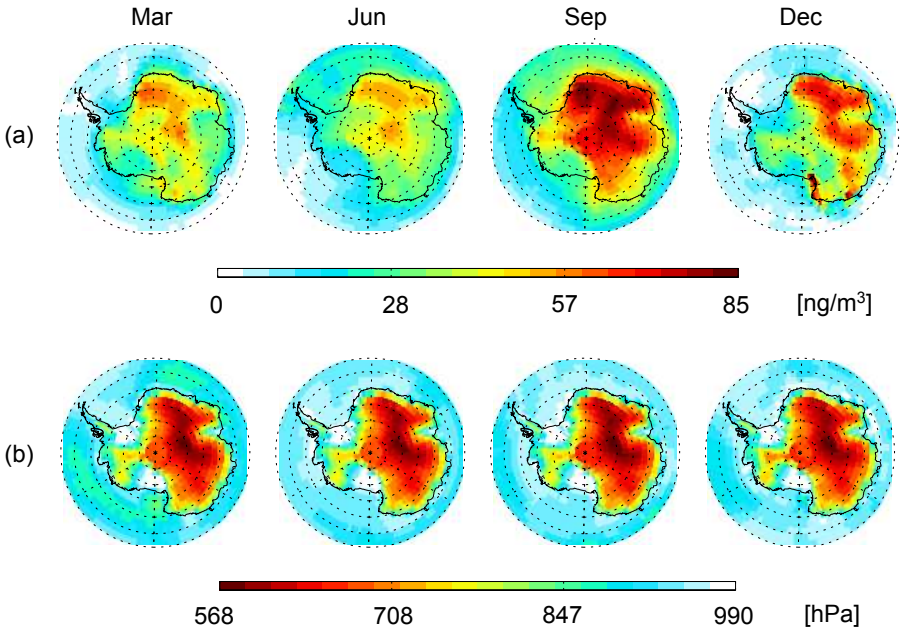

Figure 2.3: Monthly average (a) surface level concentration of TNIT estimated by GEOS-Chem and (b) boundary layer top pressure (62°S - 90°S).

Table 2.2: Global contributions of emissions and stratospheric tracers to J_{TNIT}

Month	MAM			JJA			SON			DJF		
	3	4	5	6	7	8	9	10	11	12	1	2
J (μg/m^2 hr)	3.7	2.9	1.8	2.3	1.8	3.9	4.6	2.3	2.1	2.7	4.0	2.4
Pos (%)	ffNO$_x$ 5.3	ffNO$_x$ 7.6	ffNO$_x$ 12.5	ffNO$_x$ 14.6	ffNO$_x$ 14.6	ffNO$_x$ 7.8	ffNO$_x$ 6.4	ffNO$_x$ 6.9	ffNO$_x$ 4.8	bbNO$_x$ 3.1	spNO$_x$ 3.0	liNO$_x$ 4.6
	soNO$_x$ 5.1	soNO$_x$ 5.8	soNO$_x$ 9.4	soNO$_x$ 8.2	soNO$_x$ 5.1	liNO$_x$ 3.4	soNO$_x$ 3.6	soNO$_x$ 6.7	soNO$_x$ 3.7	soNO$_x$ 2.0	spHNO$_3$ 2.3	soNO$_x$ 2.8
	spHNO$_3$ 4.1	liNO$_x$ 2.7	liNO$_x$ 3.2	liNO$_x$ 5.2	liNO$_x$ 2.9	soNO$_x$ 3.2	liNO$_x$ 3.3	naNH$_3$ 4.2	liNO$_x$ 3.5	ffNO$_x$ 1.9	bbNO$_x$ 2.1	spNO$_x$ 1.8
Neg (%)	slHNO$_3$ -4.4	slNO$_x$ -2.0	slNO$_x$ -1.0	-*	-*	slNO$_x$ -1.4	slNO$_x$ -1.7	slNO$_x$ -1.1	slNO$_x$ -2.6	slNO$_x$ -2.0	slNO$_x$ -3.4	slNO$_x$ -2.1
	slNO$_x$ -4.0	slHNO$_3$ -1.4	-*	-*	-*	-*	-*	-*	slHNO$_3$ -1.2	slHNO$_3$ -1.2	slHNO$_3$ -2.5	slHNO$_3$ -1.7
	slHNO$_4$ -1.8	slHNO$_4$ -1.0	-*	-*	-*	-*	-*	-*	-*	-*	slHNO$_4$ -1.0	-*

- MAM: March April May, JJA: June July August, SON: September October November, DJF: December January February
- ff: fossil fuel combustion, li: lightning, na: natural, sl: stratospheric loss, so: soil, sp: stratospheric production
- *: <1.0 %

While the source contributions in Table 2.2 and Fig. 2.4 show the ultimate sectors and locations of origin, they alone do not answer questions such as: which NO_x reservoir species are most responsible for transport to Antarctica, and what is the role of chemical reactions during transport? To answer these questions we quantify the roles of different chemical mechanisms transforming NO_x by calculating sensitivities of J_{TNIT} with respect to chemical reaction rate constants. Among 24 reactions directly producing HNO_3, three reactions, (R1) – (R3), are found to contribute the most, in agreement with [1],

$$NO_2 + OH \rightarrow HNO_3 \qquad \text{(R1)},$$

$$N_2O_5 + H_2O \rightarrow 2HNO_3 \qquad \text{(R2)},$$

$$NO_3 + DMS \rightarrow HNO_3 \qquad \text{(R3)},$$

where DMS is dimethylsulfide. Table 2.3 shows the globally integrated sensitivities with respect to (R1) – (R3). The relative importance of each reaction varies by season and is affected by a combination of emissions, chemistry, and meteorology. Although these are HNO_3-producing pathways, their contributions often exhibit negative values when more HNO_3 is lost than added to J_{TNIT}. This occurs when the net HNO_3 produced by a given pathway occurs too far from Antarctica for the HNO_3 to reach the continent prior to being removed from the atmosphere by

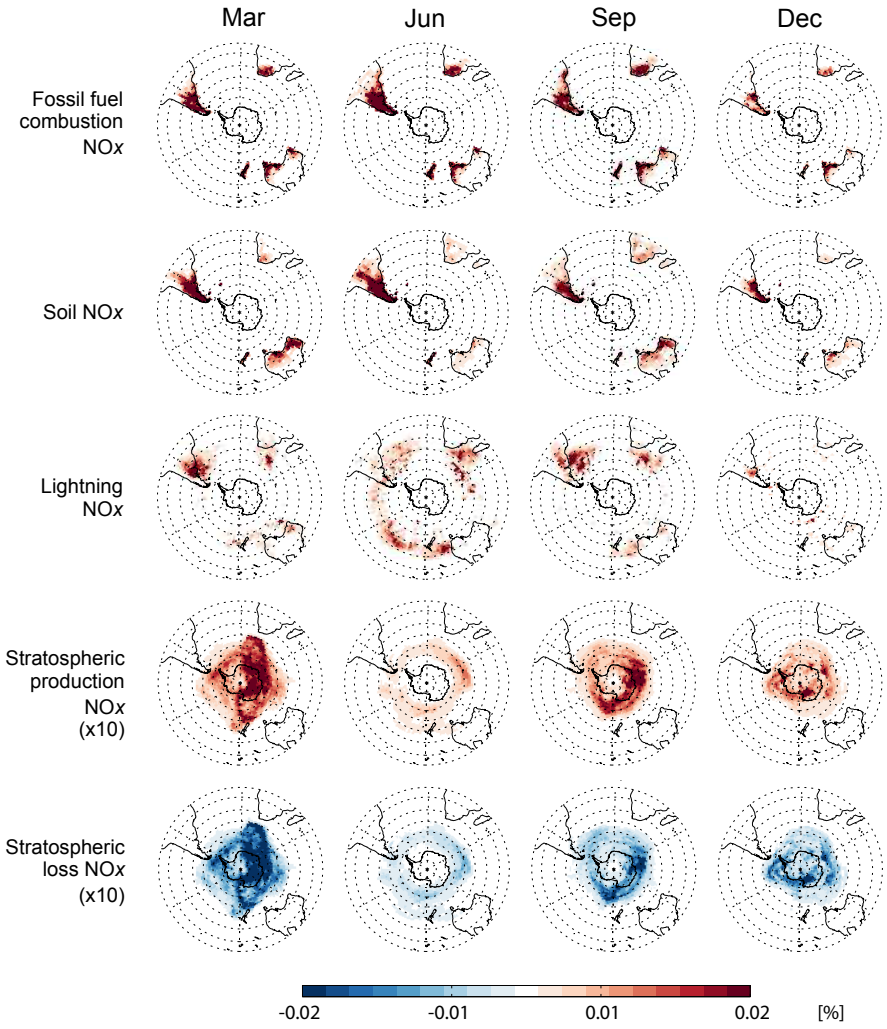

Figure 2.4: Spatial distribution of source contributions to J_{TNIT} (15°S - 90°S).

deposition. Figures 2.5 and 2.6 map the horizontal and vertical distribution of each reaction's contribution to J_{TNIT}. It is evident that when the reactions occur too far away from Antarctica, a source of J_{TNIT} is removed from the atmosphere. The lifetime of HNO_3 is short, about 2 – 5 days in the lower atmosphere, because it is readily removed near the surface by wet and dry deposition. Meanwhile, when these reactions occur closer to Antarctica they positively contribute to J_{TNIT}, showing that if the precursors involved in (R1) – (R3) reach certain latitudes the resulting HNO_3 will be transported to Antarctica. There is a vertical transition above the mid-latitudes where continental sources are emitted; if precursors ascend across this transition then the HNO_3 they form will be transported to Antarctica. The critical altitude appears to be $\sim$4 km, extending as far north as 40°S.

Table 2.3: Global total contribution of major reactions forming HNO_3 to J_{TNIT}

Month	MAM			JJA			SON			DJF		
	3	4	5	6	7	8	9	10	11	12	1	2
(R1) NO_2 + OH → HNO_3 (%)	1.4	-4.6	-6.3	-4.5	-7.8	-4.1	0.5	9.3	13.5	16.3	11.4	11.5
(R2) N_2O_5 + H_2O → 2 HNO_3 (%)	0.8	-0.2	-1.0	-1.0	-2.4	-0.6	0.8	0.4	-0.2	-0.1	-0.1	-0.6
(R3) NO_3 + DMS → HNO_3 (%)	0.3	-0.4	-0.8	-0.5	-0.6	-0.2	0.7	0.0	-0.4	-0.2	-0.1	-0.3

Surface level TNIT shows small positive sensitivities (less than 1%) to stratospheric production of tracers in most months. However, additional calculations at the 4° latitude × 5° longitude resolution show that long-term (6 month) integration of the adjoint sensitivities lead to positive sensitivities that are twice as large as those from 1-month integration, with no significant increase of sensitivities after 6 months. Thus, sensitivities to the stratospheric production from the month long, 2° × 2.5° resolution analysis shown in Table 2.2 may be an underestimate. In contrast, sensitivities with respect to emissions and stratospheric loss appear to converge within one month.

2.3.2.1 Background concentrations

The lowest J_{TNIT} values of 1.8 $\mu g/m^2$ hr appear May and July; During these months, the sensitivities are consistently dominated by fossil fuel, and then soil and lighting NO_x emissions with negligible sensitivities to stratospheric loss (Table 2.2). We therefore consider the the modeled minimum concentrations as extending from May through July. And these minimum levels are regarded as background concentrations. The range of background concentrations across Antarctica are in good agreement with observations (Fig. 2.2). Spatially, the origin of those sources are shown in Fig. 2.4. Influential NO_x emissions are distributed from 30°S – 65°S. Regarding emissions, biomass burning is greater than lightning NO_x in July, however lightning NO_x is still the third most influential source. NO_x from biomass burning originates in lower latitudes between 10°S – 30°S and at the surface, whereas lightning NO_x is produced in higher latitudes and altitudes where it can be effectively transported to Antarctica.

Total influences of reactions producing HNO_3 (R1– R3) are all negative from April to August (Table 2.3). Due to a lack of sunlight from the end of March through the next six months, there is no

local supply of OH radical in Antarctica. Thus, HNO_3 produced by (R1) during the austral winter is not produced locally in Antarctica but is imported from lower latitudes or the stratosphere. Figure 2.6 shows that J_{TNIT} is produced from precursors injected into the free troposphere at latitudes as far north as 35°S. O_3 dry deposition (2.7% – 3.5%), $NO+O_3 \rightarrow NO_2+O_2$ (1.3% – 3.1%), and thermal decomposition of PAN (1.4% – 2.4%) are the most influential reactions during May – July. J_{TNIT} is positively sensitive to these reactions since they favor NO_2, which may be further oxidized to TNIT. Spatial distributions of these reactions are shown in Fig. 2.7 – 2.9. As more O_3 is removed near the surface by dry deposition, less NO_2 is scavenged via $NO_2+O_3 \rightarrow NO_3+O_2$, and the chance for NO_2 or PAN to be lofted above the critical altitude is enhanced. NO_2 produced from $NO+O_3 \rightarrow NO_2+O_2$ over the continents near the surface also favors PAN formation. The same reaction near the tropopause contributes to TNIT in Antarctica, which is affected by high O_3 concentrations from the stratosphere. If the reaction occurs at altitudes between the two positively sensitive regions, the resulting NO_2 does not add TNIT to Antarctica but deposits in the Southern Ocean. Thermal decomposition of PAN is influential during austral fall and winter, increasing with increasing temperature towards the troposphere from the stratosphere. It occurs at altitudes lower than 6 km and photolysis of PAN occurs at higher altitudes, up to 12 km. Considering that J_{TNIT} is positively sensitive to PAN formation in the mid-latitudes (30°S – 50°S) and that thermal decomposition occurs throughout the free troposphere (Fig. 2.8 and 2.9), we conclude that PAN produced in the mid-latitudes and transported through the free troposphere can be an effective source of TNIT over Antarctica.

2.3.2.2 Peak concentrations in August

Model estimates and measurements both show a peak in TNIT concentration in August. It is interesting that the model shows high concentrations in August without a scheme describing PSC formation and sedimentation, which has been suggested from measurement studies as being a major source of the peak in August [141, 223, 192]. Decomposition of PAN has also been suggested as a source of NO_x during austral winter to early spring [192, 96]. In this study, thermal decomposition

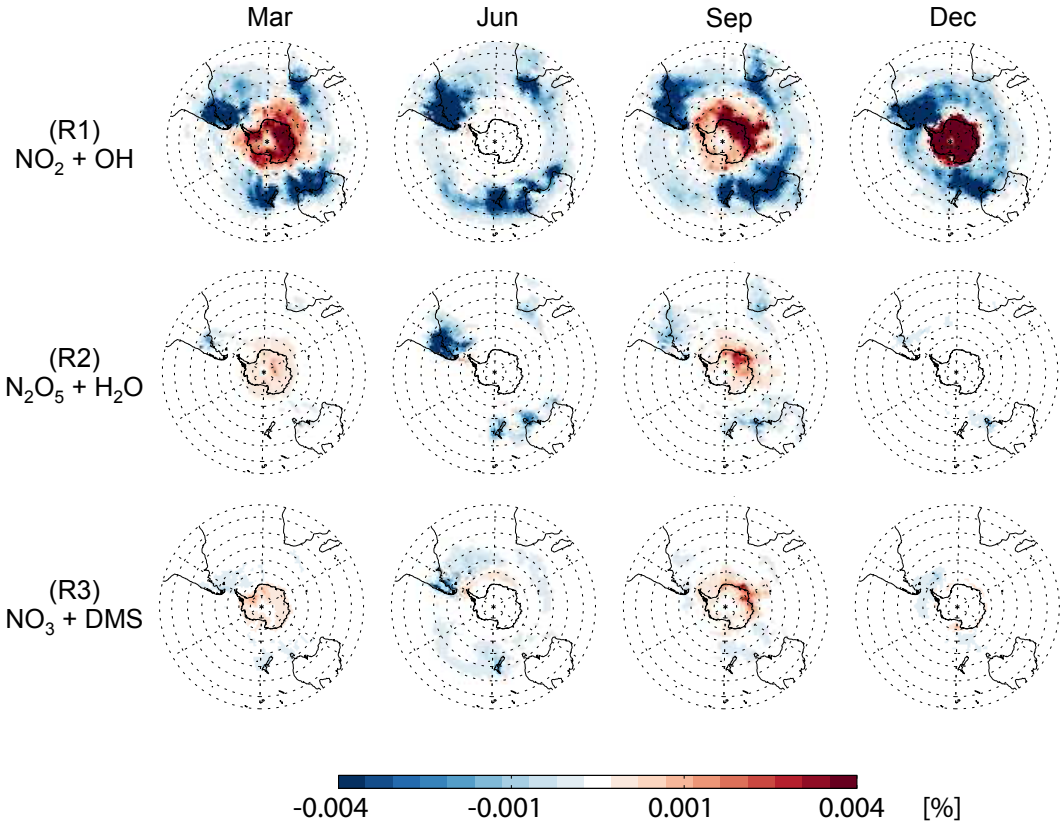

Figure 2.5: Spatial distribution of J_{TNIT} sensitivities to reactions producing HNO_3 (15°S - 90°S).

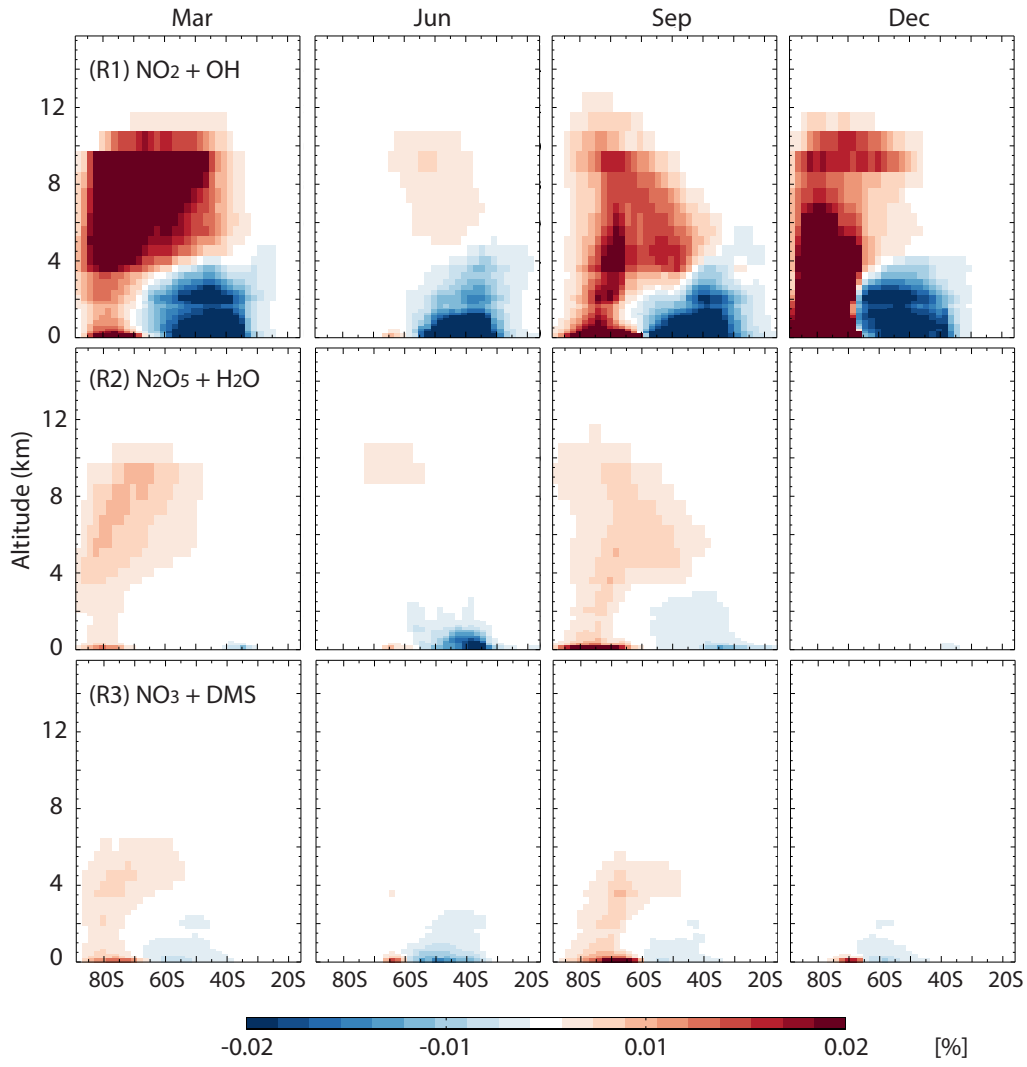

Figure 2.6: Vertical distribution of J_{TNIT} sensitivities to reactions producing HNO_3 (15°S - 90°S).

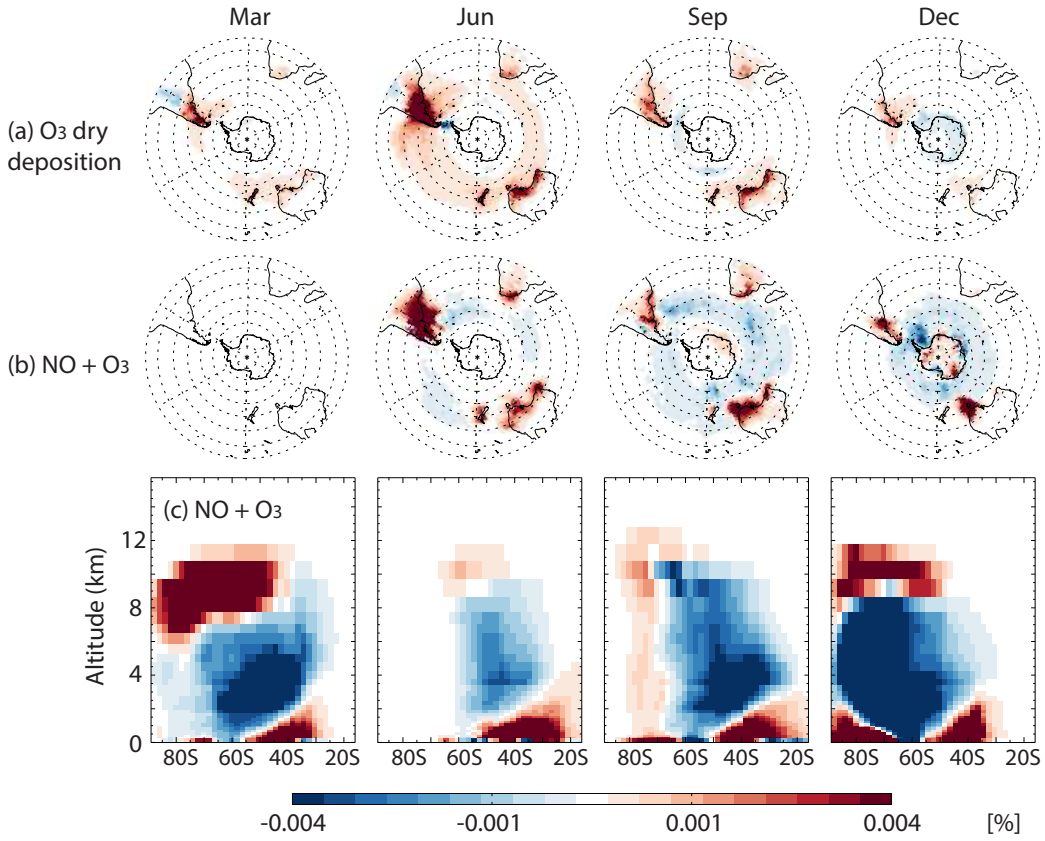

Figure 2.7: Horizontal and vertical distribution of J_{TNIT} sensitivities to (a) dry deposition and (b),(c) reaction of NO with O_3.

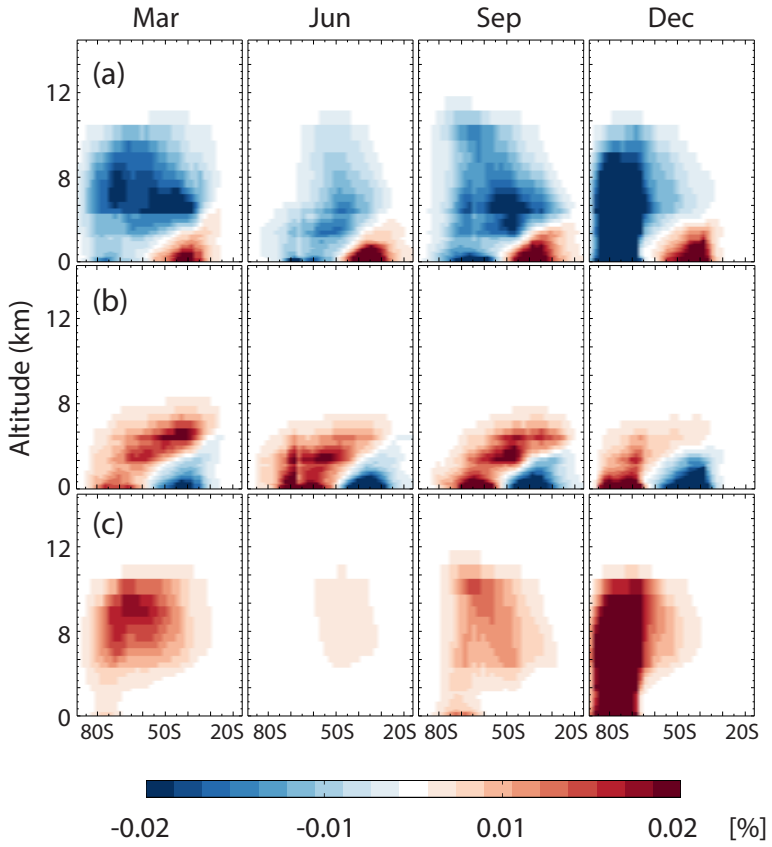

Figure 2.8: Vertical distribution of J_{TNIT} sensitivities to the formation and decomposition of PAN (15°S - 90°S). (a) PAN formation, (b) thermal decomposition, (c) photolysis.

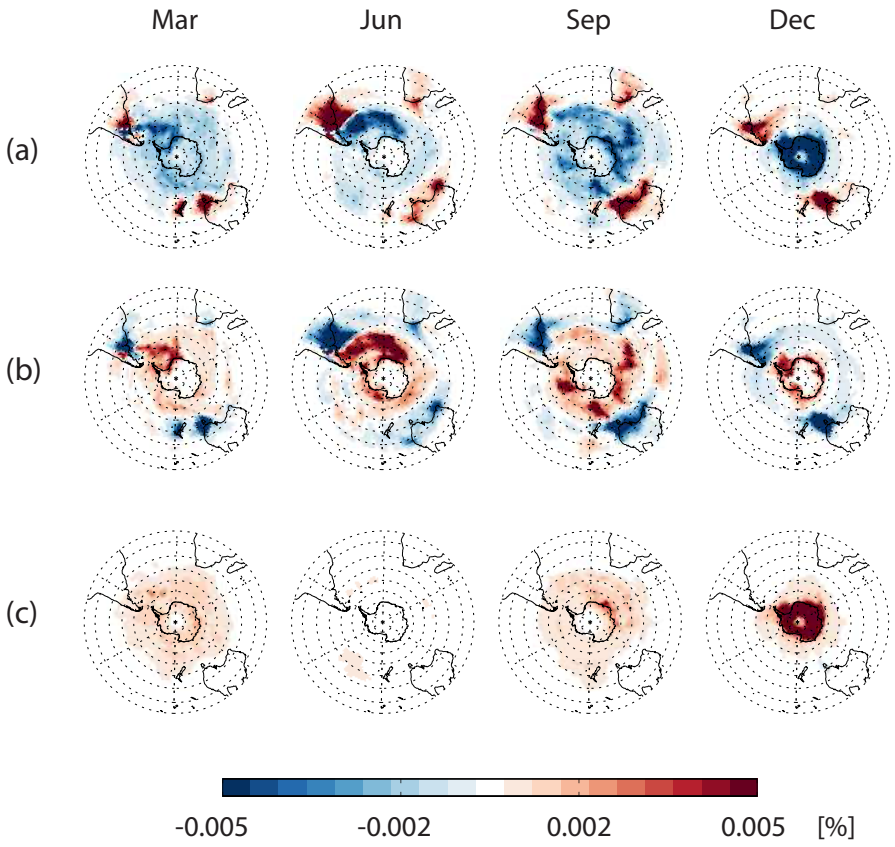

Figure 2.9: Same as Fig. 2.8 but for horizontal distribution.

of PAN is the most influential reaction in August, accounting for 2.9% of the positive sensitivity. J_{TNIT} in August is still most sensitive to fossil fuel combustion (7.8%), lightning (3.4%) and soil (3.2%) NO_x emissions from 30°S – 65°S. There is relatively less contribution from continental sources compared to May – July. August marks a transition between the season when remote influences dominate during winter and local reactions dominate during summer.

The sensitivity with respect to stratospheric production of NO_x is 1.6%. Compared to the 0.4% – 0.6% contribution in May – July, this increased stratospheric NO_x contribution shows that stratospheric influence on the August peak is represented by the model. It is worth pointing out that sensitivities with respect to stratospheric production and loss rates do not equate to the actual fluxes from and to the stratosphere, just the amount by which current stratospheric chemistry influences these fluxes. Thus, a small increase in the stratospheric production rate results in a large increase in the surface level TNIT, since the HNO_3 mixing ratio is significantly higher in the stratosphere compared to the troposphere (Fig. 2.10). Stratospheric effects seen in GEOS-Chem reflect the climatological production and loss of tracers by gas-phase chemistry in the stratosphere. However, PSC formation and sedimentation is not included in the model. Thus, this stratospheric influence is likely the effect of the polar vortex in conjunction with the lack of photolysis during the austral winter. Noting that the model does not include PSC sedimentation nor the disappearance of the tropopause, these estimates of stratospheric contributions are likely lower bounds.

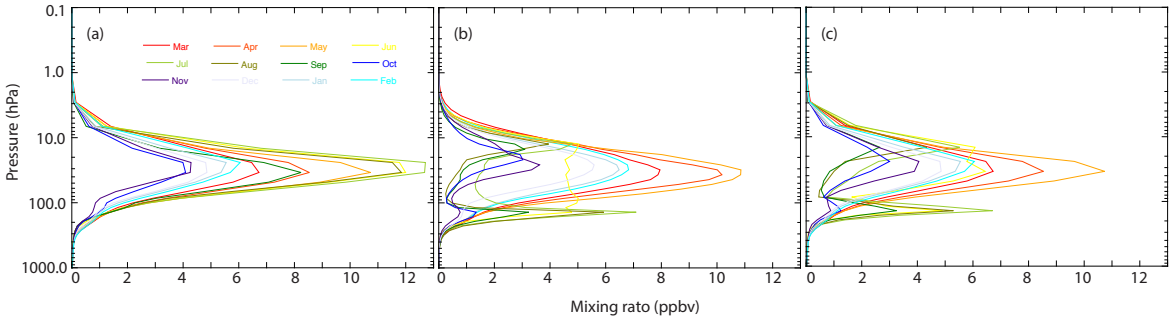

Figure 2.10: Monthly HNO_3 vertical profiles averaged over Antarctica (70°S - 90°S). (a) GEOS-Chem, (b) GMI, (c) Modified GEOS-Chem.

Although it is well known that PSCs are responsible for removal of gas-phase HNO_3 in the winter in the Antarctic stratosphere, i.e., denitrification [58, 28], whether the effect of PSC sedimentation is detectable in surface level HNO_3 concentrations is still not clear. Figure 2.10 shows vertical profiles of HNO_3 from (a) GEOS-Chem and (b) GMI. The major difference between these models is that GMI considers PSC formation and sedimentation whereas GEOS-Chem does not. We therefore modified GEOS-Chem to have similar vertical profiles of HNO_3 to that of GMI, see Fig. 2.10 (c). This profile is achieved by enforced sedimentation of HNO_3 at 14 km altitude, adjacent to the tropopause, from HNO_3 in the 15 – 25 km range during June to November. This allows us to examine the effect of enhanced HNO_3 mixing ratio in the lower stratosphere ($\sim$ 140hPa) on surface level HNO_3 concentrations in GEOS-Chem. With this modification, surface level HNO_3 increases from August through October as shown in Fig. 2.11, and more measurements of the August peak fall in the range of model estimates with this modification. This result, which does not include particles from PSCs, suggests that effects of PSCs on surface TNIT can be explained largely by gas-phase convection in August. However, the impact in October is smaller than in August and September, showing that the gas-phase convection is unlikely a factor controlling the spring maximum.

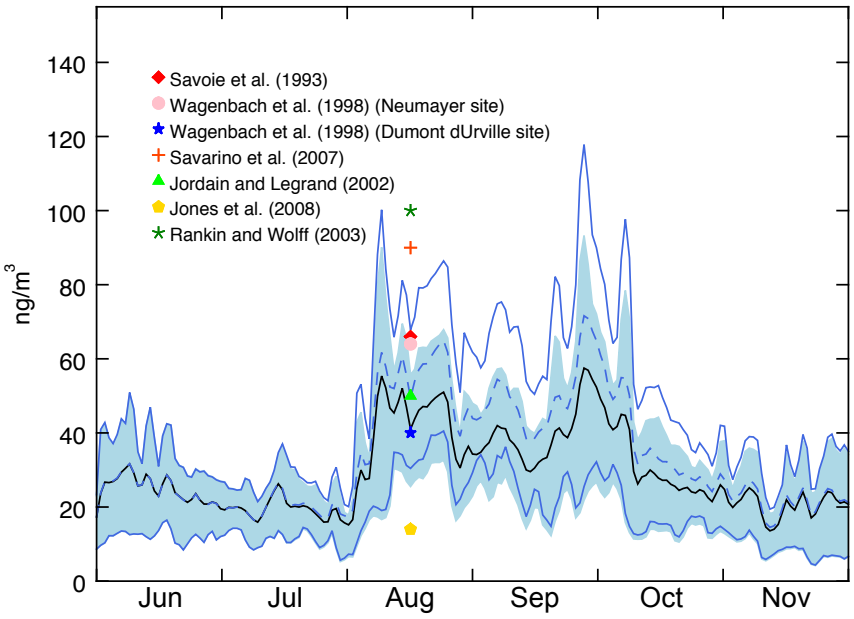

Figure 2.11: Same as Fig. 2.2 but showing impacts of enforced HNO_3 enhancement in lower stratosphere in GEOS-Chem. From June to November 2006. Blue dash line is the mean and blue solid lines are first and third quartiles of surface level TNIT concentrations calculated by modified GEOS-Chem.

2.3.2.3 Maximum concentrations

Modeled maximum TNIT concentrations appear at the end of September, however the concentration is only slightly higher than the August peak (Fig. 2.2). While measured concentrations at the end of September are comparable to modeled concentrations, the model underestimates the observed maximum concentration in November – January. Measured maximum TNIT concentrations have been attributed to the combination of PSC sedimentation [223, 231, 192] and post-depositional processing [192, 97]. Given that the model does not well represent the tropopause in winter, PSC sedimentation, nor post-depositional processing, differences between modeled and measured TNIT concentrations in November to January can be considered as an upper bound on contributions from these mechanisms.

Regarding the sensitivities of modeled maximum TNIT, NO_x emissions from fossil fuel, soil, and lightning are the three most influential sources in September. As Antarctica starts to receive more solar radiation in spring, photochemical reactions become active. J_{TNIT} starts to indicate positive sensitivities to (R1) – (R3) in September (Table 2.3). PAN photolysis is the most positively influential reaction for the modeled maximum in September. From October to February, modeled J_{TNIT} is consistently affected the most by (R1) (9% – 11%) and PAN photolysis (6% – 12%), indicating strong effects of active photolysis owing to extended daylight hours and enhanced high surface albedo. Thus, implementation of post-depositional processing, also controlled by photolysis, in the model will likely introduce more TNIT in these months. Comparing the two mechanisms of PAN decomposition in the model, contributions from photolysis dominate compared to thermal decomposition (Fig. 2.12). Global effects of PAN formation appear to be positive only when it is formed in an area where transport to Antarctica is likely.

Another thing to consider is that GEOS-Chem does not include the heterogeneous chemistry of the stratospheric ozone hole. Thus, O_3 in the polar vortex over Antarctica in austral spring during September to November is greatly overestimated, which will affect the $NO+O_3 \rightarrow NO_2+O_2$ pathway once O_3 is transported to the troposphere. Therefore, J_{TNIT} in September to November

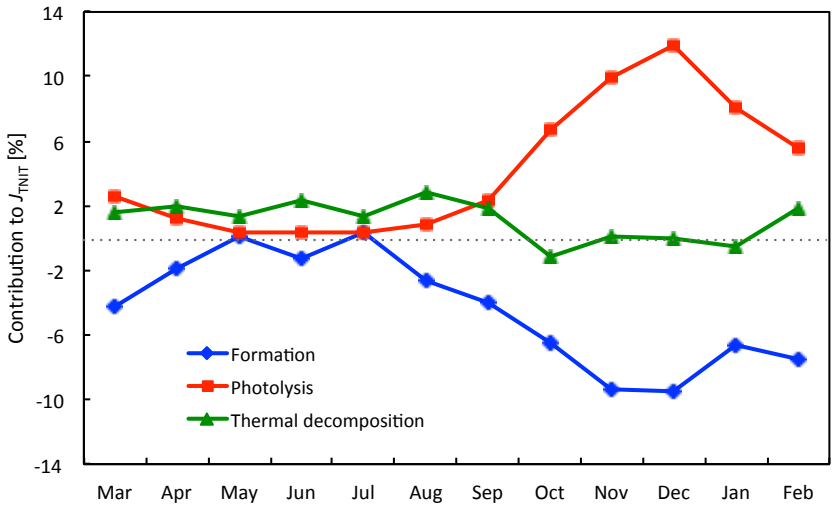

Figure 2.12: Annual variation of sensitivities of J_{TNIT} to the PAN formation and decompositions.

could be overestimated as a consequence of overestimated stratospheric O_3 transported to the troposphere.

2.4 Summary and conclusions

We have assessed sensitivities of surface level Antarctic TNIT to various emission sectors in the troposphere and production and loss of tracers in the stratosphere throughout a year using GEOS-Chem and its adjoint. Average annual minimum, August peak, and annual maximum TNIT concentrations from measurement studies are compared with modeled TNIT concentrations across Antarctica. Most seasonal minima from measurements lie within the first and third quartiles of modeled background concentrations during May to July. The first and relatively small peak of the year appearing in August, i.e., the August peak, is also captured by the model. The August peak representation in the model is improved by inclusion of enhanced HNO_3 mixing ratios in the lower stratosphere to mimic the effects of PSC formation and sedimentation. The model is not able to reproduce the maximum concentration of the year observed in November to January likely due to a lack of post-depositional processing. We anticipate this underestimation to be resolved with implementation of new snow chemistry and post-depositional processing [247] in future work. In addition, while our results only include the gas-phase influences of PSCs in August, there is still a possibility that PSC sedimentation influences surface level TNIT in early austral spring by particulate deposition.

Sensitivity calculations show that the modeled background concentrations are mostly affected by TNIT produced in the free troposphere over mid latitudes (30°S – 65°S) through the reaction $NO_2 + OH \rightarrow HNO_3$. NO_x for the reaction is mainly supplied from fossil fuel combustion, soil, lightning, and thermal decomposition and photolysis of PAN. It is evident from horizontal sensitivity maps that surface level Antarctica receives more influences from outside Antarctica during winter than summer. August is a transitional month; thus, the modeled August peak is comparably affected by tropospheric and stratospheric sources. In summer, surface level TNIT is negatively sensitive to stratospheric gas-phase chemistry that consumes NO_x, HNO_3, and HNO_4 in the strato-

sphere. Thus TNIT concentrations decrease in summer even though total emissions from south of 15°S increase. Given that the model lacks post-depositional processing, photochemical decomposition of PAN accounts for the largest fraction of NO_x supply for the HNO_3 forming reaction during the austral summer.

Chapter 3

Sources of nitrogen deposition in Federal Class I areas in the US

3.1 Introduction

Excessive deposition of reactive nitrogen (Nr) is of interest due to its cascading impact on the environment [221]. The primary impacts of Nr deposition appear in terrestrial and aquatic ecosystems as imbalanced nutrition [65], decreased biological diversity [189, 202, 39], eutrophication [61, 51], and acidification [65, 204]. Each of these primary impacts lead to subsequent consequences such as disturbances in ecosystems [65] and changes in greenhouse gas emissions and uptakes [73, 181].

The potential impact of Nr deposition on ecosystems can be evaluated using critical loads (CLs), a quantitative estimate of an exposure to one or more pollutants below which no significant harmful effects occur over the long term [162]. The magnitude of the CL varies across different types of receptors, e.g., alpine lakes, lichens in forests, alpine vegetation, etc. It can be estimated using various methods [167], which include empirical studies [18], steady-state mass balance approach [214], and dynamic modeling [222]. Pardo et al.[167] synthesized current research related to Nr deposition and comprehensively assessed empirical CLs for major ecoregions across the US.

National Parks (Organic Act of 1916, 16 USC 1-4) and wilderness areas (Wilderness Act of 1964, 16 USC 1131-1136) in the US are required to be protected to conserve natural and historic objects and the wildlife therein. Of these, Federal Class I areas are defined as those where visibility is important (Clean Air Act Amendments of 1977, 40 CFR 81). In the US, current Nr deposition exceeds CLs in many Class I areas. Fenn et al.[60] estimated that one-third of the land area of

California vegetation types is in excess of the CL for Nr deposition. Bowman et al.[21] empirically determined CLs for vegetation and soils in Rocky Mountain National Park and found ongoing vegetation change due to excessive Nr deposition. Benedict et al.[13] found substantial exceedance of CLs for Nr deposition in Grand Teton National Park. Ellis et al.[54] estimated that exceedances will become more pervasive in the coming decades.

It is desired to reduce the number of regions in CL exceedance and the amount of excessive Nr deposited above CLs. To reach this goal, it is necessary to understand the sources contributing to Nr deposition, which include both natural and anthropogenic emissions of NO_x and NH_3. Chemical transport models (CTM) can be used to study sources of Nr deposition. Zhang et al.[250] used a 3-D CTM, GEOS-Chem, to investigate the distribution, sources, and processes of Nr deposition in the US. By toggling emissions on and off in consecutive model simulations, they found that Nr deposition was dominated by contributions from domestic NO_x and NH_3 emissions, followed by natural and foreign sources. While this approach provided estimates of the role of the total emissions from these sectors throughout the US, refined estimates of source contributions from specific locations can be calculated using the adjoint of a CTM, which is a computationally efficient tool for such sensitivity analysis [81]. For example, Paulot et al.[175] used the adjoint method to identify the sources and processes that control Nr deposition in biodiversity hotspots worldwide and two US national parks (Cuyahoga and Rocky Mountain) and found that anthropogenic sources dominate deposition at all continental sites and are mainly located with 1000 km of the hotspots themselves.

The primary purpose of this study is to evaluate the origin of Nr that specifically impacts Federal Class I areas throughout the US, identifying the source locations, species and sectors that contribute to both total deposition and deposition above CLs. The results can thus be used to identify how regionally specific emissions mitigation efforts will impact ecosystems in these protected areas. To accomplish this goal, we evaluate source contributions to the deposition at the collection of all Class I areas as well as eight specific regions: Voyageurs national park (VY), Smoky Mountain national park (SM), Shenandoah national park (SD), Big Bend national park (BB), Rocky

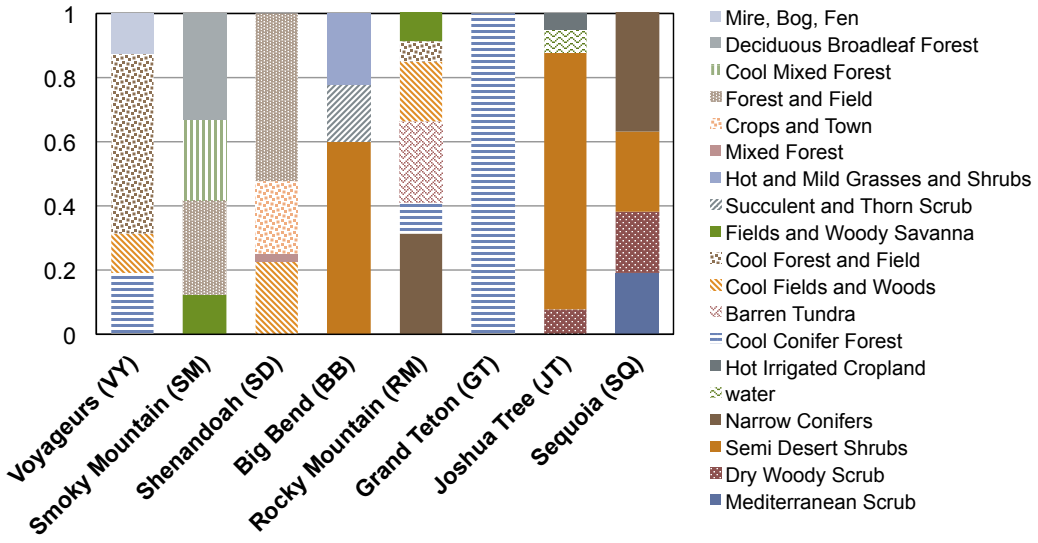

Figure 3.1: Composition of vegetation types of select Class I areas used in this study based on Olson et al.[165].

Mountain national park (RM), Grand Teton national park (GT), Joshua Tree wilderness (JT), and Sequoia national park (SQ). Following Ellis et al.[54], we use the lowest estimate of CL for these areas from [167] which are based on CLs for lichens in most regions because lichen is among the most sensitive bio-indicators of N in terrestrial ecosystems. These 8 focus areas are selected as they have low CLs (VY, SM, SD, BB, JT: 3 kg N/ha/yr, RM, GT, SQ: 2.5 kg N/ha/yr) and are thus most likely impacted by Nr deposition. We also choose this set of areas to highlight different spatial distributions of sources and mechanisms governing Nr deposition in regions of the country that are spatially disparate, are subject to a range of nitrogen emission profiles, encompass several types of ecosystems (see Fig. 3.1), and are subject to Nr deposition at levels close to or above CLs.

The secondary purpose is to evaluate the impact of uncertainties in NH_3 emissions on source attribution of Nr deposition. NH_3 emissions are known to have uncertainties of more than a factor of two in total US emissions in some seasons [81, 174]. Thus, NH_3 emissions inventories are often updated through top-down approaches, using constraints provided through inverse modeling of wet deposition measurements [69, 70, 250, 174] or, more recently, remote sending observations [257]. Here we consider constraints on NH_3 emissions throughout the US from Zhu et al.[257] that were

derived from 4D variational assimilation of NH_3 remote sensing observations from the Thermal Emissions Spectrometer (TES) aboard the Aura satellite [198]. We investigate the impacts of these adjustments to NH_3 emissions, relative to those from a national emissions inventory, on source attribution of Nr deposition in 3 Class I areas (VY, SD, and RM). Another consideration is that the air-surface exchange of NH_3 emissions is actually bi-directional [159, 206], an aspect that has recently begun to be implemented to air quality models [42, 8, 177, 256]. Zhu et al.[256] found increased net NH_3 emissions in July (5.9%) and decreased net NH_3 emission in April (23.3%) and October (13.9%) over the US when including the bi-directional flux of NH_3 in the GEOS-Chem model. As bi-directional flux of NH_3 is not considered in our present work, this provides additional motivation for studying the response of Nr source attribution to uncertainties in NH_3 emissions.

The organization of this manuscript is as follows. Modeled seasonality of Nr deposition is compared with measurement data in section 3.3.1. Sensitivity analysis using the adjoint model is presented in section 3.3.2. In section 3.3.3, we examine the impacts of uncertainties in our model's NH_3 emissions in the source attribution results. The paper concludes with summary and discussions in section 3.4.

3.2 Methods

3.2.1 Measurement data

The National Trends Network (NTN) (http://nadp.sws.uiuc.edu) of the National Atmospheric Deposition Program [157] provides weekly records of precipitation amount and chemical properties (i.e., ion concentration, acidity, and conductance) at as many as 250 sites across the US. Rainfall is recorded to the nearest 0.01 inch with a weighing-bucket rain gauge at each site. Chemical properties are analyzed at the Central Analytical Laboratory [157]. Table 3.1 lists sites used in this study. We use monthly aggregate wet deposition of NH_4^+ and NO_3^- for select sites. However, no data are available for SQ in JJA. For GT, we use the average of Yellowstone and Pinedale, WY, measurements because there are no wet deposition measurements made in 2010 in

GT. For RM, there are three collocated monitoring sites, and we use the average of them.

The Clean Air Status and Trends Network (CASTNET, http://epa.gov/castnet) measures ambient concentration of nitrogen and sulfur weekly at about 90 sites across the US and Canada. More than 20 of these sites are within Class I areas. A 3-stage filter pack is used to measure nitrogen concentrations. Dry deposition flux is then calculated using the dry deposition velocity estimated by the Multi-Layer Model (MLM) [30]. For simplicity when discussing these values along with other observations, we refer to these derived quantities as dry deposition measurements, although we recognize here that dry deposition is not directly measured. We use monthly aggregate dry deposition of NH_4^+, NO_3^-, and HNO_3 for select sites. Yellowstone and Pinedale, WY, measurements are used for GT since there is no CASTNET site in GT.

3.2.2 GEOS-Chem model description

GEOS-Chem (www.geos-chem.org) is a 3-dimensional atmospheric CTM driven by meteorological input from the Goddard Earth Observing System (GEOS) of the NASA Global Modeling and Assimilation Office [16]. We use GEOS-Chem adjoint version 35 with a nested grid resolution of $1/2^\circ$ latitude $\times$ $2/3^\circ$ longitude with 47 vertical layers up to 0.01 hPa [228, 35, 251] for the modeling domain over the contiguous US (126W - 66W, 13N - 57N). The model includes detailed tropospheric gas-phase chemistry of the O_3-NO_x-hydrocarbon system [86]. Aerosols are assumed to be externally mixed and the thermodynamic equilibrium between gases and aerosol of NH_3-H_2SO_4-HNO_3 is calculated using RPMARES [170]. Wet deposition includes sub-grid scavenging in convective updrafts, large scale in-cloud rainout, and below-cloud washout [128]. Dry deposition is calculated using a resistance-in-series model [234, 227]. Resistances are aerodynamic resistance, quasi-laminar sublayer resistance, and bulk surface resistance. Bulk surface resistances are specified by different surface type, i.e., vegetation types [234]. We use vegetation types from Olson et al.[165], shown in Fig. 3.1.

Anthropogenic emissions of NO_x, SO_2, and NH_3 in GEOS-Chem are taken from the National Emissions Inventory produced by the US EPA (EPA/NEI2008). Annual emissions of NO_x and

Table 3.1: NADP and CASTNET sites used for Nr deposition measurements.

Class I area name	NADP		CASTNET	
	ID	Location (lat, lon)	ID	Location (lat, lon)
Voyaguers (VY)	MN32	(48.4, -92.8)	VOY413	(48.4, -92.8)
Smoky Mountain (SM)	TN11	(35.7, -83.6)	GRS420	(35.6, -83.9)
Shenandoah (SD)	VA28	(38.5, -78.4)	SHN418	(38.5, -78.4)
Big Bend (BB)	TX04	(29.3, -103.2)	BBE401	(29.3, -103.2)
	CO19	(40.4, -105.6)	ROM206	(40.3, -105.5)
Rocky Mountain (RM)[a]	CO89	(40.3, -105.7)	ROM406	(40.3, -105.5)
	CO98	(40.3, -105.7)	-	-
Pinedale (GT)	WY06	(42.9, -109.8)	PND165	(42.9, -109.8)
Yellowstone (GT)[b]	WY08	(44.9, -110.7)	YEL408	(44.6, -110.4)
Joshua Tree (JT)	CA67	(34.1, -116.4)	JOT403	(34.1, -116.4)
Sequoia (SQ)	CA75	(36.6, -118.4)	SEK430	(36.5, -118.8)

[a]Average of three collocated sites of NADP and 2 collocated sites of CASTET is used.
[b]Average of Yellowstone and Pinedale is used.

Table 3.2: NO_x and NH_3 emissions in the contiguous US in 2010.

	Sectors	Emissions (Tg N/yr)
NH_3	Total	3.2
	Livestock	2.7
	Fertilizer	0.3
	Natural	0.1
NO_x	Total	4.9
	Surface	2.6
	EGUs[a]	0.57
	Non-EGU	0.38
	Aircraft	0.13
	Lightning	0.69
	Soil	0.43

[a] Electric generating units

NH_3 in the contiguous US in 2010 are shown in Table 3.2. Mobile emissions of NH_3 are not shown explicitly here, as they are <4% of the US total in the NEI2008, although this may be an underestimate in urban areas [100]. Anthropogenic sources of NO_x includes surface sources, electric generating units (EGUs), and non-EGU industrial point sources. Surface sources of NO_x comprises on-road (diesel and gasoline exhaust from cars and trucks, 68.4%), non-road (off-road vehicles, construction equipment, industrial, commercial, and agricultural engines, 17.2%), and non-point (not otherwise included, e.g., residential heating, oil and gas development, 14.4%) sources. Biomass burning emissions are taken from the 3-hour GFED3 inventory [151, 218]. NO_x emissions from aircraft are described in Wang et al.[227]. Natural emissions of NO_x are from lightning [156] and soil [243, 227]. Natural emissions of NH_3 from soil, vegetation, and ocean sources are from the GEIA inventory [20]. In section 3.3.3, we consider NH_3 emissions constrained by remote sensing observations from Zhu et al.[257], which we refer to as optimized NEI2005. Bidirectional NH_3 exchange is not considered in this study.

3.2.3 Nr deposition metrics in Federal Class I areas

Here we consider several metrics (cost functions) for quantifying Nr deposition and CL exceedances in Federal Class I areas. When considering strategies for reducing Nr deposition in Class I areas, several possible questions of interest arise, such as: 1) How do emissions from different source locations and sectors affect Nr deposition in specific individual Class I areas? 2) Which emissions contribute the most to the spatial extent of all Class I regions in exceedance? and 3) What is the amount by which emissions contribute to the severity of Nr deposition in Class I areas above CLs? Each of these three questions corresponds to a unique approach to defining the cost function for our sensitivity calculations. The cost functions in this study include the following constituents: the sum of wet and dry deposition of NH_3, NH_4^+, NO_3^-, and HNO_3, and dry deposition of NO_2, PANs (peroxyacetyl nitrate and higher peroxyacyl nitrates: peroxymethacroyl nitrate, peroxypropionyl nitrate), alkyl nitrate, and N_2O_5. Although dry deposition of NO_2, PANs, alkyl nitrate, and N_2O_5 are not part of the CL estimates by Pardo et al.[167], the sum of these species does not significantly contribute to our modeled Nr deposition or comparison to these CLs.

We first consider a cost function formulated for source attribution of Nr deposition in an individual Class I area. It is defined as the annual Nr deposition in a region [kg N/ha/yr],

$$J_p = \sum_{i=1}^{N} \text{annDep}_i \beta_i, \tag{3.1}$$

where annDep_i is the annual Nr deposition in grid cell i, β_i is the fraction of grid cell i that is contained within the Class I area, and N is number of grid cells for which β_i is nonzero for an individual Class I area. Sensitivities of this cost function provide a first order estimate of the contribution of emissions to annual Nr deposition in a particular Class I area.

We next consider a cost function that is the sum of Nr deposition in all Class I areas in CL exceedance, J_a [kg N/ha/yr], defined as

$$J_a = \sum_{i=1}^{L} \text{annDep}_i \beta_i, \tag{3.2}$$

where L is the number of grid cells containing Federal Class I areas in which annual modeled Nr

deposition has exceeded the CL values we use in this study and β_i is the fraction of grid cell i that is contained within each Class I area. This metric is proportional to the total area of Class I regions in CL exceedance. Sensitivities of J_a with respect to emissions thus identify which emissions contribute to the total spatial extent of Class I areas that have Nr deposition above their CL by any amount.

Lastly, we consider a third cost function that is the sum of square of the difference of annual Nr deposition and CL in all Class I areas in CL exceedance, J_c [(kg N/ha/yr)^2], which defined as

$$J_c = 0.5 \sum_{i=1}^{L} (\text{annDep}_i \text{ - } \text{CL}_i)^2 \beta_i, \tag{3.3}$$

where L and β_i are same as Eq. 3.2 and CL_i is the critical load in grid cell i. While both Eq. 3.2 and Eq. 3.3 include only regions where annual Nr deposition is higher than the CL, Eq. 3.3 is more strongly related to the magnitude of the Nr deposition in exceedance (the factor of 0.5 is habitually included for sensitivity calculations based on the first derivative of J). Sensitivities of J_c quantify the contribution of emissions to the magnitude of Nr deposition above CL loads, which can then guide analysis of mitigation efforts for reducing the most severe levels of Nr deposition.

3.2.4 GEOS-Chem adjoint model

The GEOS-Chem adjoint model [80] is a tool for receptor-based inverse modeling and sensitivity analysis [106, 230, 257]. When it is used for a sensitivity analysis, gradients of the user defined cost function with respect to all model parameters are calculated simultaneously, making the model a very efficient tool for source attribution [225, 175, 116, 121]. Here we use the model to evaluate the sensitivity of Nr deposition to emission sources, including for the first time all chemical species of Nr present in the GEOS-Chem "full-chemistry" simulation, which considers NO_x-O_x-HC-aerosol chemisry.

Non-normalized sensitivities quantify the change in the cost function per change in kg emission. We thus refer to this type of sensitivity as an efficiency in that large non-normalized sensitivities indicate areas where reducing Nr emissions would have a very strong impact on Nr deposition

in terms of the response of Nr deposition achieved per amount of emissions reduced (as opposed to locations where reducing emissions would have little effect on Nr deposition in the areas of interest, or locations where Nr emissions are just large in magnitude). These are defined as

$$\lambda_{i,j} \equiv \frac{\partial J}{\partial E_{i,j}}, \tag{3.4}$$

where J is any of the cost functions defined in Section 4.2.4, and $\lambda_{i,j}$ is found from solution of the adjoint model. $E_{i,j}$ is the emission at grid cell i of species j. Details of the adjoint model description and validation have been presented previously [80, 81]. We also consider the semi-normalized sensitivity [kg N/ha/yr], defined as,

$$\chi_{i,j,k} \equiv \lambda_{i,j} \cdot E_{i,j,k}, \tag{3.5}$$

where $E_{i,j,k}$ is the emission at grid cell i of species j from sector k. This sensitivity linearly approximates the contribution to the cost function of the emission in location i, of species j, from sector k. While the adjoint model computes sensitivities with respect to all emissions (e.g., SO_2, VOCs, etc.), here we focus our analysis on sensitivities with respect to emissions of NH_3 and NO_x from anthropogenic and natural sources, which are the largest. Sensitivity calculations are performed monthly, including a one week spin-up for each month to capture the influence of emissions from the end of the previous month.

3.3 Results

3.3.1 Evaluation of simulated Nr deposition

Figure 3.2 shows the spatial distribution of total, reduced, and oxidized annual Nr deposition in the contiguous US in 2010 calculated with GEOS-Chem. Total Nr deposition consists of all chemical species included in the cost function, reduced Nr deposition is the sum of wet and dry deposition of NH_3 and NH_4^+, and oxidized Nr deposition is total minus reduced. Total Nr deposition ranges from 2 to 5 kg N/ha/yr in the West, except in some parts of California where is it >12 kg N/ha/yr, and from 6 to 20 kg N/ha/yr in the East. Annual total Nr deposition over the contiguous

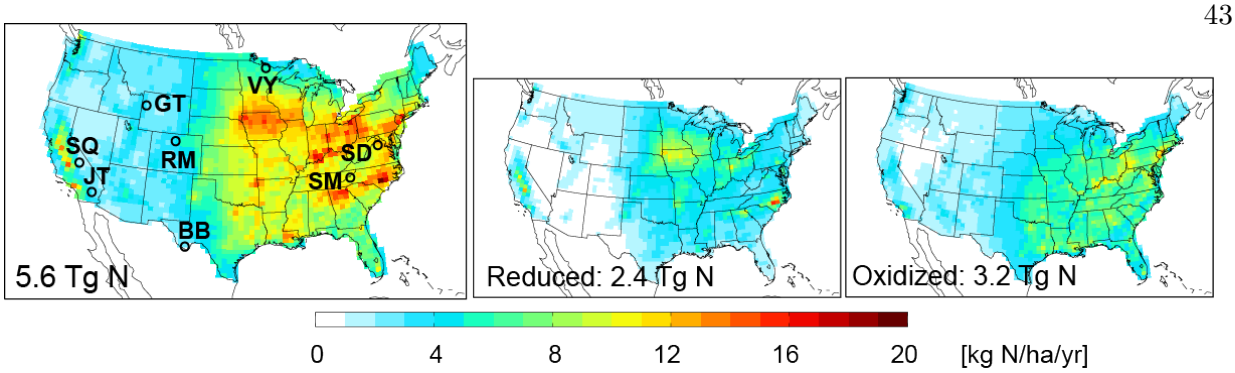

Figure 3.2: GEOS-Chem modeled Nr deposition in 2010. Select Class I areas for case studies are indicated by initials. Inset number is the annual contiguous US total Nr deposition.

US is 5.6 Tg N (3.2 oxidized, 2.4 reduced). Oxidized Nr is higher than reduced Nr overall, while reduced Nr is higher in mid-California, Iowa, and eastern North Carolina.

The spatial distribution of reduced and oxidized Nr deposition is comparable with other studies [250, 50, 196] yet a few differences and uncertainties are worth considering. Du et al.[50] found greater wet deposition of NH_4^+ compared to wet deposition of NO_3^- over the contiguous US except in the Northeast region. The larger fraction of reduced wet Nr deposition in their work may be related to the year being analyzed (increased NH_3 and decreased NO_x emissions in their study period of 2011- 2012 compared to ours in 2010) and to the overestimation of HNO_3 in our study that is discussed below.

Zhang et al.[250], using the same model we use but with the different emissions, found that wet and dry HNO_3 deposition is overestimated compared to observations when the model's isoprene nitrate is treated as HNO_3, as in our simulation, rather than being treated separately as organic nitrate. Further, comparison of modeled to measured HNO_3 deposition in Zhang et al.[250] required consideration of sub-grid concentration gradients near the surface. Simulated ambient HNO_3 concentrations are also overestimated [79], possibly owing to excessive N_2O_5 hydrolysis. This suggests that oxidized Nr may be overestimated in our study. Schwede et al.[196] generated maps of Nr deposition for multiple years, including 2010. These maps display localized hotspots in parts of Colorado and Idaho that are not evident in our results. The high Nr deposition in these regions

is attributed to dry deposition of reduced nitrogen [196], whereas in our result the contribution of reduced nitrogen deposition is generally less than that of oxidized nitrogen deposition (Fig. 3.2), possibly owing to the aforementioned overestimation of HNO_3.

For the eight selected Class I areas, we compare seasonal average values from measurements provided by NADP/NTN and CASTNET versus GEOS-Chem model estimates (Fig. 3.3). Total modeled Nr deposition in each Class I area (J_p, which includes non-measured species) is also plotted in Fig. 3.3 as blue diamonds to show the role of non-measured species. Seasonal averages are calculated from monthly values. Measured Nr correspond to the sum of modeled wet deposition of NH_3, NH_4^+, HNO_3, and NO_3^-, and dry deposition of NH_4^+, NO_3^-, and HNO_3. The squared correlation coefficient (R^2) of measured and modeled Nr is shown in each plot. For SQ, R^2 is calculated with spring, fall, and winter data. The model well reproduces the seasonality of measurements ($R^2 > 0.6$) except at JT. For all sites, measurements and model estimates have maximum values in the summer. Seasonally averaged measured Nr range from 0 to 0.6 kg N/ha/month (monthly value 0 to 1.3 kg N/ha/month), modeled Nr range from 0.0 to 1.2 kg N/ha/month (monthly value 0 to 1.3 kg N/ha/month) and J_p (modeled Nr including non-measured species) range from 0.1 to 1.3 kg N/ha/month (monthly value 0 to 1.4 kg N/ha/month). Modeled Nr deposition is also higher than the measured Nr in the spring and summer in SM and SD, likely owing to overestimated HNO_3 as discussed above. Additionally, our model grid-cell size ($\sim$3350 km^2) is larger than the largest Class I area (BB, 2866 km^2). Representational error may thus also contribute to the discrepancy between the model and the measurement for regions with large emissions within grid cells containing the Class I area (e.g., SM and SD). Lastly, comparison to dry deposition measurements warrants some additional considerations. The MLM model used for deriving the CASTNET dry deposition values is subject to uncertainty in estimating dry deposition velocities [195] because of a height dependent non-physical component that can lead to overestimate of HNO_3 deposition by 10-30% [194]. Additionally, Hicks et al.[83] found that measurements of HNO_3 dry deposition in a clearing, such as the CASTNET sites in SM and SD from which dry deposition measurements are derived, are lower than measurements of dry deposition to the surrounding forest canopy. Thus, measured Nr

deposition in Class I areas that have large forested areas (such as SM, SD, RM, GT, and SQ, see Fig. 3.1) is likely underestimated.

Annual modeled Nr deposition in each Class I area (J_p) ranges from 2.2 to 10.7 kg N/ha/yr, and is highest in SD and SM and lowest in BB. The dotted lines in Fig. 3.3 show the annual CLs from [54] divided by twelve. Class I areas considered to be in CL exceedance on an annual basis based on simulated values are VY, SM, SD, RM, GT, and SQ and those in exceedance based on measurement are VY, SM, SD, RM, and SQ. Within California, annual Nr deposition in SQ is about 70% larger than that in JT. This is influenced by the position of these parks relative to large upwind anthropogenic sources, as well as different vegetation types of the two parks (Fig 3.1). JT is 80% desert where very low Nr deposition is expected; in contrast, SQ has narrow conifers and mediterranean scrub. The lowest annual Nr deposition in BB is explained, in part, by the large fraction of desert (60%) and succulent and thorn scrub (18%); it is also far from large anthropogenic sources.

Figure 3.4 shows the model speciation of J_p. Non-measured species are dry deposition of NO_2, PANs, alkyl nitrate, N_2O_5 (lumped as others in Fig. 3.4) and dry NH_3. Non-measured species account for 0.5% (winter, SM) to 55.6% (summer, SQ) of seasonally averaged J_p values in the model. Dry deposition of NH_3 accounts for 14% of contiguous US total annual Nr deposition. The summer maximum of J_p is mainly driven by wet deposition of HNO_3 (VY, SM, SD, BB, RM) and dry deposition of HNO_3 (VY, GT, JT, SQ). Dry deposition of NH_3 is a major contributor in SQ. Organics (PANs and alkyl nitrate) make only a small contribution ($< 5\%$) to Nr deposition in the model. While it is known that organics account for $\sim$30% of total Nr deposition [158, 43], we expect organics to be underestimated in our model because only dry deposition is included for these species and isoprene nitrate is not explicitly treated [250].

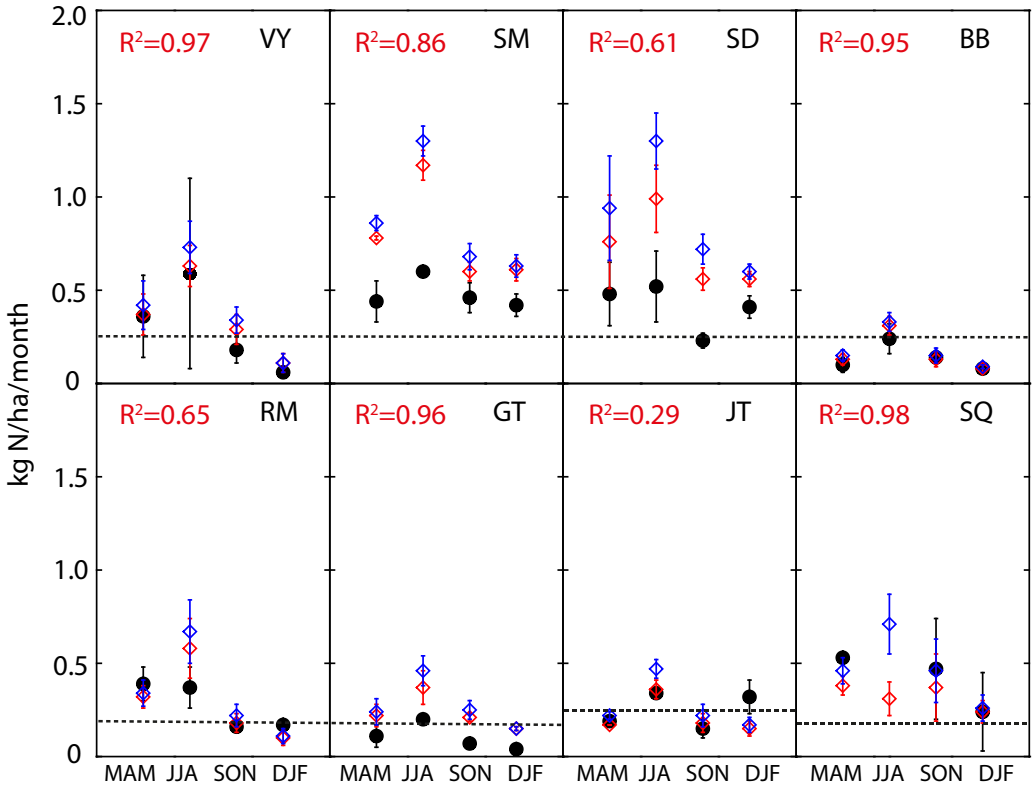

Figure 3.3: Seasonal variation of Nr deposition in select Class I areas. Model values (open red diamond) correspond to only those species that are measured (closed black circle). Cost function values (J_p, open blue diamond) also include dry deposition of NH_3, NO_2, PANs, alkyl nitrate, and N_2O_5. Bars indicate standard deviation of monthly averages in the season. R^2 is squared correlation coefficient for measured and modeled seasonal deposition. Dotted lines are for annual CLs divided by twelve in each site. MAM: March April May, JJA: June July August, SON: September October November, DJF: December January February.

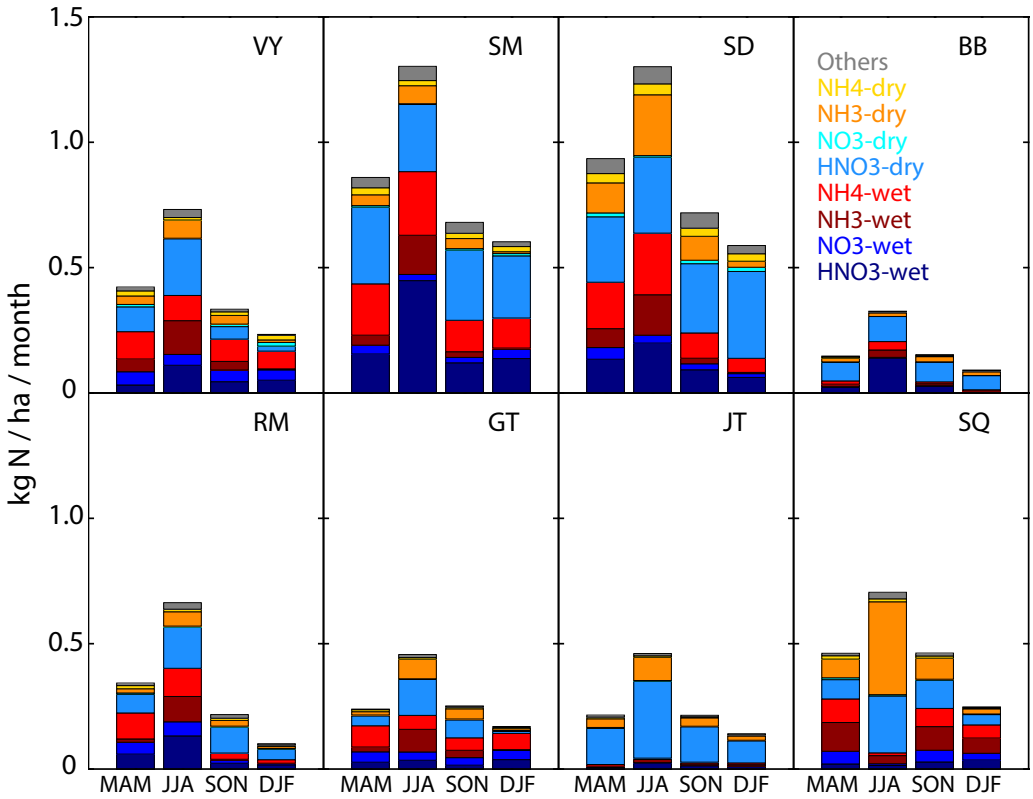

Figure 3.4: Stacked bar of modeled seasonal Nr deposition showing speciation. Others includes dry deposition of NO_2, PANs, alkyl nitrate, and N_2O_5. Blueish: oxidized N, reddish: reduced N, dark: wet deposition, light: dry deposition.

3.3.2 Source attribution using GEOS-Chem adjoint

3.3.2.1 Spatial and sectoral footprints of Nr deposition

The sensitivity of total annual Nr deposition (J_p) to emission sources is calculated by the GEOS-Chem adjoint model. The results can be understood as the contribution of emissions in each grid cell to the Nr deposition in each Class I area. Figure 3.5 shows spatial distributions of the sensitivities of Nr deposition to NO_x and NH_3 emissions – the so called source footprint (Eq. 3.5) – for each region. Inset numbers are the annual Nr deposition in each area from all sources (J_p). Pie charts show the relative contributions to this value from specific emission sectors (sectors contributing $< 1\%$ are not shown).

The source attribution results show significant variability in terms of the sectors contributing to Nr deposition in different Class I areas. Livestock NH_3 and surface source NO_x, i.e., mobile sources, are the major sources of Nr deposition, contributing more than 65% to SM, SD, RM, GT, JT, and SQ. Livestock NH_3 contributions are largest for SQ (54%) and smallest for BB (15%). Mobile NO_x is the major emission source for JT (63%), SM (40%) and SD (38%). Fertilizer NH_3 is the third most important source of Nr deposition for VY (14%), GT (11%), and SQ (8%). In contrast to the other sites, for BB the contribution of natural sources of Nr (the sum of natural NH_3, lightning and soil NO_x equal to 47%) is comparable to that of anthropogenic contributions. NO_x from EGUs is the third most important source for RM (12%) and SD (9%). Lightning is a considerable source not only for BB but for SM (9%). Aircraft emissions have a noticeable impact only for JT (2%).

The results of the adjoint sensitivity calculations show that the spatial footprint of emissions affecting different Class I regions can vary by several hundred kilometers. Even though NO_x and NH_3, by themselves, have very short lifetimes (< 1 day), in the form of aerosol species they can influence Nr deposition over quite large distances, which is reflected in the maps in Fig. 3.5. To provide a quantitative means of evaluating the spatial extent of the footprint for each region, Fig. 3.6 shows cumulative contributions of annual average monthly Nr deposition by radial distance from

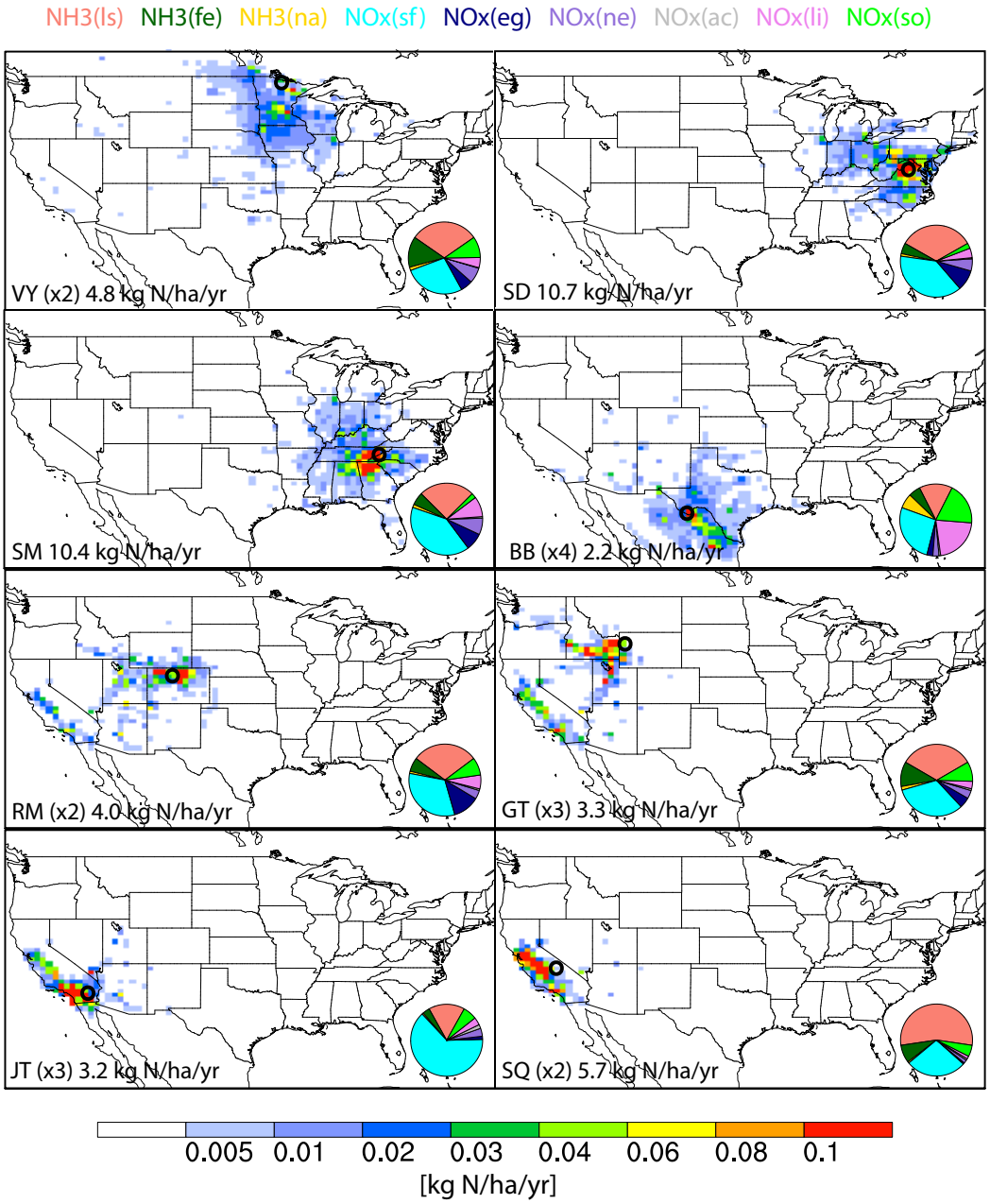

Figure 3.5: Annual-averaged monthly footprint (χ) of Nr deposition in each Class I area and pie chart of fractional contribution from emission sectors. ls: livestock, fe: fertilizer, na: natural, sf: surface inventory, eg: electric generating units, ne: non-eg industrial stacks, ac: aircraft, li: lightning, so: soil. Inset numbers are cost function (J_p), annual Nr deposition in each Class I area. Site locations are shown with open circles. Footprint values are scaled for visibility with numbers in parenthesis.

each site. Blue and red lines indicate distances for which the cumulative influence is 50% and 90% of the total, respectively. For reference, the greatest distance within the contiguous US, from Florida to Washington, is about 4500 km. It can be inferred from the shape of the plot that VY, SM, and BB have broad source regions spreading ∼1500 km from the site. In contrast, JT and SQ are mostly (90%) influenced by sources within 700 km (JT) and 400 km (SQ). Local sources (within 50 km) contribute more than 20% of total Nr deposition for SD, while the rest are from more distant regions spread across ∼1100 km. For RM and GT, there is a jump in the cumulative distribution around 1200 km which is due to sources in California. Steep initial rises for JT and SQ correspond to the influence of local urban centers (Los Angeles and San Francisco, respectively).

Additional analysis was performed for RM, given the prevalence of studies on Nr deposition in this area [14, 132, 209]. Figure 3.7 shows the source distributions of oxidized and reduced Nr deposition. Our results suggest that reduced Nr deposition originates primarily from east of the park, while in contrast a large fraction of oxidized Nr deposition originates from west of that park. This is consistent with the spatial distributions of the emissions of NH_3 compared to those of NO_x surrounding the park. The high sensitivity of reduced Nr to sources west of RM in California and Idaho agrees with other recent studies [14, 132, 209].

3.3.2.2 Efficiency of emission impacts on Nr deposition

For each Class I area, we also calculate non-normalized adjoint sensitivities as defined in Eq. 3.4 using the cost function defined in Eq. 3.1. These provide estimates of the response of Nr deposition (J_p) in each park per kg emissions of NH_3-N, NO_x-N, and SO_2-S in each month. These are a measure of transport efficiency of each species, largely determined by meteorology and aerosol partitioning. Figure 3.8 shows a few select results with unique seasonal features in JJA and DJF.

In JT, there is a clear seasonal trend (Fig. 3.8 (a)). Nr deposition in the park is impacted most efficiently by sources in the NW-SE direction during the summer and by sources in the NE-SW direction in the winter, due to changes in wind patterns. In RM, Nr deposition is owing to the sources from California during the summer, whereas the source footprints are much more localized

during the winter (Fig. 3.8 (b)). While stronger winds ($\geq$ 6 m/s) are actually more frequent in the winter, larger NH_3 emissions in the summer facilitate formation of NH_4NO_3 and thus long-range Nr transport. In SD, NH_3 emissions make a positive contribution to Nr deposition during the summer, while emissions north of the park contribute negatively during the winter (Fig. 3.8 (c)). These negative sensitivities occur because NH_4NO_3 formation is limited by NH_3 in the winter in SD. In these conditions, emissions of NH_3 promote formation of NH_4NO_3. Since NH_4NO_3 has a longer lifetime in the atmosphere than gas-phase NH_3 or HNO_3, formation of NH_4NO_3 causes Nr to be transported further away, and thus less Nr deposits in the park. Thus, the deposition of Nr in the park has a negative sensitivity with respect to NH_3 emissions. This tradeoff is also manifested by SO_2 emissions having positive sensitivities during winter and negative sensitivities during summer. In NH_3 limited conditions (winter), increased SO_2 emissions would tie up NH_3 as aerosol $(NH_4)_2SO_4$ or NH_4HSO_4, leaving less NH_3 available to form NH_4NO_3.

3.3.2.3 Analysis of all Class I areas in critical load exceedance

CL exceedance in Class I areas are shown in Fig. 3.9. In order to see the number of grid cells in CL exceedance, the area of the regions are not reflected in this map; they are shown as filled cells if the fraction that the region occupies in the cell is greater than zero (although fractional grid cell areas, β_i, are considered in the model simulations themselves). The West/East contrast is clear. The number of cells in CL exceedance is larger in the West while the magnitude of the CL exceedance is larger in the East. This is not surprising considering the spatial distribution of Nr deposition (Fig. 3.2) and Class I areas. Among the 149 Class I areas in the contiguous US only 38 are located in the East. Figure 3.10 (a) shows the sensitivity of J_a to NO_x and NH_3 emissions. This sensitivity indicates the regions where reducing emission will result in the largest decrease in the extent of Class 1 areas in CL exceedance. Figure 3.10 (b) is the sensitivity of J_c to emissions. This sensitivity shows the sources that are causing the largest values of Nr deposition, relative to the CLs (i.e., excessive or severe values).

Comparison of the two types of sensitivity analysis suggests how different emissions control

strategies might be considered to meet different objectives. Decreasing Nr emissions in California and regions surrounding RM and SM would be useful for reducing both the extent of Class I areas in CL exceedance (Fig. 3.10 (a)) and the amount of excessive Nr in Class I areas (Fig. 3.10 (b)).

Nr originating from Idaho, Utah, Washington, and Arizona contribute more to reduce the extent of Class I areas in CL exceedance but less to the amount of excessive Nr in Class I areas, as the Nr deposition in these regions is not as excessive as it is in other regions, as shown in Fig. 3.9. Reducing Nr emissions from the tip of Florida would reduce the area of regions in CL exceedance, while reductions to emissions in this area are not as beneficial for avoiding excessively high deposition, as this region has the highest CL (5kg N/ha/yr) of those considered here. For reduction of excessive Nr above the CL, sources with the largest impact are located in the East (i.e., Tennessee, Alabama, and Georgia) and the San Joaquin Valley in California. Interestingly, the distribution of contributions across sectors is similar for both J_a and J_c; surface NO_x and livestock NH_3 are the major emission sectors contributing to both the extent and severity of CL exceedances.

3.3.3 Uncertainty caused by NH_3 emissions

To evaluate the robustness of our source attribution analysis with respect to NH_3 emissions uncertainties we compare our base case results using NEI2008 emissions to sensitivity results using NEI2005 NH_3 emissions optimized using remote sensing observations [198] from [257]. This is of interest not only because the magnitude of NH_3 emissions may change the contribution of NH_3 to Nr deposition, but also because Nr deposition is sensitive to long-range transport of ammonium and nitrate aerosol and NH_3 abundance exerts a strong, nonlinear, influence on nitrate partitioning. As shown in [257], in the optimized NEI2005 the overall NH_3 emissions have increased compared to the original NEI2005 inventory; emissions in California, the central US, and the Midwest are especially enhanced. Figure 3.11 shows the NH_3 emissions from the optimized NEI2005 and those used in this study, NEI2008. The NEI2008 inventory has even larger NH_3 emissions over the Midwest compared to the optimized NEI2005 in all three months shown here. In July, NH_3 emissions in the central US (Kansas, Nebraska, eastern Colorado, and Texas) and Washington are higher with the optimized

NEI2005.

Case studies are performed for VY, SD, and RM, whose Nr deposition footprint (Fig. 3.5) includes regions showing noticeable differences between the two NH_3 emission inventories (Fig. 3.11). The non-normalized sensitivity, $\lambda_{i,j}$, remains constant with the changes in emissions but the semi-normalized sensitivity, $\chi_{i,j,k}$, is perturbed by the differences in $E_{i,j,k}$. Figure 3.12 shows the sensitivities of J_p (total modeled Nr deposition in individual Class I areas) to NH_3 emissions for these sites. Overall, when using NEI2008 the contribution of NH_3 emissions to J_p is larger than when using the optimized NEI2005 inventory in all cases. Differences in NH_3 emissions clearly affect sensitivities in VY. Differences in emissions between the two inventories in Minnesota and Iowa mainly contribute to changes in the sensitivities for Nr deposition in VY. The source footprint for VY site gradually accumulates to 90% of the total Nr deposition at a distance of 1700 km from VY (see Fig. 3.5 and 3.6), which encompasses the regions in Iowa where the emissions have changed, which are ∼840 km away. SD is not affected much by different NH_3 inventories in July and October as up to 50% of total Nr deposition is owing to sources within 250 km (Fig. 3.6). However, NEI2008 leads to broader estimates of the source footprints in April. Local influences become more pronounced for SD in the footprints estimated using the NEI2005 emissions. For the base case, Nr deposition was found to have significant long range influences for RM. However, when using the optimized NEI2005 emissions, where NH_3 sources in eastern Colorado are estimated to be much larger, the relative role of long-range influence from east of the park is reduced.

3.4 Discussion and conclusions

We used the GEOS-Chem CTM and its adjoint model for Nr deposition source attribution in Federal Class I areas in the US. Among the eight selected Class I areas, Voyageurs, Smoky Mountain, Shenandoah, Rocky Mountain, Grand Teton, and Sequoia are estimated to be in exceedance of the most conservative estimates of CLs from [167]. Modeled Nr deposition is compared with NADP/NTN [157] and CASTNET [30] measurements and other modeling studies [250, 196]. The seasonality of measured species is generally well represented by the model ($R^2 > 0.6$), except in

Joshua Tree. Modeled Nr deposition contains large contributions from wet HNO_3 deposition which is likely overestimated in the version of the model used here [250], leading to overestimates of Nr deposition in Smoky Mountain and Shenandoah of up to 0.6 kg N/ha/month. Still, adequate model performance in other seasons and locations suggests a considerable contribution of dry deposition of NH_3 in some locations and seasons, consistent with [196]. A significant fraction of Nr deposition in the central mountain region (including Rocky Mountain National Park) is estimated to be in the form of reduced nitrogen, similar to several other recent studies [14, 132, 209], although such estimates are sensitive to model uncertainties in NH_3 emissions and modeled NO_3^-.

The spatial and sectoral distribution of annual Nr deposition sources are investigated using the adjoint of GEOS-Chem. Quantifying the contribution of local versus long-range transport and the contribution of different sectors to Nr deposition may serve as a guide for devising locally-tailored strategies to reduce Nr deposition in different Class I areas. NH_3 emissions from livestock and NO_x emissions from mobile sources are the major sectors that contribute to Nr deposition in all selected Class I areas, except Big Bend where natural sources contribute comparably with anthropogenic sources. Nr deposition in Joshua Tree and Sequoia, both located in California, tends to originate from local (< 700 km) sources, whereas Nr deposition in the mountain regions (Grand Teton and Rocky Mountain) are $\sim$50% from nearby sources (< 400 km) and the rest from sources as far away as California ($\sim$1300 km). For other parks (Voyageurs, Smoky Mountain, Shenandoah, and Big Bend), sources are broadly distributed radially. Overall, these results suggest that mitigating Nr deposition in many specific areas may require substantial consideration of interstate transport.

The efficiency of emissions to impact Nr deposition is evaluated at the per-kg emission level for NH_3-N, NO_x-N, and SO_2-S. This result represents the response of Nr deposition to additional emissions, which is useful for consideration of the impact of future emission. As it is expected [54] that NH_3 emissions will increase and NO_x emissions will decrease in the US in the coming decades, the formation of ammonium nitrate will increasingly be limited by NO_x. This will cause the sensitivities of deposition that contains considerable contributions from ammonium nitrate, such as Voyageurs and Grand Teton national parks, to be increasingly sensitivity to perturbations in

NO_x emissions, even though NH_3 emissions will make larger contributions to total Nr deposition. In Joshua Tree, NH_3 emission efficiencies show distinct seasonality in terms of their locations. The NW-SE impact is strongest in summer and the NE-SW impact is dominant in winter. In Rocky Mountain, effective regions, where emissions from the region would contribute to more than $\sim \pm 1.0\times10^{-8}$ kg N/ha/yr per kg N emission or $\sim \pm 1.0\times10^{-9}$ kg N/ha/yr per kg S emission, are broader in the summer even though stronger winds are more frequent in the winter (Fig. 3.8), owing to larger NH_3 sources in the summer. In Shenandoah, NH_3 emissions to the north of the park inhibit Nr deposition in the park during the winter. This response is interesting, and explainable from consideration of aerosol partitioning and transport, although the absolute significance is not that large owing to the small levels of deposition here in the winter.

Sources of Nr deposition in all Class I areas in CL exceedance throughout the US are studied using two approaches: emissions contributing to the extent of the total area of Class I areas that are in CL exceedance (J_a) and emissions contributing to the magnitude of the excessive Nr deposition above CLs (J_c). Our result suggests that one of the largest source regions contributing to the spatial extent of Class I regions in CL exceedance is California. On the other hand, Nr sources in the Eastern US, i.e., Tennessee, Alabama, and Georgia, in addition to California, contribute the most to excessive Nr above the CL in Class I areas. Thus, strategies for reducing the spatial extent of ecological damage from excessive Nr deposition may differ from those aimed at reducing its severity.

Lastly, case studies are performed for Voyageurs, Shenandoah, and Rocky Mountain national parks using different NH_3 emission inventories, which have large uncertainties, in order to evaluate how sensitive our source footprint estimates are to underlying model emissions. We adopted NH_3 emissions optimized using remote sensing observations [257] to compare with our results using the NEI2008 inventory, which has greater NH_3 emissions in the Midwest and California. Difference in semi-normalized sensitivity is most apparent in April and July. Differences of NH_3 emissions in Minnesota and Iowa are mainly reflected in the source footprint for Voyageurs. Estimated local influences become more important for Shenandoah when using the optimized NEI2005 inventory. For

Rocky Mountain, when using the optimized NEI2005 emissions, NH_3 sources in eastern Colorado are estimated to be much larger, but the role of long-range influences is reduced.

Overall, the results presented here provide useful information for considering how emissions control strategies both regionally and nationally may impact Nr deposition in Federal Class I areas. Future work may strive to apply such methods to higher resolution models, as model resolution may impact the ability to resolve fine-scale features delineating specific sources or areas of influence and complex topography in Class I areas. In addition, considering the role of bi-directional NH_3 exchange [256], which can effectively extend the source footprint owing to reemission of NH_3 from NH_3 rich soils, would be of interest. Lastly, as source attribution estimates for Nr deposition are intrinsically sensitive to uncertainties in the balance of emissions between NH_3 and NO_x, even if the total nitrogen emissions are correct, further effort should be made to improve knowledge of the distributions and trends in NH_3 and NO_x emissions.

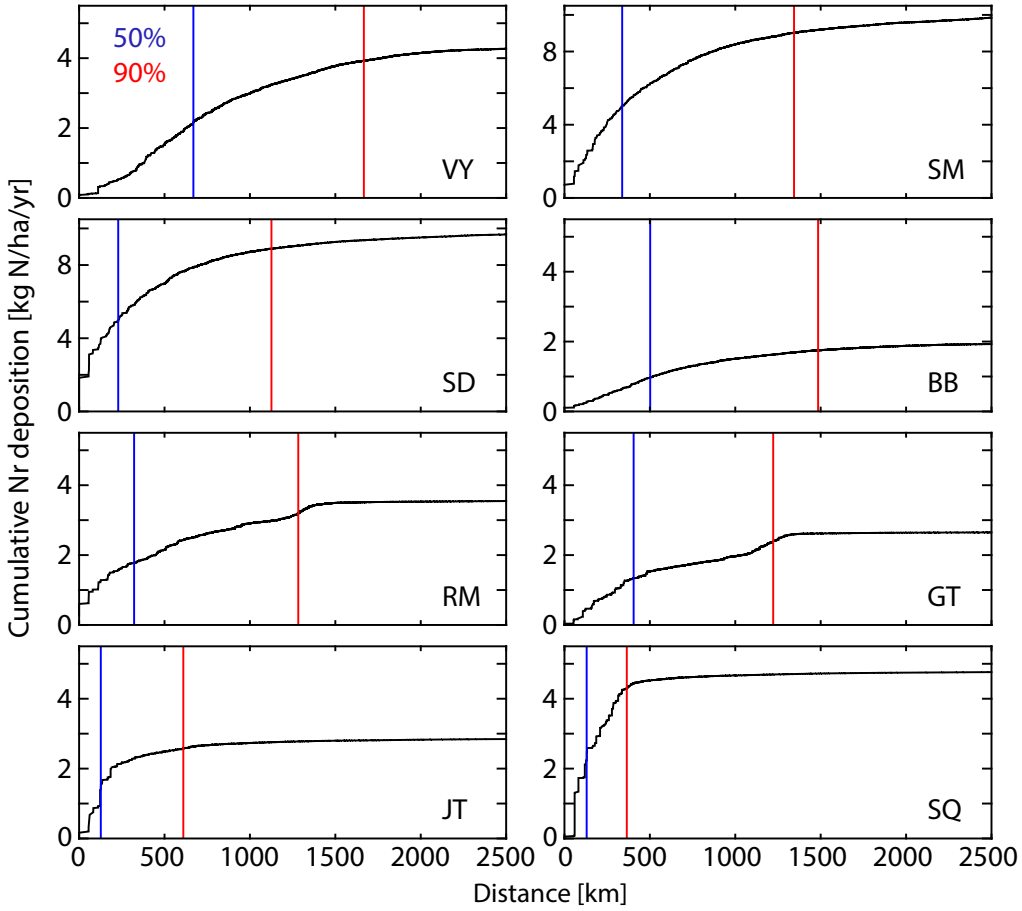

Figure 3.6: Annual averaged monthly cumulative contribution as a function of distance from the site. Vertical lines are for 50% (blue) and 90% (red) of total Nr deposition. Note that the change in scale of the y-axis for SM and SD.

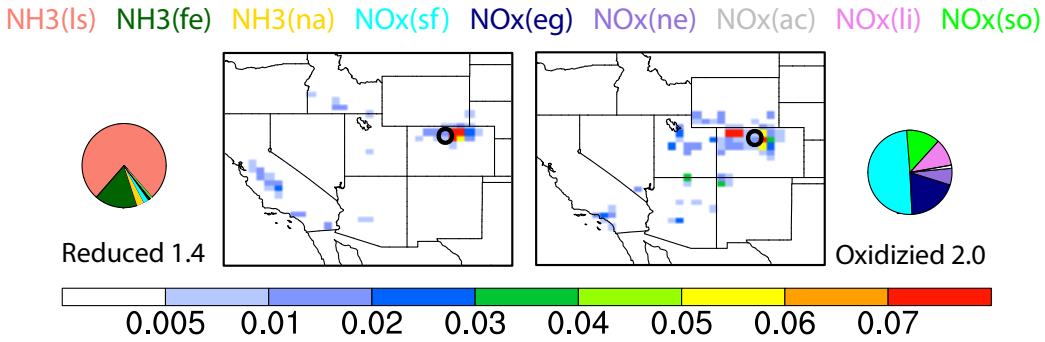

Figure 3.7: Same as Fig. 3.5 but for oxidized and reduce Nr deposition in RM. Units for the pie charts and colorbar are kg N/ha/yr. The sum of the oxidized and reduced Nr deposition is smaller than the inset number in Fig. 3.5 because the number here excludes Nr from "other species."

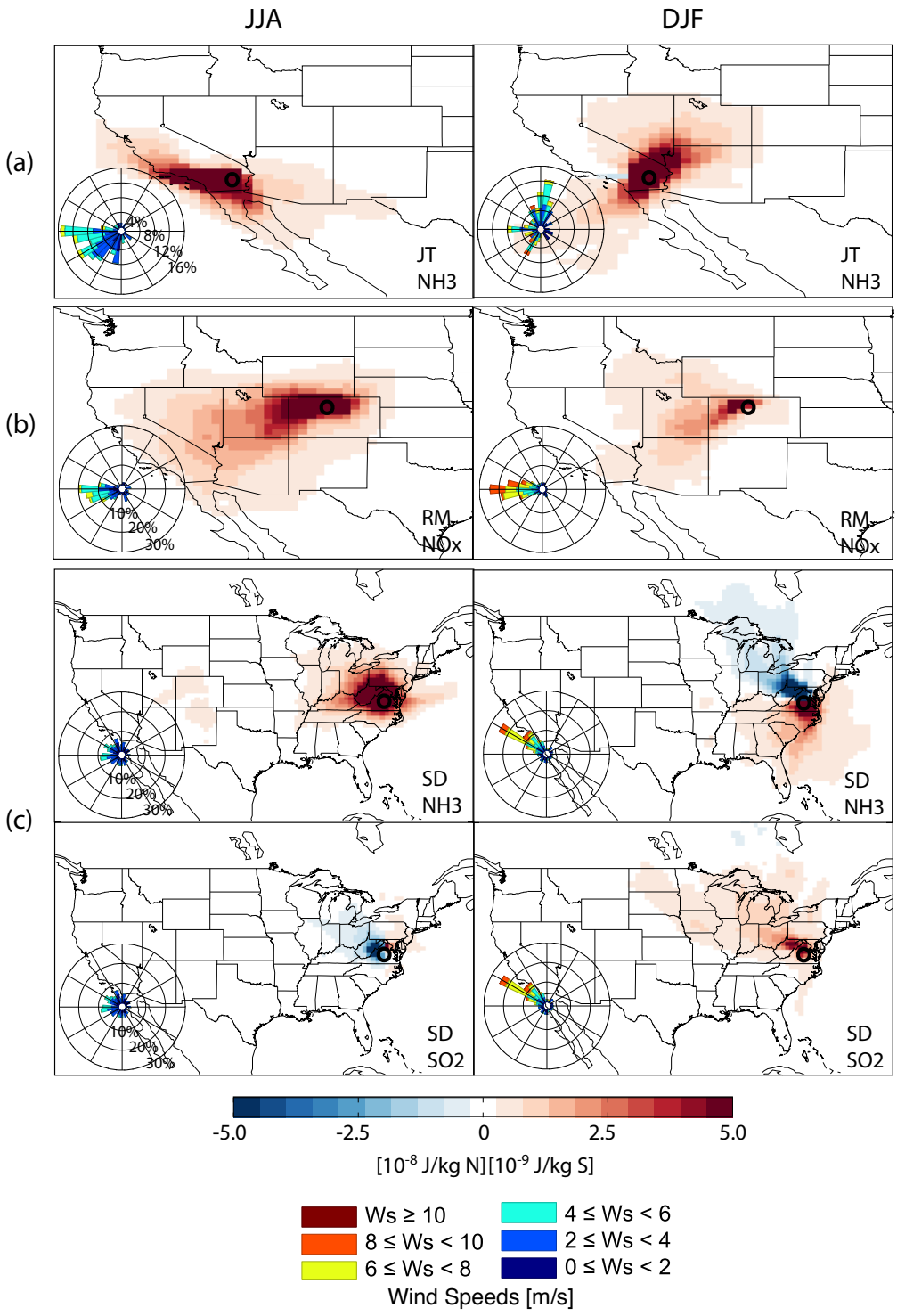

Figure 3.8: Efficiencies of impacts on Nr deposition showing cost function (J_p) change per kg N or kg S emission for the tracer and season indicated in the plot. (a) Joshua Tree (b) Rocky Mountain (c) Shenandoah national parks. Wind-roses for each site show fraction of wind frequencies based on daily surface winds during the season.

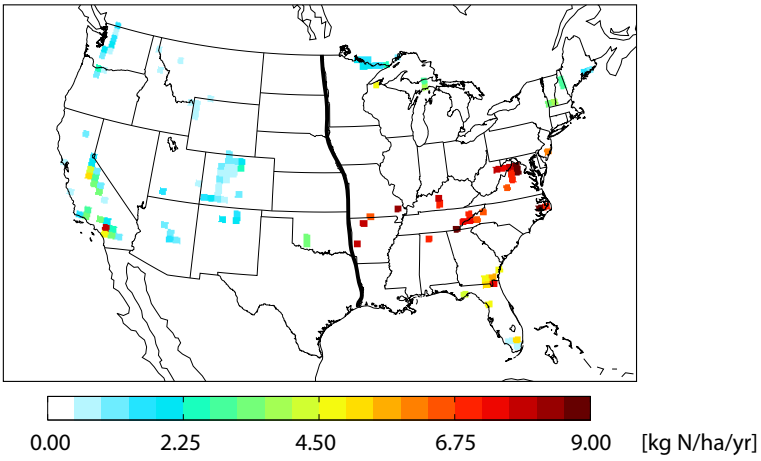

Figure 3.9: CL exceedance in Class I areas; color indicates magnitude of exceedance. The size of Class I areas are not reflected. Grid cells containing Class I areas are shown as colored regardless of the fraction of Class I areas. Bold line divides Western and Eastern US.

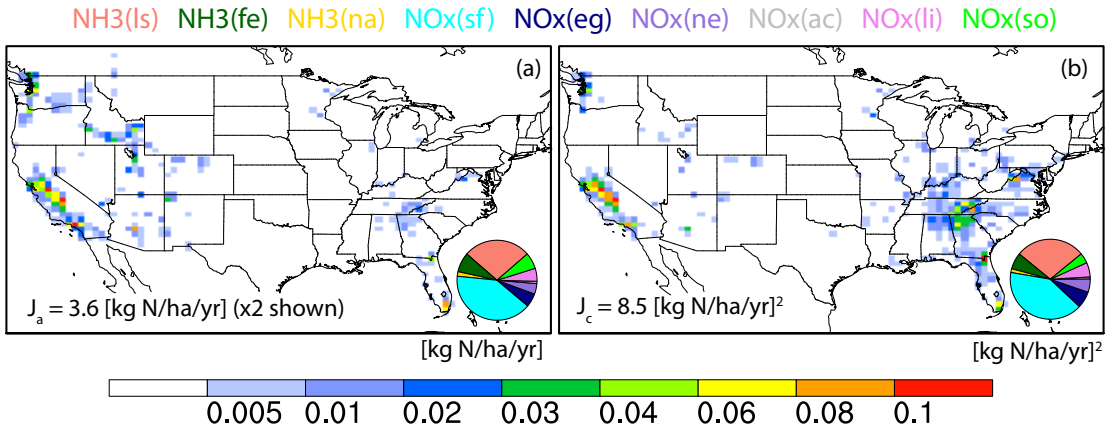

Figure 3.10: Same figure as Fig. 3.5 but with different cost functions. (a) J_a, the sum of Nr deposition in all Class I areas in CL exceedance, (b) J_c, the sum of square of the difference of annual Nr deposition and CL in all Class I areas in CL exceedance. Sensitivities of (a) are scaled by $\times 2$ to share the colorbar with (b).

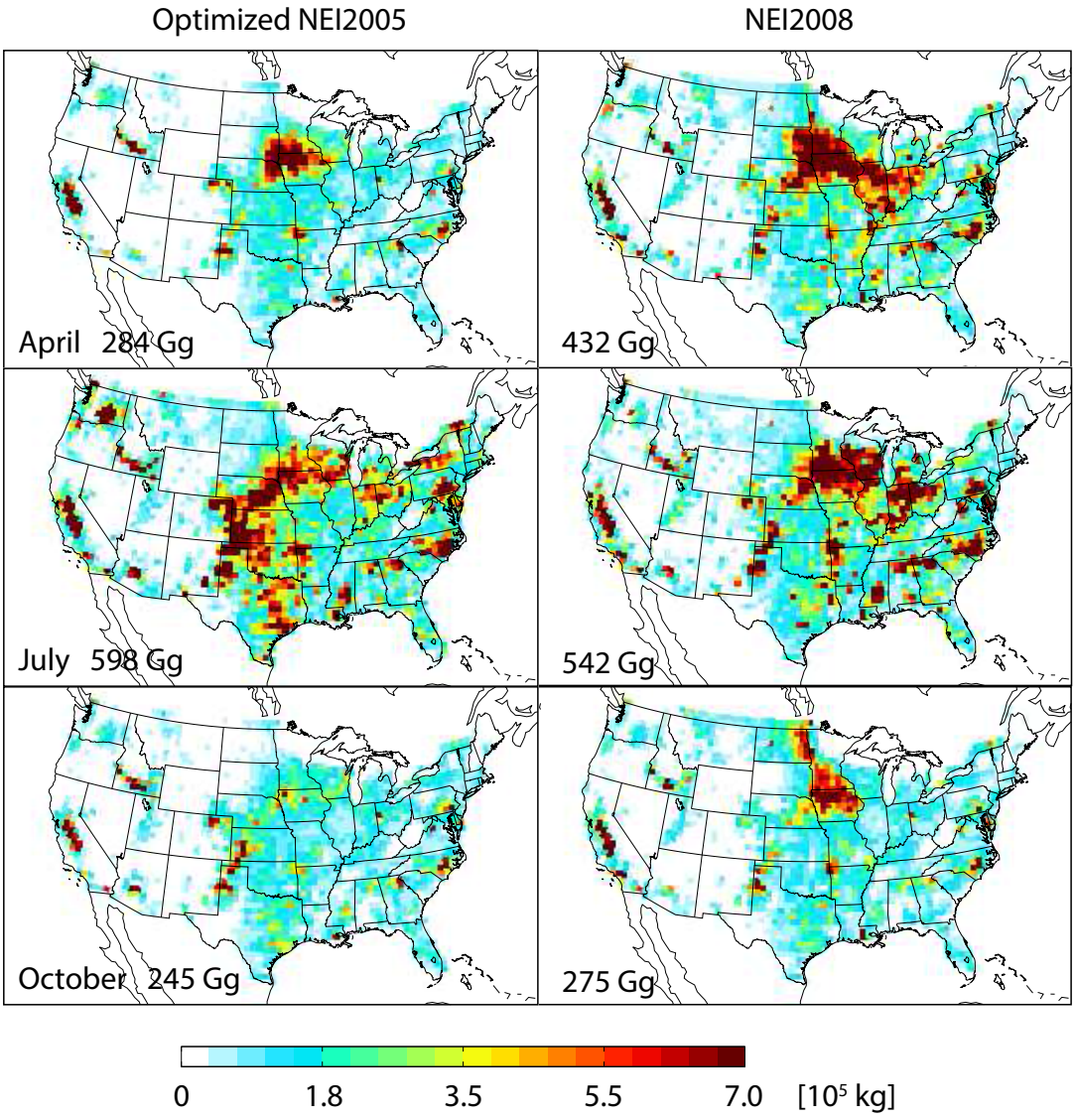

Figure 3.11: Sum of NH_3 emissions from anthropogenic, natural, biomass burning, and biofuel sources. Inset numbers are contiguous US total NH_3 emissions in each month.

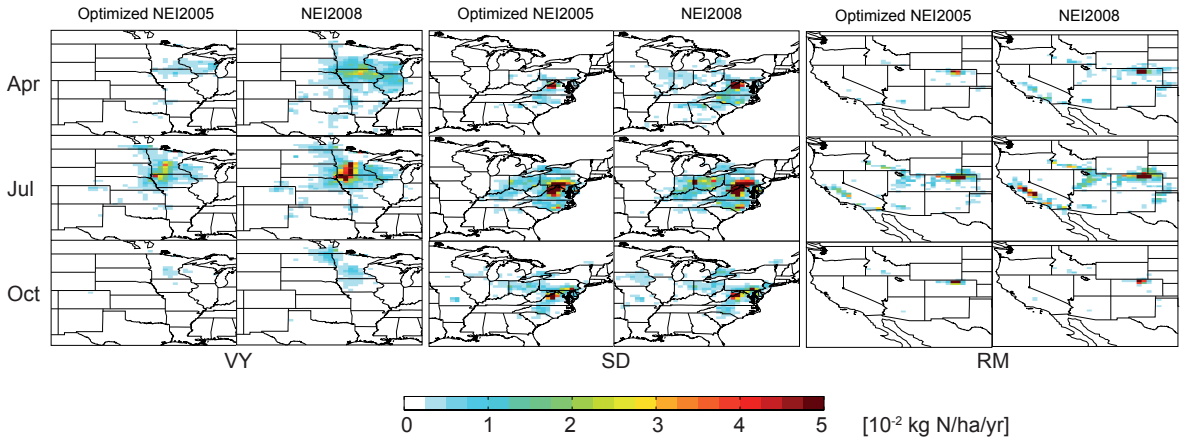

Figure 3.12: Map of sensitivities of J_p to NH_3 emissions for 3 selected Class I areas (VY, SD, and RM) for two different NH_3 emission inventories (optimized NEI2005 and default NEI2008) in each month.

Chapter 4

$PM_{2.5}$ source attribution for Seoul in May from 2009 to 2013 using GEOS-Chem and its adjoint model

4.1 Introduction

Particulate matter with aerodynamic diameter less than 2.5 μm ($PM_{2.5}$) is known to have detrimental impacts on human health, causing increased respiratory disease and stroke related mortalities (e.g.[23, 64, 12]). The Seoul metropolitan area (Seoul, Incheon, and Geonggi) is one of the most densely populated mega-cities worldwide, having more than 23 million residents (49% of national population) in about 12,000 km^2 (12% of the Korean peninsula) [107]. Air quality standards for $PM_{2.5}$ have only recently been implemented in Seoul. The Korean Ministry of Environment devised a Special Act legislation for improving air quality in the Seoul metropolitan area in 2003 (enacted in 2005). The first Seoul Metropolitan Air Quality Improvement Plan (2005 - 2014) aimed at reducing PM_{10} and NO_2 concentrations. In the second master plan, formulated for 2015 - 2024, $PM_{2.5}$ and O_3 were added to the regulations. This plan includes $PM_{2.5}$ standards of 50 $\mu g/m^3$ for 24 hours, and 25 $\mu g/m^3$ for a year. The goal of the second master plan is reducing annual $PM_{2.5}$ from 27 $\mu g/m^3$ in 2010 to 20 $\mu g/m^3$ in the Seoul metropolitan area by 2024 [146].

In order to help monitor and enforce these air quality regulations, the National Institute of Environmental Research (NIER) runs 7 sites over South Korea that provide intensive obciteservations of ambient air quality. Intensive monitoring for the Seoul metropolitan area started in 2008 at a site in Bulgwang-dong, Seoul (37.5°N, 126.6°E). The data provided include wind speed, temperature, relative humidity, concentrations of gaseous tracers (SO_2, CO, NO_x, O_3), particulate

matter (PM_{10}, $PM_{2.5}$), carbonaceous components (black carbon (BC), organic carbon (OC)), ion components (SO_4^{2-}, NO_3^-, Cl^-, Na^+, NH_4^+, K^+, Mg^{2+}, Ca^{2+}), and heavy metals (Pb, Cd, Cr, Cu, Mn, Fe, Ni, As, Be).

Although the continuous and intensive federal monitoring program began in 2008, there have been several prior institutional studies of $PM_{2.5}$ in Seoul. Both local emissions and long-range transport from major industrial areas in China have been identified as sources of $PM_{2.5}$ observed in Seoul [82]. It has been found that major components of $PM_{2.5}$ in Seoul are sulfate, nitrate, and ammonium, and those secondary aerosols are likely transported with air parcels originated from China [99, 102, 82]. Recently, [68] analyzed $PM_{2.5}$ and PM_{10} measurements from ambient air monitoring stations in Seoul between 2002 to 2009 and interpreted the observed temporal variations of $PM_{2.5}$ in terms of variability of local NO_x emissions, secondary formations, and mixing height variation.

However, quantitative analysis of the relative contribution of local versus distant sources to $PM_{2.5}$ in Seoul are still limited, possibly owing to a lack of consistent measurements and suitable source-receptor models. Recent activities have lead to enhanced interest in $PM_{2.5}$ source attribution in Seoul, such as an intensive ground-based and airborne measurement campaign (KORUS-AQ) in May to June, 2016. This season of the year shows high $PM_{2.5}$ concentrations [120, 102]. Combinations of local and remote sources and anthropogenic, natural, and dust storms have been suggested as contributing sectors [37, 102].

In this study, we use the 3-dimensional atmospheric chemical transport model (CTM) GEOS-Chem and its adjoint model to investigate trends and sources of $PM_{2.5}$ in Seoul, Korea, from 2009 to 2013 in May. The model is evaluated using surface measurements, and several set of emission inventories are considered to determine which best reproduce observed $PM_{2.5}$ concentrations. High $PM_{2.5}$ concentration episodes that exceed 24 hr air quality standards are selected for emissions source attribution. The spatial and sectoral distribution of emissions for high $PM_{2.5}$ episodes are determined. Findings from this study may guide interpretation of observations obtained in the KORUS-AQ measurement campaign.

4.2 Methods

4.2.1 Measurement data

We use speciated and total surface aerosol concentration measurements to evaluate the modeled $PM_{2.5}$ concentrations. The intensive monitoring site that provides both $PM_{2.5}$ and component measurements for the Seoul metropolitan area is located in Bulgwang-dong, Seoul (37.5°N, 126.6°E). Hourly concentrations of $PM_{2.5}$ are measured using the β-ray attenuation method (BAM) (BAM-1020, Met One, USA). SO_4^{2-}, NO_3^-, and NH_4^+ are measured by ambient ion monitor (AIM) (URG-9000D, URG Corporation, USA) utilizing ion-chromatography. BC and OC are measured by thermal-optical-transmittance (SOCEC, Sunset, USA) following the National Institute for Occupational Safety and Health of USA (NIOSH) protocol. $PM_{2.5}$ measured by BAM pass through a heating oven and are conditioned to maintain 35% relative humidity and are thus assumed to be dry. AIM and SOCEC measure unconditioned aerosols, which may contain water.

4.2.2 GEOS-Chem model

GEOS-Chem (www.geos-chem.org) is a 3-dimensional atmospheric CTM driven by assimilated meteorological input from the Goddard Earth Observing System (GEOS) of the NASA Global Modeling and Assimilation Office [16]. We use the nested model configuration with a resolution of 0.5° latitude ×0.667° longitude with 47 vertical layers up to 0.01 hPa [35, 251] for a domain over East Asia (100E - 150E, 20N - 50N). Boundary conditions are provided by two steps of one-way nested simulations. A global simulation at 4° latitude × 5° longitude resolution provides boundary conditions every 3 hours for the first nesting at 0.5° latitude ×0.667° longitude resolution over larger East Asian domain (70E - 150E, 11S - 55N). Then these nested simulations provide boundary (every hour) and initial conditions for the smaller East Asian domain (100E - 150E, 20N - 50N). This smaller domain is used to minimize computational requirements of the adjoint model used for source attribution.

GEOS-Chem includes detailed tropospheric gas-phase chemistry of the O_3-NO_x-hydrocarbon

system [87]. Aerosols are assumed to be externally mixed, and the thermodynamic equilibrium between gases and aerosol of K^+-Ca^{2+}-Mg^{2+}-NH_4^+-Na^+-SO_4^{2-}-NO_3^--Cl^--H_2O is calculated using ISORROPIA II [63, 179, 27]. We estimate $PM_{2.5}$ as the sum of SO_4^{2-}, NO_3^-, NH_4^+, BC, and 1.8×OC. The conversion factor of 1.8 is used to convert OC to OM (organic matter) [213]. Wet deposition includes sub-grid scavenging in convective updrafts, large scale in-cloud rainout, and below-cloud washout [128]. Dry deposition is calculated using a resistance-in-series model [234, 227], which includes aerodynamic resistance, quasi-laminar sublayer resistance, and bulk surface resistance.

Anthropogenic emissions will be described in the following section. Biomass burning emissions are taken from the 3-hour GFED3 inventory [151, 218]. Natural emissions of NO_x are from lightning [156] and soil [243, 227]. Natural emissions of NH_3 from soil, vegetation, and ocean sources are from the GEIA inventory [20].

4.2.3 Anthropogenic emission inventories

4.2.3.1 Gaseous and carbonaceous emissions

Monthly total anthropogenic emissions used in this study are shown in Fig.4.1. As a default, the model uses the Emissions Database for Global Atmospheric Research (EDGAR) inventory for global anthropogenic emissions. For the East Asian region, the emissions are overwritten by the Streets regional inventory for Intercontinental Chemical Transport Experiment-Phase B (INTEX-B) [253] for SO_2, NO_x, and NH_3. BC and OC emissions are from [19]. These inventories are updated with a more recently developed anthropogenic emission inventories for the East Asian region, NIER/KU-CREATE [241], for SO_2, NO_x, NH_3, BC, and OC. With the replacement with NIER/KU-CREATE emission inventory, NH_3 emissions have finer resolution and show increased emissions over Eastern China and western South Korea. SO_2 emissions have also increased in industrial regions in China. NO_x emissions remains almost constant, excluding an increase in Beijing. BC and OC have increased over China; however, their emissions largely decrease in South Korea.

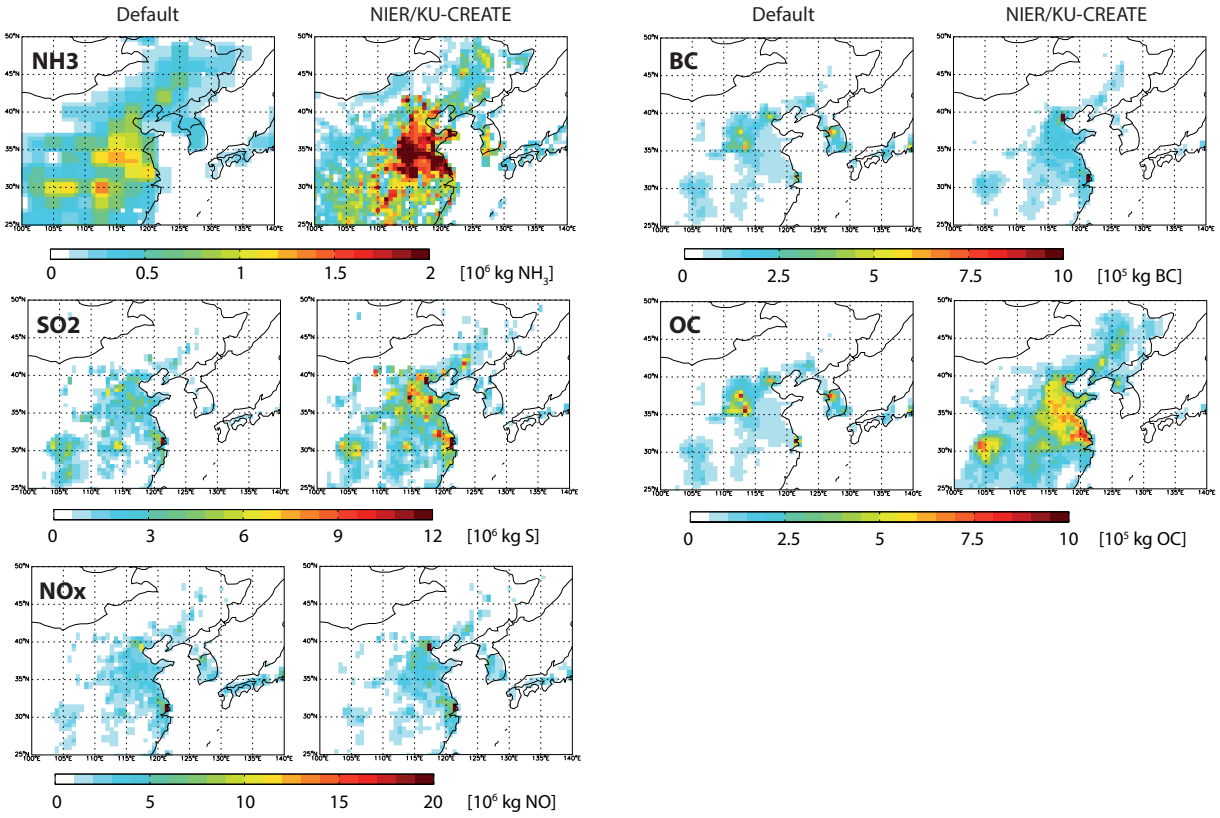

Figure 4.1: Monthly emissions in May used in modeling. (a) Default inventory and (b) KU-CREATE inventory. See text for details.

4.2.3.2 Diurnal variation of NH_3 emissions

Diurnal variation is applied to the daily NH_3 emissions. We refer readers to [258] for a detailed description of the method; here we provide a brief explanation of the scheme. The diurnal fraction of NH_3 emissions are calculated using Eqs.4.1 and 4.2.

$$E_{NH3}(t) = \frac{H_t \overline{E_{NH3}}}{\sum_{i=1}^{24} H_i} \tag{4.1}$$

$$H_t = \frac{161500}{T_t Ra} e^{(-\frac{10380}{T_t})} \tag{4.2}$$

where $E_{NH3}(t)$ is the NH_3 emission at time of day t, $\overline{E_{NH3}}$ is the daily average NH_3 emission, H is the Henry's equilibrium constant, T is surface temperature (K), and Ra is aerodynamic resistance of the surface. The impact of this scheme is that more NH_3 is emitted at higher temperatures and stronger winds. This scheme is adopted to adjust all NH_3 emissions that are overestimated during the nighttime and underestimated during the daytime [131], causing overall overestimation of NO_3^-. We recognize that this scheme was originally developed to account for diurnal variations in livestock emissions [258]. For urban sites such as the Seoul metropolitan area, where sources of NH_3 other than livestock emission (e.g., transportation) may be significant, representation of NH_3 diurnal profiles for other sectors, e.g., motor vehicles, should be developed; here the scheme for livestock emissions is used as a proxy [131].

4.2.4 GEOS-Chem adjoint model and cost function

We use the GEOS-Chem adjoint [80] v35i for source attribution. The adjoint model is a tool for efficiently calculating the gradient (i.e., sensitivity) of a scalar model response function with respect to numerous model parameters, in our case emissions. This tool can be utilized in inverse modeling (e.g.,[135, 85]) and sensitivity analyses (e.g.,[118, 119]). The normalized sensitivity is defined as

$$\lambda_E \equiv \frac{\partial J}{\partial E} \cdot \frac{E}{J} \tag{4.3}$$

where $\frac{\partial J}{\partial E}$ is found from solution of the adjoint model. Here, E is the emission of a $PM_{2.5}$ precursor in a single grid-cell, and J is a scalar function of forward model estimates called the cost function. In this study, the cost function is the daily average $PM_{2.5}$ concentration in the grid cell containing the Seoul metropolitan area at times when both measured and modeled daily $PM_{2.5}$ concentrations exceed the daily air quality standard (50 $\mu g/m^3$) during May from 2009 to 2013,

$$J \equiv \frac{1}{M} \sum_{i=1}^{N} \sum_{j=1}^{M} c_{ij} \tag{4.4}$$

where c_{ij} is the daily average concentration of aerosol species i in day j, M is the number of days when $PM_{2.5}$ is higher than 50 $\mu g/m^3$, and N is the number of tracers composing $PM_{2.5}$ (SO_4^{2-}, NO_3^-, NH_4^+, BC, OM). The definition of cost function used in this study is discussed more in Section 4.3.3.

4.3 Results

4.3.1 Total and speciated $PM_{2.5}$ measurements

Figure 4.2 shows the comparison between $PM_{2.5}$ concentrations measured using BAM and the tracer sum (TrcSum) of those species measured by AIM and carbonaceous species by SOCEC. We define TrcSum the same way as we define modeled $PM_{2.5}$ as the sum of SO_4^{2-}, NO_3^-, NH_4^+, BC, and 1.8×OC. The correlation coefficient and the normalized mean bias (NMB) are calculated as

$$NMB = \frac{\sum_{k=1}^{L} (TrcSum_k - BAM_k)}{\sum_{k=1}^{L} BAM_k}$$

for L days when both measurements are obtained, are also indicated in the figure. NMB estimates the mean offset of one dataset from the other. It shows that TrcSum data agree well with $PM_{2.5}$ measurements using BAM, within a 5% underestimation. Although TrcSum is the best measurement for direct comparison between modeled and measured values, there are 41 days of missing data out of 155 days in AIM and SOCEC measurements, whereas there are only 3 hours of missing data among 3720 hourly data in BAM measurements. We thus use BAM data for selecting source attribution cases.

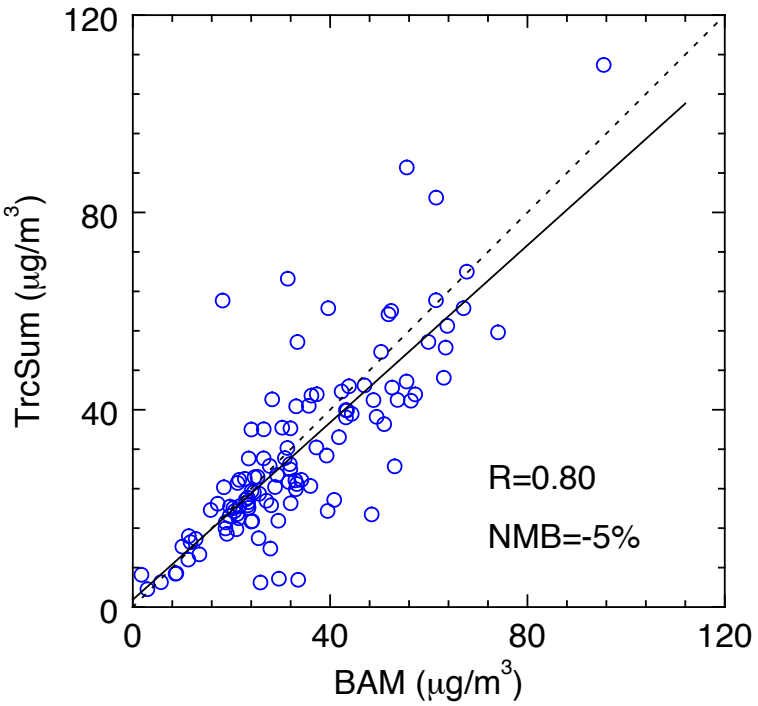

Figure 4.2: Daily averaged concentrations of $PM_{2.5}$ in May during 2009 - 2013 measured by BAM and TrcSum. See text for details.

4.3.2 Forward model evaluation

We first compare modeled and measured $PM_{2.5}$ concentrations for model evaluation. Figure 4.3 shows monthly average $PM_{2.5}$ and component concentrations in May from 2009 to 2013 in Seoul. With the default emission inventories (blue), nitrate, BC, and OC are overestimated by the model, resulting in overestimation (NMB = 29%) of $PM_{2.5}$ concentrations in all years except for 2009. Nitrate is overestimated during 2009 to 2012 (NMB = 36%), BC is constantly overestimated (NMB = 254%), and OC is largely overestimated (NMB = 52%) in 2010, 2012, and 2013. Sulfate (NMB = -7%) and ammonium (NMB = -1%) estimates are in good agreement with observed values, except for 2009 when they are noticeably underestimated.

To reduce the discrepancies between the model and the measurements, we first replace the anthropogenic emission inventory for gaseous species (SO_2, NO_x, NH_3) and carbonaceous species (BC and OC) with NIER/KU-CREATE (Fig.4.1). We additionally applied diurnal variation to the NH_3 emission for better estimation of nitrate aerosols. Results including both updates are shown in Fig. 4.3 as red lines. The correlation coefficient of measured and modeled $PM_{2.5}$ concentrations has increased from 0.38 using the default model to 0.68. Sulfate, nitrate, and ammonium estimates are also improved in terms of their correlation coefficients. The absolute NMB for ammonium is still small but has increased, possibly due to inaccurate representation of the diurnal profile of NH_3 emissions from livestock applied to an anthropogenic sector as a whole. The magnitude of BC estimates become closer to the measured values (NMB decreases from 254% to -28%). However, carbonaceous species (BC, OC) still have low correlations and larger NMB compared to other species. Modeled OC does not reproduce the annual variation, potentially due to missing sources in the emission inventory in 2009 and 2011.

4.3.3 Source attribution of high $PM_{2.5}$ episodes

The GEOS-Chem adjoint model is used to investigate source attribution for the high $PM_{2.5}$ episodes, J. We define the high $PM_{2.5}$ episodes as occurring when both modeled and measured

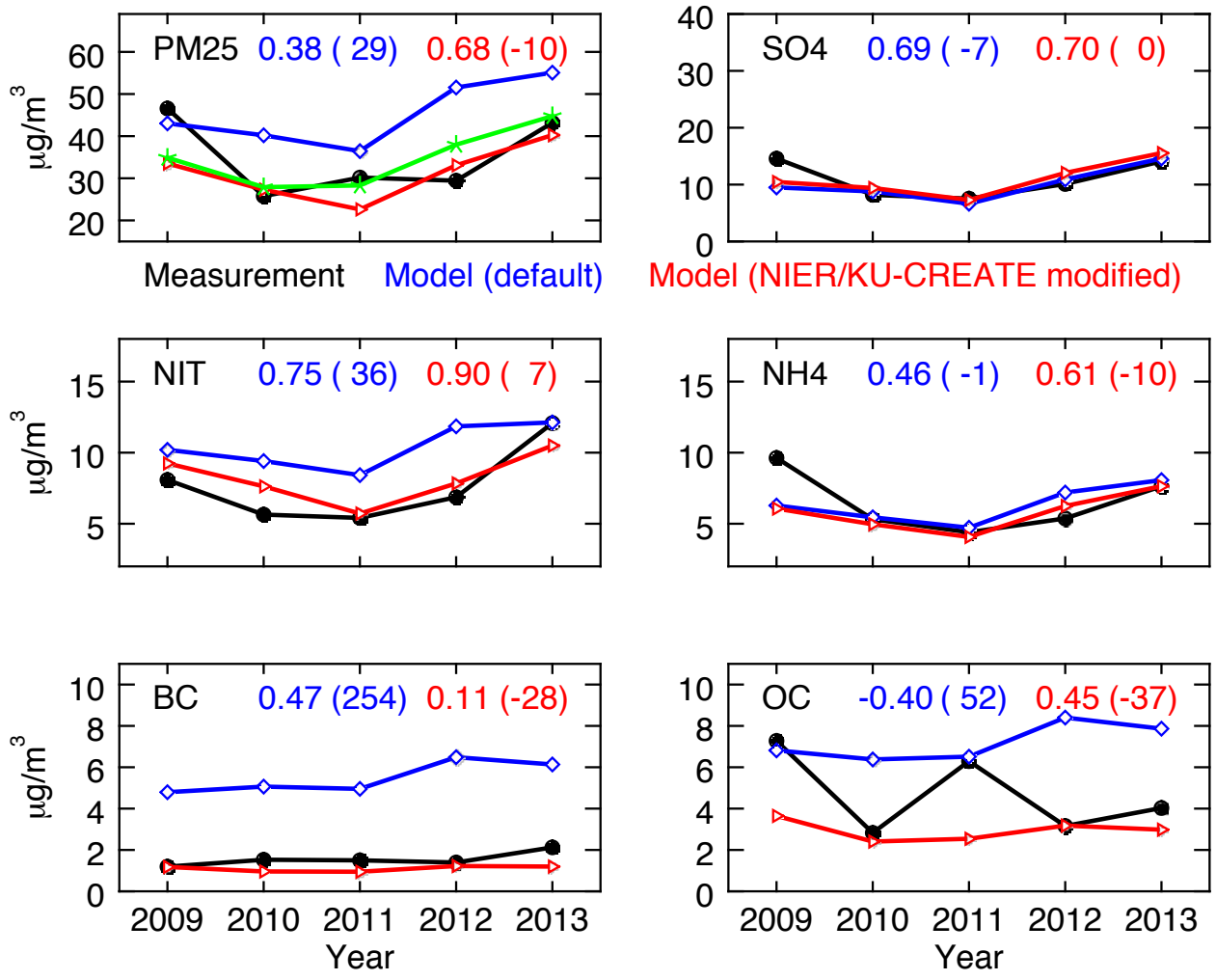

Figure 4.3: Monthly average concentrations of $PM_{2.5}$ and components in May from 2009 to 2013 in Seoul. Green is the measured $PM_{2.5}$ using β-ray absorption method, black is the sum of measured SO_4^{2-}, NO_3^-, NH_4^+, BC, and 1.8×OC, blue is the corresponding model estimates using default emissions, and red is the model values using NIER/KU-CREATE emissions including diurnal variation of NH_3 emissions. Inset numbers are correlation coefficient between the measurements and each model result, with NMB(%) in the parenthesis.

concentrations exceed the daily air quality standard of 50 μg/m^3 (Eqn. 4.4). Figure 4.4 shows measured (BAM) and modeled daily $PM_{2.5}$ concentrations in Seoul in May from 2009 to 2013. A total of 10 episodes are identified, shown with yellow shading. There are five more observed peaks (1 in 2011, 3 in 2012, 1 in 2013) that are not replicated by the model, which we do not include in J.

We conducted adjoint calculations for each episode shown in Fig. 4.4 for three days prior to the onset of the episode. Figure 4.5 shows the spatial distribution of the contributions to the cost function from the five most influential emission sectors averaged over all high $PM_{2.5}$ episodes. Regional contributions are summarized with pie charts; we consider the eight source regions indicated by different colors in Fig. 4.5 (a): South Korea; North Korea; north of the Korean peninsula; regions including Beijing, Shandong, and Shanghai; ocean in-between Korea and China; and the rest of the domain. Contributions from the Shandong region have the highest fractional contribution for each emission sector. Considering the total contribution from all sectors, emissions from South Korea account for 15.1% of the $PM_{2.5}$ peak episode concentration, whereas the Shandong region accounts for 38.5%, the Shanghai region accounts for 15.7%, and the Beijing region accounts for 13.6%. There are considerable contributions from local sources (i.e., South Korea) for all sectors ($> 6\%$) except for SO_2 (2%). NH_3 and NO_x emissions from shipping also have considerable contributions (7% and 10%).

4.4 Discussion and conclusions

An intensive ground-based and airborne collaborative (Korea and US) measurement campaign, KORUS-AQ, was conducted in May to mid-June of 2016 in the Seoul metropolitan area. To gain insight on the trends and sources of $PM_{2.5}$ for the campaign season, we analyze total and speciated $PM_{2.5}$ concentrations from a surface measurement site in Bulgwang-dong, Seoul, in May from 2009 to 2013. The measurement data is used to evaluate the 3-D atmospheric CTM, GEOS-Chem, and the model's emission inventory has updated with NIER-KU/CREATE for improved representation of daily variation of $PM_{2.5}$ concentrations. The GEOS-Chem adjoint model is used

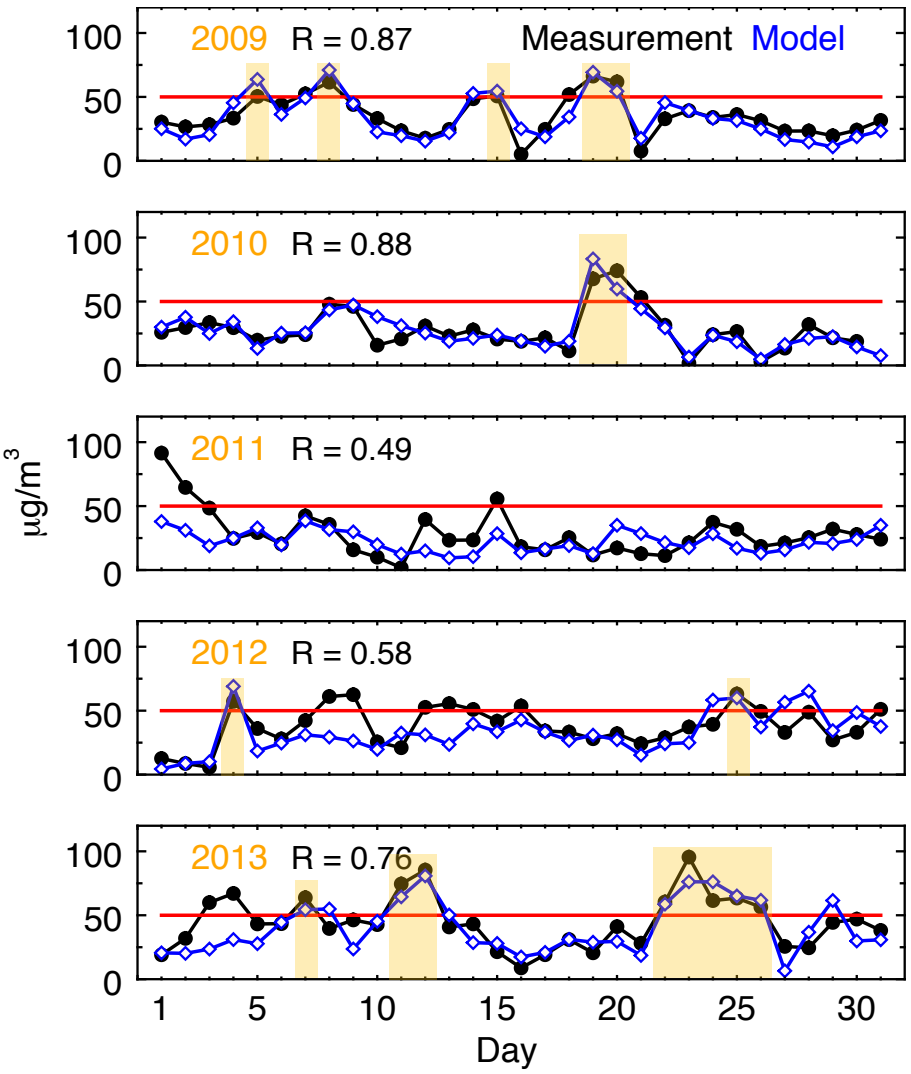

Figure 4.4: Daily $PM_{2.5}$ concentration ($\mu g/m^3$) in Seoul from 2009 to 2013. Red line indicates 24-h $PM_{2.5}$ air quality standard for Seoul (50 $\mu g/m^3$). R is correlation coefficient. Shadings indicate high $PM_{2.5}$ episode. See text for details.

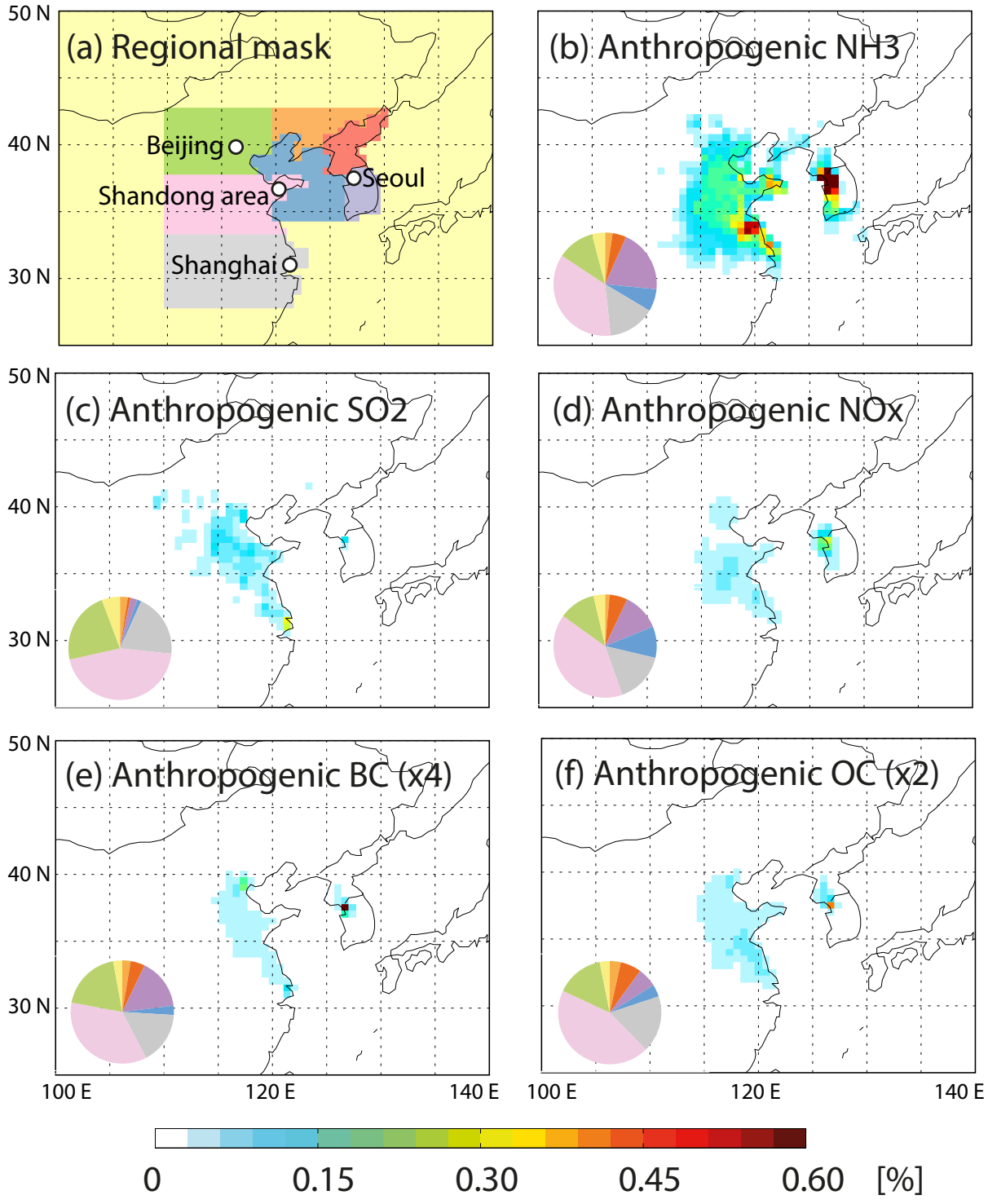

Figure 4.5: Averaged sensitivities (normalized gradient) with respect to emissions sectors for high $PM_{2.5}$ episodes that exceed the Korean daily air quality standard (50 $\mu g/m^3$) shown in Fig. 4.4.

for regional and sectoral source attributions.

Monthly average measured $PM_{2.5}$ concentration in May range from 28 (2010) to 45 (2013) $\mu g/m^3$, without a distinct increasing or decreasing annual trend. The mass concentration of $PM_{2.5}$ is explained by the sum of sulfate, nitrate, ammonium, BC, and OC concentrations, leaving less than 5% residual bias. However, the residual could be greater than 5% since the $PM_{2.5}$ is measured as dry aerosol while $PM_{2.5}$ collected for species measurement are unconditioned and may contain water.

From the comparison of measured and modeled total and speciated $PM_{2.5}$, the GEOS-Chem model tends to overestimate $PM_{2.5}$ due to overestimated nitrate, BC, and OC concentrations with the default emissions inventories. By replacing the emissions with those more recently developed for the East Asian region, NIER-KU/CREATE, and applying diurnal variation to the NH_3 emissions, the model NMB has decreased from 29% to -10%. This underestimation is mainly owing to discrepancies in OC estimates. Daily OC concentrations are consistently underestimated by the model throughout May in 2009 and 2011, possibly due to the missing emission sources (e.g., forest fire events) in the inventory. Also, secondary organic aerosols not included in the model estimates, whereas is is included in the measured OC, which also likely contributes to the discrepancy.

Using the GEOS-Chem adjoint model, the dominant emission sources to the $PM_{2.5}$ of Seoul are identified by sector and region. High $PM_{2.5}$ episodes that exceed 24h air quality standard, (50 $\mu g/m^3$), are most sensitive to anthropogenic NH_3 emissions, and regionally most sensitive to emissions from the Shandong region of China. The average contribution from all emission sectors to the high $PM_{2.5}$ episodes is 69% from Eastern China (39% from the Shandong region, 16% from the Shanghai region, 14% from the Beijing region), and 15% from South Korea.

Our results imply that attainment of air quality standard for $PM_{2.5}$ in the Seoul metropolitan area depends on anthropogenic emissions control in Eastern China. A recent study using satellite observations showed that there are decreasing trend of SO_2 and NO_x emissions in Eastern China from 2013 to 2015 [110]. It would be interesting to compare our results to the output from KORUS-AQ to see if there was improvement in $PM_{2.5}$ in the Seoul metropolitan area.

Chapter 5

Conclusions

This thesis presents three studies using the GEOS-Chem model and its adjoint to investigate sources and mechanisms of air pollutants encompassing a broad range of regional and temporal scales. We first show the model can be used for understanding background concentrations of surface level total nitrate in Antarctica. The model is able to calculate the sensitivities with respect to not only emissions distributed in the surface level but also chemical reaction rates in 3-dimensional space. Our results suggest that the background concentrations of total nitrate at the Antarctic surface in austral winter are most sensitive to NO_x emissions from mid-latitudes. Total nitrate is transported to Antarctica as nitric acid formed above continental source regions in the free troposphere through the gas-phase reaction $NO_2 + OH \rightarrow HNO_3$. In other seasons, NO_x is transported as a reservoir species such as PAN through the free troposphere, transforming into total nitrate within a cone of influence that extends to 35° S and above 4 km altitude. In addition to background concentrations, the annual variation of surface level nitrate measurements across the Antarctic continent is characterized to have first peak concentration in August and annual maximum values during austral summer. Sources such as stratospheric air mass intrusion in mid-winter, polar stratospheric clouds sedimentation in early spring, and re-emission from snow in summer have been suggested for the observed nitrate variability. In the absence of features like the disappearance of the tropopause in mid-winter, which is responsible for active air mixing between the troposphere and stratosphere, particulate deposition from polar stratospheric sedimentation, and re-emission from snow by photolysis of deposited nitrate, our analysis is limited to the source

attribution of background concentrations and to some extent of the peak in August. For future work, it is encouraged to quantify the source contribution to the summer maximum values with the recently implemented snow nitrate photolysis scheme to the model [246].

We then present a practical use of the model which may help guide the review of the SO_x/NO_x secondary air quality standard in the US. We quantify the sources of reactive nitrogen deposition in Class I areas in the US using three different cost functions implemented in a regional, high resolution ($0.5^\circ \times 0.667^\circ$) version of GEOS-Chem adjoint. We find that while it is effective to control NH_3 and NO_x emissions in the western US to reduce the area of regions in critical loads exceedance, it can be more effective to control NH_3 and NO_x emissions in the eastern US to reduce the magnitude of nitrogen deposition above the critical loads. From case studies of specific Class I areas, NH_3 and SO_2 emissions are found to contribute negatively to nitrogen deposition in Class I areas in some cases due to the longer atmospheric lifetime of nitrate aerosols compared to NO_x. As the US EPA is examining NO_x and SO_x compounds together in reviewing secondary (welfare-based) national ambient air quality standards, future works to quantify how SO_2 emissions contribute to both nitrogen and sulfur deposition in sensitive and protected regions throughout the country will be helpful.

In our final study, we use the adjoint model to review sources of $PM_{2.5}$ concentrations in the Seoul metropolitan area, Korea. Air quality standards for $PM_{2.5}$ have only recently been implemented in Seoul, with regulations started in 2015. After evaluating forward model estimates using measurement data from an intensive monitoring site in Seoul in May from 2009 to 2013, the relative contributions from emission sources are regionally quantified. Shandong region, China is found to contribute the most to $PM_{2.5}$ in Seoul. Total contribution from China is more than four times the contribution form Korea. Results from this study suggest future studies investigating the mechanisms of $PM_{2.5}$ transport from Shandong are needed. This suggestion may be applied to the data obtained from the KORUS-AQ measurement campaign.

Bibliography

[1] B. Alexander, M. G. Hastings, D. J. Allman, J. Dachs, J. A. Thornton, and S. A. Kunasek. Quantifying atmospheric nitrate formation pathways based on a global model of the oxygen isotopic composition (δ^{17}o) of atmospheric nitrate. Atmos. Chem. Phys., 9(14):5043–5056, July 2009.

[2] Aubrey P. Altshuller. Atmospheric sulfur dioxide and sulfate. distribution of concentration at urban and nonurban sites in united states. Environ. Sci. Technol., 7(8):709–712, 1973.

[3] S. C. Anenberg, K. Talgo, S. Arunachalam, P. Dolwick, C. Jang, and J. J. West. Impacts of global, regional, and sectoral black carbon emission reductions on surface air quality and human mortality. Atmos. Chem. Phys., 11(14):7253–7267, 2011.

[4] Shigeru Aoki, Stephen R. Rintoul, Shuki Ushio, Shuichi Watanabe, and Nathaniel L. Bindoff. Freshening of the adélie land bottom water near 140 °e. Geophys. Res. Lett., 32:4 PP., 2005.

[5] R. Arimoto, T. Zeng, D. Davis, Y. Wang, H. Khaing, C. Nesbit, and G. Huey. Concentrations and sources of aerosol ions and trace elements during ANTCI-2003. Atmos. Environ., 42(12):2864–2876, April 2008.

[6] Robert J. Arthern, Dale P. Winebrenner, and David G. Vaughan. Antarctic snow accumulation mapped using polarization of 4.3-cm wavelength microwave emission. J. Geophys. Res.-Atmos., 111(D6), 2006.

[7] Willem a. H. Asman, Mark A. Sutton, and Jan K. Schjørring. Ammonia: emission, atmospheric transport and deposition. New Phytologist, 139(1):27–48, May 1998.

[8] J. O. Bash, E. J. Cooter, R. L. Dennis, J. T. Walker, and J. E. Pleim. Evaluation of a regional air-quality model with bidirectional NH3 exchange coupled to an agroecosystem model. Biogeosciences, 10(3):1635–1645, March 2013.

[9] S. J.-B. Bauguitte, W. J. Bloss, M. J. Evans, R. A. Salmon, P. S. Anderson, A. E. Jones, J. D. Lee, A. Saiz-Lopez, H. K. Roscoe, E. W. Wolff, and J. M. C. Plane. Summertime nox measurements during the chablis campaign: can source and sink estimates unravel observed diurnal cycles? Atmos. Chem. Phys., 12(2):989–1002, 2012.

[10] G. I. Baylor. Up, up and away. Proc. Roy. Soc., London A, 294:456–475, 1959.

[11] J. Beer, A. Blinov, G. Bonani, R. C. Finkel, H. J. Hofmann, B. Lehmann, H. Oeschger, A. Sigg, J. Schwander, T. Staffelbach, B. Stauffer, M. Suter, and W. Wötfli. Use of 10be in polar ice to trace the 11-year cycle of solar activity. Nature, 347(6289):164–166, September 1990.

[12] Michelle L. Bell, Francesca Dominici, Keita Ebisu, Scott L. Zeger, and Jonathan M. Samet. Spatial and Temporal Variation in PM2.5 Chemical Composition in the United States for Health Effects Studies. Environmental Health Perspectives, 115(7):989–995, 2007.

[13] Katherine B. Benedict, Xi Chen, Amy P. Sullivan, Yi Li, Derek Day, Anthony J. Prenni, E. J. T. Levin, Sonia M. Kreidenweis, William C. Malm, Bret A. Schichtel, and Jeffrey L. Collett. Atmospheric concentrations and deposition of reactive nitrogen in grand teton national park. J. Geophys. Res. Atmos., 118(20):11,875–11,887, 2013.

[14] Katherine B. Benedict, Derek Day, Florian M. Schwandner, Sonia M. Kreidenweis, Bret Schichtel, William C. Malm, and Jeffrey L. Collett Jr. Observations of atmospheric reactive nitrogen species in rocky mountain national park and across northern colorado. Atmos. Environ., 64:66–76, January 2013.

[15] N. Bertler, P.A. Mayewski, A. Aristarain, P. Barrett, S. Becagli, R. Bernardo, S. Bo, C. Xiao, M. Curran, D. Qin, D. Dixon, F. Ferron, H. Fischer, M. Frey, M. Frezzotti, F. Fundel, C. Genthon, R. Gragnani, G. Hamilton, M. Handley, S. Hong, E. Isaksson, J. Kang, J. Ren, K. Kamiyama, S. Kanamori, E. Kärkäs, L. Karlöf, S. Kaspari, K. Kreutz, A. Kurbatov, E. Meyerson, Y. Ming, M. Zhang, H. Motoyama, R. Mulvaney, H. Oerter, E. Osterberg, M. Proposito, A. Pyne, U. Ruth, J. Simões, B. Smith, S. Sneed, K. Teinilä, F. Traufetter, R. Udisti, A. Virkkula, O. Watanabe, B. Williamson, J-G. Winther, Y. Li, E. Wolff, Z. Li, and A. Zielinski. Snow chemistry across antarctica. Ann. Glaciol., 41(1):167–179, 2005.

[16] Isabelle Bey, Daniel J. Jacob, Robert M. Yantosca, Jennifer A. Logan, Brendan D. Field, Arlene M. Fiore, Qinbin Li, Honguy Y. Liu, Loretta J. Mickley, and Martin G. Schultz. Global modeling of tropospheric chemistry with assimilated meteorology: Model description and evaluation. J. Geophys. Res.-Atmos., 106(D19):PP. 23,073–23,095, 2001.

[17] Francis S. Binkowski and Shawn J. Roselle. Models-3 community multiscale air quality (cmaq) model aerosol component 1. model description. J. Geophys. Res.-Atmos., 108(D6):4183, 2003.

[18] R. Bobbink, K. Hicks, J. Galloway, T. Spranger, R. Alkemade, M. Ashmore, M. Bustamante, S. Cinderby, E. Davidson, F. Dentener, B. Emmett, J-W. Erisman, M. Fenn, F. Gilliam, A. Nordin, L. Pardo, and W. De Vries. Global assessment of nitrogen deposition effects on terrestrial plant diversity: a synthesis. Ecol. Appl., 20(1):30–59, January 2010.

[19] Tami C. Bond, Ekta Bhardwaj, Rong Dong, Rahil Jogani, Soonkyu Jung, Christoph Roden, David G. Streets, and Nina M. Trautmann. Historical emissions of black and organic carbon aerosol from energy-related combustion, 1850–2000. Global Biogeochem. Cy., 21(2):GB2018, June 2007.

[20] A. F. Bouwman, D. S. Lee, W. a. H. Asman, F. J. Dentener, K. W. Van Der Hoek, and J. G. J. Olivier. A global high-resolution emission inventory for ammonia. Global Biogeochem. Cy., 11(4):561–587, 1997.

[21] William D. Bowman, John Murgel, Tamara Blett, and Ellen Porter. Nitrogen critical loads for alpine vegetation and soils in rocky mountain national park. J. Environ. Manage., 103:165–171, July 2012.

[22] Timothy P. Boyer, S. Levitus, J. I. Antonov, R. A. Locarnini, and H. E. Garcia. Linear trends in salinity for the world ocean, 1955–1998. Geophys. Res. Lett., 32:4 PP., 2005.

[23] R. T. Burnett, J. Brook, T. Dann, C. Delocla, O. Philips, S. Cakmak, R. Vincent, M. S. Goldberg, and D. Krewski. Association Between Particulate- and Gas-Phase Components of Urban Air Pollution and Daily Mortality in Eight Canadian Cities. Inhal Toxicol, 12(sup4):15–39, January 2000.

[24] Douglas A Burns, Tamara Blett, Richard Haeuber, and Linda H Pardo. Critical loads as a policy tool for protecting ecosystems from the effects of air pollutants. Front. Ecol. Environ., 6(3):156–159, April 2008.

[25] CAAA. Clean air act amendments §162(a)(4), 1977.

[26] Jun-Ji Cao, Zhen-Xing Shen, Judith C. Chow, John G. Watson, Shun-Cheng Lee, Xue-Xi Tie, Kin-Fai Ho, Ge-Hui Wang, and Yong-Ming Han. Winter and Summer PM2.5 Chemical Compositions in Fourteen Chinese Cities. J. Air. Pollut. Control Assoc., 62(10):1214–1226, October 2012.

[27] S. L. Capps, D. K. Henze, A. Hakami, A. G. Russell, and A. Nenes. Anisorropia: the adjoint of the aerosol thermodynamic model isorropia. Atmos. Chem. Phys., 12(1):527–543, 2012.

[28] K. S. Carslaw, B. P. Luo, S. L. Clegg, Th. Peter, P. Brimblecombe, and P. J. Crutzen. Stratospheric aerosol growth and HNO3 gas phase depletion from coupled HNO3 and water uptake by liquid particles. Geophys. Res. Lett., 21(23):2479–2482, 1994.

[29] Kenneth S. Carslaw, Beiping Luo, and Thomas Peter. An analytic expression for the composition of aqueous HNO3-H2SO4 stratospheric aerosols including gas phase removal of HNO3. Geophys. Res. Lett., 22(14):1877–1880, 1995.

[30] CASTNET. U.s. environmental protection agency clean air markets division clean air status and trends network (castnet) data table accessed (nh4, no3, hno3 weekly dry deposition) available at www.epa.gov/castnet date accessed: 09 november, 2014.

[31] Center for History and New Media. Zotero quick start guide. http://zotero.org/support/quick_start_guide.

[32] T. Chai, H.-C. Kim, P. Lee, D. Tong, L. Pan, Y. Tang, J. Huang, J. McQueen, M. Tsidulko, and I. Stajner. Evaluation of the United States National Air Quality Forecast Capability experimental real-time predictions in 2010 using Air Quality System ozone and NO2 measurements. Geosci. Model Dev., 6(5):1831–1850, October 2013.

[33] Tianfeng Chai, Gregory R. Carmichael, Youhua Tang, Adrian Sandu, Michael Hardesty, Peter Pilewskie, Sallie Whitlow, Edward V. Browell, Melody A. Avery, Philippe Nédélec, John T. Merrill, Anne M. Thompson, and Eric Williams. Four-dimensional data assimilation experiments with International Consortium for Atmospheric Research on Transport and Transformation ozone measurements. J. Geophys. Res.-Atmos., 112(D12):D12S15, June 2007.

[34] G. Chavent. Identification of functional parameters in partial differential equations. In Joint Automatic Control Conference, volume 12, pages 155–156, 1974.

[35] D. Chen, Y. Wang, M. B. McElroy, K. He, R. M. Yantosca, and P. Le Sager. Regional CO pollution and export in China simulated by the high-resolution nested-grid GEOS-Chem model. Atmos. Chem. Phys., 9(11):3825–3839, June 2009.

[36] Mian Chin, Paul Ginoux, Stefan Kinne, Omar Torres, Brent N. Holben, Bryan N. Duncan, Randall V. Martin, Jennifer A. Logan, Akiko Higurashi, and Teruyuki Nakajima. Tropospheric aerosol optical thickness from the GOCART model and comparisons with satellite and sun photometer measurements. J. Atmos. Sci., 59(3):461–483, February 2002.

[37] Jae C. Choi, Meehye Lee, Youngsin Chun, Jiyoung Kim, and Sungnam Oh. Chemical composition and source signature of spring aerosol in Seoul, Korea. J. Geophys. Res.-Atmos., 106(D16):18067–18074, August 2001.

[38] Na Rae Choi, Se Pyo Lee, Ji Yi Lee, Chang Hoon Jung, and Yong Pyo Kim. Speciation and source identification of organic compounds in PM10 over Seoul, South Korea. Chemosphere, 144:1589–1596, February 2016.

[39] Christopher M. Clark, Philip E. Morefield, Frank S. Gilliam, and Linda H. Pardo. Estimated losses of plant biodiversity in the United States from historical N deposition (1985–2010). Ecology, 94(7):1441–1448, July 2013.

[40] David W. Clow, Heidi A. Roop, Leora Nanus, Mark E. Fenn, and Graham A. Sexstone. Spatial patterns of atmospheric deposition of nitrogen and sulfur using ion-exchange resin collectors in Rocky Mountain National Park, USA. Atmos. Environ., 101:149–157, January 2015.

[41] D. B. Considine, A. R. Douglass, P. S. Connell, D. E. Kinnison, and D. A. Rotman. A polar stratospheric cloud parameterization for the global modeling initiative three-dimensional model and its response to stratospheric aircraft. J. Geophys. Res.-Atmos., 105(D3):PP. 3955–3973, February 2000.

[42] Ellen J. Cooter, Jesse O. Bash, John T. Walker, M. R. Jones, and Wayne Robarge. Estimation of NH3 bi-directional flux from managed agricultural soils. Atmos. Environ., 44(17):2107–2115, June 2010.

[43] Sarah E. Cornell. Atmospheric nitrogen deposition: Revisiting the question of the importance of the organic component. Environ. Pollut., 159(10):2214–2222, October 2011.

[44] M. E. Crow. Aerodynamic sound emission as a singular perturbation problem. Stud. Appl. Math., 29:21–44, 1968.

[45] Nguyen Ba Cuong, Bernard Bonsang, and Gérard Lambert. The atmospheric concentration of sulfure dioxide and sulfate aerosols over antarctic, subantarctic areas and oceans. Tellus, 26(12):241–249, February 1974.

[46] Douglas D. Davis, Jon Seelig, Greg Huey, Jim Crawford, Gao Chen, Yuhang Wang, Marty Buhr, Detlev Helmig, William Neff, Don Blake, Rich Arimoto, and Fred Eisele. A reassessment of antarctic plateau reactive nitrogen based on antci 2003 airborne and ground based measurements. Atmos. Environ., 42(12):2831–2848, April 2008.

[47] Robert Delmas, Martine Briat, and Michel Legrand. Chemistry of south polar snow. J. Geophys. Res.-Atmos., 87(C6):PP. 4314–4318, 1982.

[48] Julian D. Dole. Perturbation Methods in Applied Mathematics. Winsdell Publishing Company, 1967.

[49] G.A.M. Dreschhoff, E.J. Zeller, D. Qin, and B.C. Parker. Major solar flares and long-term variability in antarctic ice cores. Adv. Space. Res., 13(9):443–446, September 1993.

[50] Enzai Du, Wim de Vries, James N. Galloway, Xueyang Hu, and Jingyun Fang. Changes in wet nitrogen deposition in the United States between 1985 and 2012. Environ. Res. Lett., 9(9):095004, September 2014.

[51] R. A. Duce, J. LaRoche, K. Altieri, K. R. Arrigo, A. R. Baker, D. G. Capone, S. Cornell, F. Dentener, J. Galloway, R. S. Ganeshram, R. J. Geider, T. Jickells, M. M. Kuypers, R. Langlois, P. S. Liss, S. M. Liu, J. J. Middelburg, C. M. Moore, S. Nickovic, A. Oschlies, T. Pedersen, J. Prospero, R. Schlitzer, S. Seitzinger, L. L. Sorensen, M. Uematsu, O. Ulloa, M. Voss, B. Ward, and L. Zamora. Impacts of Atmospheric Anthropogenic Nitrogen on the Open Ocean. Science, 320(5878):893–897, May 2008.

[52] Bryan N. Duncan, Randall V. Martin, Amanda C. Staudt, Rosemarie Yevich, and Jennifer A. Logan. Interannual and seasonal variability of biomass burning emissions constrained by satellite observations. J. Geophys. Res.-Atmos., 108(4100), January 2003.

[53] Hendrik Eibern and Hauke Schmidt. A four-dimensional variational chemistry data assimilation scheme for Eulerian chemistry transport modeling. J. Geophys. Res.-Atmos., 104(D15):18583–18598, August 1999.

[54] R. A. Ellis, D. J. Jacob, M. P. Sulprizio, L. Zhang, C. D. Holmes, B. A. Schichtel, T. Blett, E. Porter, L. H. Pardo, and J. A. Lynch. Present and future nitrogen deposition to national parks in the united states: critical load exceedances. Atmos. Chem. Phys., 13(17):9083–9095, September 2013.

[55] Ronald M. Errico. What Is an Adjoint Model? B. Am. Meteorol. Soc., 78(11):2577–2591, November 1997.

[56] D. M. Etheridge, L. P. Steele, R. L. Langenfelds, R. J. Francey, J.-M. Barnola, and V. I. Morgan. Natural and anthropogenic changes in atmospheric CO2 over the last 1000 years from air in antarctic ice and firn. J. Geophys. Res.-Atmos., 101(D2):PP. 4115–4128, 1996.

[57] J. S. Fabnis, H. J. Giblet, and H. McDormand. Navier-stokes analysis of solid rocket motor internal flow. J. Prop. and Power, 2:157–164, 1980.

[58] D. W. Fahey, K. K. Kelly, S. R. Kawa, A. F. Tuck, M. Loewenstein, K. R. Chan, and L. E. Heidt. Observations of denitrification and dehydration in the winter polar stratospheres. Nature, 344(6264):321–324, March 1990.

[59] T. Duncan Fairlie, Daniel J. Jacob, and Rokjin J. Park. The impact of transpacific transport of mineral dust in the united states. Atmos. Environ., 41(6):1251–1266, February 2007.

[60] M. E. Fenn, E. B. Allen, S. B. Weiss, S. Jovan, L. H. Geiser, G. S. Tonnesen, R. F. Johnson, L. E. Rao, B. S. Gimeno, F. Yuan, T. Meixner, and A. Bytnerowicz. Nitrogen critical loads and management alternatives for N-impacted ecosystems in California. J. Environ. Manage., 91(12):2404–2423, December 2010.

[61] Mark E. Fenn, Jill S. Baron, Edith B. Allen, Heather M. Rueth, Koren R. Nydick, Linda Geiser, William D. Bowman, James O. Sickman, Thomas Meixner, Dale W. Johnson, and Peter Neitlich. Ecological effects of nitrogen deposition in the western united states. BioScience, 53(4):404–420, April 2003.

[62] Hubertus Fischer, Dietmar Wagenbach, and Joseph Kipfstuhl. Sulfate and nitrate firn concentrations on the greenland ice sheet 1. large-scale geographical deposition changes. J. Geophys. Res.-Atmos., 103(D17):934, 1998.

[63] C. Fountoukis and A. Nenes. ISORROPIA II: a computationally efficient thermodynamic equilibrium model for K+–Ca2+–Mg2+–NH4+–Na+–SO42–NO3–Cl–H2O aerosols. Atmos. Chem. Phys., 7(17):4639–4659, 2007.

[64] Meredith Franklin, Ariana Zeka, and Joel Schwartz. Association between PM2.5 and all-cause and specific-cause mortality in 27 US communities. J Expo Sci Env Epid, 17(3):279–287, September 2006.

[65] James N. Galloway, John D. Aber, Jan Willem Erisman, Sybil P. Seitzinger, Robert W. Howarth, Ellis B. Cowling, and B. Jack Cosby. The nitrogen cascade. BioScience, 53(4):341–356, April 2003.

[66] S. Gassó, A. Stein, F. Marino, E. Castellano, R. Udisti, and J. Ceratto. A combined observational and modeling approach to study modern dust transport from the patagonia desert to east antarctica. Atmos. Chem. Phys., 10(17):8287–8303, 2010.

[67] Kristi A. Gebhart, Bret A. Schichtel, William C. Malm, Michael G. Barna, Marco A. Rodriguez, and Jeffrey L. Collett Jr. Back-trajectory-based source apportionment of airborne sulfur and nitrogen concentrations at rocky mountain national park, colorado, USA. Atmos. Environ., 45(3):621–633, January 2011.

[68] Young Sung Ghim, Young-Soo Chang, and Kweon Jung. Temporal and spatial variations in fine and coarse particles in seoul, korea. Aerosol Air Qual Res, 2015(3):842–852, 2015.

[69] Alice B. Gilliland, Robin L. Dennis, Shawn J. Roselle, and Thomas E. Pierce. Seasonal NH3 emission estimates for the eastern United States based on ammonium wet concentrations and an inverse modeling method. J. Geophys. Res., 108(D15):4477, August 2003.

[70] Alice B. Gilliland, K. Wyat Appel, Robert W. Pinder, and Robin L. Dennis. Seasonal NH3 emissions for the continental united states: Inverse model estimation and evaluation. Atmos. Environ., 40(26):4986–4998, August 2006.

[71] Tianyi Gou and Adrian Sandu. Continuous versus discrete advection adjoints in chemical data assimilation with CMAQ. Atmos. Environ., 45(28):4868–4881, September 2011.

[72] Georg A. Grell, Steven E. Peckham, Rainer Schmitz, Stuart A. McKeen, Gregory Frost, William C. Skamarock, and Brian Eder. Fully coupled "online" chemistry within the WRF model. Atmos. Environ., 39(37):6957–6975, December 2005.

[73] Nicolas Gruber and James N. Galloway. An Earth-system perspective of the global nitrogen cycle. Nature, 451(7176):293–296, January 2008.

[74] A. Guenther, T. Karl, P. Harley, C. Wiedinmyer, P. I. Palmer, and C. Geron. Estimates of global terrestrial isoprene emissions using megan (model of emissions of gases and aerosols from nature). Atmos. Chem. Phys., 6(11):3181–3210, 2006.

[75] F. Guillot and Z. Javalon. Acoustic boundary layers in propellant rocket motors. J. Prop. and Power, 5:331–339, 1989.

[76] A. Hakami, D. K. Henze, J. H. Seinfeld, T. Chai, Y. Tang, G. R. Carmichael, and A. Sandu. Adjoint inverse modeling of black carbon during the asian pacific regional aerosol characterization experiment. J. Geophys. Res.-Atmos., 110:17 PP., July 2005.

[77] E. Hall, A. Eyth, S. Phillips, and R. Mason. Hierarchical bayesian model (hbm) - derived estimates of air quality for 2008: Annual report. Technical Report EPA/600/R-12/048 (NTIS PB2012-113297), U.S. Environmental Protection Agency, Washington, DC, 2012.

[78] Lijian Han, Weiqi Zhou, and Weifeng Li. City as a major source area of fine particulate (PM2.5) in China. Environ Pollut, 206:183–187, November 2015.

[79] C. L. Heald, J. L. Collett Jr., T. Lee, K. B. Benedict, F. M. Schwandner, Y. Li, L. Clarisse, D. R. Hurtmans, M. Van Damme, C. Clerbaux, P.-F. Coheur, S. Philip, R. V. Martin, and H. O. T. Pye. Atmospheric ammonia and particulate inorganic nitrogen over the United States. Atmos. Chem. Phys., 12(21):10295–10312, November 2012.

[80] D. K. Henze, A. Hakami, and J. H. Seinfeld. Development of the adjoint of GEOS-Chem. Atmos. Chem. Phys., 7(9):2413–2433, May 2007.

[81] D. K. Henze, J. H. Seinfeld, and D. T. Shindell. Inverse modeling and mapping us air quality influences of inorganic pm2.5precursor emissions using the adjoint of geos-chem. Atmos. Chem. Phys., 9:5877–5903, August 2009.

[82] J.-B. Heo, P. K. Hopke, and S.-M. Yi. Source apportionment of PM2.5 in Seoul, Korea. Atmos. Chem. Phys., 9(14):4957–4971, July 2009.

[83] Bruce B. Hicks. Dry deposition to forests—On the use of data from clearings. Agr Forest Meteorol, 136(3–4):214–221, February 2006.

[84] Min Sun Hong and Gregory R. Carmichael. An investigation of sulfate production in clouds using a flow-through chemical reactor model approach. J. Geophys. Res.-Atmos., 88(C15):PP. 10,733–10,743, 1983.

[85] Min Huang, Kevin W. Bowman, Gregory R. Carmichael, Meemong Lee, Tianfeng Chai, Scott N. Spak, Daven K. Henze, Anton S. Darmenov, and Arlindo M. da Silva. Improved western U.S. background ozone estimates via constraining nonlocal and local source contributions using Aura TES and OMI observations. J. Geophys. Res.-Atmos., 120(8):2014JD022993, April 2015.

[86] R. C. Hudman, D. J. Jacob, S. Turquety, E. M. Leibensperger, L. T. Murray, S. Wu, A. B. Gilliland, M. Avery, T. H. Bertram, W. Brune, R. C. Cohen, J. E. Dibb, F. M. Flocke,

A. Fried, J. Holloway, J. A. Neuman, R. Orville, A. Perring, X. Ren, G. W. Sachse, H. B. Singh, A. Swanson, and P. J. Wooldridge. Surface and lightning sources of nitrogen oxides over the united states: Magnitudes, chemical evolution, and outflow. J. Geophys. Res. Atmos., 112(D12), 2007.

[87] R. C. Hudman, D. J. Jacob, S. Turquety, E. M. Leibensperger, L. T. Murray, S. Wu, A. B. Gilliland, M. Avery, T. H. Bertram, W. Brune, R. C. Cohen, J. E. Dibb, F. M. Flocke, A. Fried, J. Holloway, J. A. Neuman, R. Orville, A. Perring, X. Ren, G. W. Sachse, H. B. Singh, A. Swanson, and P. J. Wooldridge. Surface and lightning sources of nitrogen oxides over the United States: Magnitudes, chemical evolution, and outflow. J. Geophys. Res.-Atmos., 112(D12):D12S05, June 2007.

[88] Bruce A. Hungate, Jeffrey S. Dukes, M. Rebecca Shaw, Yiqi Luo, and Christopher B. Field. Nitrogen and Climate Change. Science, 302(5650):1512–1513, November 2003.

[89] IBM. SPSS Statistics. download from vendor site, 2012. version 21.

[90] H.-W Jacobi, R Weller, A.E Jones, P.S Anderson, and O Schrems. Peroxyacetyl nitrate (PAN) concentrations in the antarctic troposphere measured during the photochemical experiment at neumayer (PEAN'99). Atmos. Environ., 34(29–30):5235–5247, 2000.

[91] Stanley S. Jacobs. Bottom water production and its links with the thermohaline circulation. Antarct. Sci., 16(04):427–437, 2004.

[92] Mark Z. Jacobson. Computation of global photochemistry with SMVGEAR II. Atmos. Environ., 29(18):2541–2546, September 1995.

[93] Jaein I. Jeong, Rokjin J. Park, Jung-Hun Woo, Young-Ji Han, and Seung-Muk Yi. Source contributions to carbonaceous aerosol concentrations in Korea. Atmos. Environ., 45(5):1116–1125, February 2011.

[94] Zhe Jiang, Dylan B. A. Jones, Monika Kopacz, Jane Liu, Daven K. Henze, and Colette Heald. Quantifying the impact of model errors on top-down estimates of carbon monoxide emissions using satellite observations. J. Geophys. Res.-Atmos., 116(D15):D15306, August 2011.

[95] A. E. Jones, R. Weller, E. W. Wolff, and H. W. Jacobi. Speciation and rate of photochemical NO and NO2 production in antarctic snow. Geophys. Res. Lett., 27(3):PP. 345–348, 2000.

[96] A. E. Jones, E. W. Wolff, D. Ames, S. J.-B. Bauguitte, K. C. Clemitshaw, Z. Fleming, G. P. Mills, A. Saiz-Lopez, R. A. Salmon, W. T. Sturges, and D. R. Worton. The multi-seasonal NOy budget in coastal antarctica and its link with surface snow and ice core nitrate: results from the CHABLIS campaign. Atmos. Chem. Phys., 11(17):9271–9285, 2011.

[97] A. E. Jones, E. W. Wolff, R. A. Salmon, S. J.-B. Bauguitte, H. K. Roscoe, P. S. Anderson, D. Ames, K. C. Clemitshaw, Z. L. Fleming, W. J. Bloss, D. E. Heard, J. D. Lee, K. A. Read, P. Hamer, D. E. Shallcross, A. V. Jackson, S. L. Walker, A. C. Lewis, G. P. Mills, J. M. C. Plane, A. Saiz-Lopez, W. T. Sturges, and D. R. Worton. Chemistry of the antarctic boundary layer and the interface with snow: an overview of the CHABLIS campaign. Atmos. Chem. Phys., 8(14):3789–3803, July 2008.

[98] Bruno Jourdain and Michel Legrand. Year-round records of bulk and size-segregated aerosol composition and HCl and HNO3 levels in the dumont d'Urville (coastal antarctica) atmosphere: Implications for sea-salt aerosol fractionation in the winter and summer. J. Geophys. Res.-Atmos., 107(D22):ACH 20–1–ACH 20–13, 2002.

[99] Choong-Min Kang, Hak Sung Lee, Byung-Wook Kang, Sang-Kwun Lee, and Young Sunwoo. Chemical characteristics of acidic gas pollutants and PM2.5 species during hazy episodes in Seoul, South Korea. Atmos. Environ., 38(28):4749–4760, September 2004.

[100] A. J. Kean, D. Littlejohn, G. A. Ban-Weiss, R. A. Harley, T. W. Kirchstetter, and M. M. Lunden. Trends in on-road vehicle emissions of ammonia. Atmos. Environ., 43(8):1565–1570, March 2009.

[101] S. K. Kharol, R. V. Martin, S. Philip, S. Vogel, D. K. Henze, D. Chen, Y. Wang, Q. Zhang, and C. L. Heald. Persistent sensitivity of Asian aerosol to emissions of nitrogen oxides. Geophys. Res. Lett., 40(5):1021–1026, March 2013.

[102] Hyun-Sun Kim, Jong-Bae Huh, Philip K. Hopke, Thomas M. Holsen, and Seung-Muk Yi. Characteristics of the major chemical constituents of PM2.5 and smog events in Seoul, Korea in 2003 and 2004. Atmos. Environ., 41(32):6762–6770, October 2007.

[103] Yong Pyo Kim, Kil-Choo Moon, Jong Hoon Lee, and Nam Jun Baik. Concentrations of carbonaceous species in particles at Seoul and Cheju in Korea. Atmos. Environ., 33(17):2751–2758, August 1999.

[104] M. Kopacz, D. J. Jacob, J. A. Fisher, J. A. Logan, L. Zhang, I. A. Megretskaia, R. M. Yantosca, K. Singh, D. K. Henze, J. P. Burrows, M. Buchwitz, I. Khlystova, W. W. McMillan, J. C. Gille, D. P. Edwards, A. Eldering, V. Thouret, and P. Nedelec. Global estimates of CO sources with high resolution by adjoint inversion of multiple satellite datasets (MOPITT, AIRS, SCIAMACHY, TES). Atmos. Chem. Phys., 10(3):855–876, February 2010.

[105] M. Kopacz, D. L. Mauzerall, J. Wang, E. M. Leibensperger, D. K. Henze, and K. Singh. Origin and radiative forcing of black carbon transported to the himalayas and tibetan plateau. Atmos. Chem. Phys., 11(6):2837–2852, March 2011.

[106] Monika Kopacz, Daniel J. Jacob, Daven K. Henze, Colette L. Heald, David G. Streets, and Qiang Zhang. Comparison of adjoint and analytical bayesian inversion methods for constraining asian sources of carbon monoxide using satellite (MOPITT) measurements of CO columns. J. Geophys. Res., 114(D4):D04305, February 2009.

[107] KOSIS. Korean statistical information service. 2010.

[108] G. Krinner and C. Genthon. Tropospheric transport of continental tracers towards antarctica under varying climatic conditions. Tellus B, 55(1):54–70, 2003.

[109] Laura Krnavek, William R. Simpson, Daniel Carlson, Florent Domine, Thomas A. Douglas, and Matthew Sturm. The chemical composition of surface snow in the arctic: Examining marine, terrestrial, and atmospheric influences. Atmos. Environ., 50(0):349–359, April 2012.

[110] N. A. Krotkov, C. A. McLinden, C. Li, L. N. Lamsal, E. A. Celarier, S. V. Marchenko, W. H. Swartz, E. J. Bucsela, J. Joiner, B. N. Duncan, K. F. Boersma, J. P. Veefkind, P. F. Levelt,

V. E. Fioletov, R. R. Dickerson, H. He, Z. Lu, and D. G. Streets. Aura OMI observations of regional SO2 and NO2 pollution changes from 2005 to 2015. Atmos. Chem. Phys., 16(7):4605–4629, April 2016.

[111] C. M. Laluraj, M. Thamban, S. S. Naik, B. L. Redkar, A. Chaturvedi, and R. Ravindra. Nitrate records of a shallow ice core from east antarctica: Atmospheric processes, preservation and climatic implications. The Holocene, 21(2):351–356, March 2011.

[112] J.-F. Lamarque, J. T. Kiehl, G. P. Brasseur, T. Butler, P. Cameron-Smith, W. D. Collins, W. J. Collins, C. Granier, D. Hauglustaine, P. G. Hess, E. A. Holland, L. Horowitz, M. G. Lawrence, D. McKenna, P. Merilees, M. J. Prather, P. J. Rasch, D. Rotman, D. Shindell, and P. Thornton. Assessing future nitrogen deposition and carbon cycle feedback using a multimodel approach: Analysis of nitrogen deposition. J. Geophys. Res., 110(D19):D19303, October 2005.

[113] Henry Lao. Linear Acoustic Processes in Rocket Engines. PhD thesis, University of Colorado at Boulder, 1979.

[114] Q. Lao, M. N. Cassoy, and K. Kirkpatrick. Acoustically generated vorticity from internal flow. J. Fluid Mechanics, 2:122–133, 1996.

[115] Q. Lao, D. R. Kassoy, and K. Kirkkopru. Nonlinear acoustic processes in rocket engines. J. Fluid Mechanics, 3:245–261, 1997.

[116] Kateryna Lapina, Daven K. Henze, Jana B. Milford, Min Huang, Meiyun Lin, Arlene M. Fiore, Greg Carmichael, Gabriele G. Pfister, and Kevin Bowman. Assessment of source contributions to seasonal vegetative exposure to ozone in the u.s. J. Geophys. Res. Atmos., 119(1):324–340, 2014.

[117] Natalie E. Latysh and Gregory Alan Wetherbee. Improved mapping of national atmospheric deposition program wet-deposition in complex terrain using PRISM-gridded data sets. Environ. Monit. Assess., 184(2):913–928, January 2012.

[118] Colin J. Lee, Randall V. Martin, Daven K. Henze, Michael Brauer, Aaron Cohen, and Aaron van Donkelaar. Response of Global Particulate-Matter-Related Mortality to Changes in Local Precursor Emissions. Environ. Sci. Technol., 49(7):4335–4344, April 2015.

[119] H.-M. Lee, F. Paulot, D. K. Henze, K. Travis, D. J. Jacob, L. H. Pardo, and B. A. Schichtel. Sources of nitrogen deposition in Federal Class I areas in the US. Atmos. Chem. Phys., 16(2):525–540, January 2016.

[120] Hak Sung Lee, Choong-Min Kang, Byung-Wook Kang, and Hui-Kang Kim. Seasonal variations of acidic air pollutants in Seoul, South Korea. Atmos. Environ., 33(19):3143–3152, August 1999.

[121] Hyung-Min Lee, Daven K. Henze, Becky Alexander, and Lee T. Murray. Investigating the sensitivity of surface-level nitrate seasonality in antarctica to primary sources using a global model. Atmos. Environ., 89:757–767, June 2014.

[122] Miyeon Lee. An analysis on the concentration characteristics of PM2.5 in Seoul, Korea from 2005 to 2012. Asia-Pac J Atmos Sci, 50(1):585–594, October 2014.

[123] Sihye Lee, Young Sung Ghim, Sang-Woo Kim, and Soon-Chang Yoon. Seasonal characteristics of chemically apportioned aerosol optical properties at seoul and gosan, korea. Atmos. Environ., 43(6):1320–1328, February 2009.

[124] Michel Legrand and Paul Mayewski. Glaciochemistry of polar ice cores: A review. Rev. Geophys., 35(3):PP. 219–243, 1997.

[125] Michel R. Legrand and Séverine Kirchner. Origins and variations of nitrate in south polar precipitation. J. Geophys. Res.-Atmos., 95(D4):PP. 3493–3507, 1990.

[126] Michel R. Legrand, Frode Stordal, Ivar S. A. Isaksen, and Bjørg Rognerud. A model study of the stratospheric budget of odd nitrogen, including effects of solar cycle variations. Tellus B, 41(4), 1989.

[127] M.R. Legrand, C. Lorius, N.I. Barkov, and V.N. Petrov. Vostok (antarctica) ice core: Atmospheric chemistry changes over the last climatic cycle (160,000 years). Atmos. Environ., 22(2):317–331, 1988.

[128] Hongyu Liu, Daniel J. Jacob, Isabelle Bey, and Robert M. Yantosca. Constraints from 210Pb and 7Be on wet deposition and transport in a global three-dimensional chemical tracer model driven by assimilated meteorological fields. J. Geophys. Res. Atmos., 106(D11):12109–12128, 2001.

[129] Jane J. Liu, Dylan B. A. Jones, John R. Worden, David Noone, Mark Parrington, and Jay Kar. Analysis of the summertime buildup of tropospheric ozone abundances over the middle east and north africa as observed by the tropospheric emission spectrometer instrument. J. Geophys. Res.-Atmos., 114(D5), 2009.

[130] A. L. Lockwood, P. B. Shepson, M. N. Fiddler, and M. Alaghmand. Isoprene nitrates: preparation, separation, identification, yields, and atmospheric chemistry. Atmos. Chem. Phys., 10(13):6169–6178, July 2010.

[131] C. R. Lonsdale, J. D. Hegarty, K. Cady-Pereira, M. J. Alvarado, D. K. Henze, M. D. Turner, S. L. Capps, J. B. Nowak, J. A. Neuman, A. M. Middlebrook, R. Bahreini, J. G. Murphy, M. Markovic, T. C. VandenBoer, L. M. Russell, and A. J. Scarino. Modeling the Diurnal Variability of Agricultural Ammonia in Bakersfield, California during CalNex. Atmos. Chem. Phys. Discuss., pages 1–30, March 2016.

[132] William C. Malm, Bret A. Schichtel, Michael G. Barna, Kristi A. Gebhart, Marco A. Rodriguez, Jeffrey L. Collett Jr, Christian M. Carrico, Katherine B. Benedict, Anthony J. Prenni, and Sonia M. Kreidenweis. Aerosol species concentrations and source apportionment of ammonia at Rocky Mountain National Park. J. Air Waste Manage., 63(11):1245–1263, November 2013.

[133] William C. Malm, Bret A. Schichtel, Marc L. Pitchford, Lowell L. Ashbaugh, and Robert A. Eldred. Spatial and monthly trends in speciated fine particle concentration in the united states. J. Geophys. Res. Atmos., 109(D3):n/a–n/a, 2004.

[134] Stanley E. Manahan. Environmental chemistry. CRC Press, 2005.

[135] Y. H. Mao, Q. B. Li, D. K. Henze, Z. Jiang, D. B. A. Jones, M. Kopacz, C. He, L. Qi, M. Gao, W.-M. Hao, and K.-N. Liou. Estimates of black carbon emissions in the western United States using the GEOS-Chem adjoint model. Atmos. Chem. Phys., 15(13):7685–7702, July 2015.

[136] Céline Mari, Daniel J. Jacob, and Peter Bechtold. Transport and scavenging of soluble gases in a deep convective cloud. J. Geophys. Res.-Atmos., 105(D17):PP. 22,255–22,267, 2000.

[137] Milos Z. Markovic, Trevor C. VandenBoer, and Jennifer G. Murphy. Characterization and optimization of an online system for the simultaneous measurement of atmospheric water-soluble constituents in the gas and particle phases. Journal of Environmental Monitoring, 14(7):1872, 2012.

[138] Randall V. Martin, Daniel J. Jacob, Jennifer A. Logan, Isabelle Bey, Robert M. Yantosca, Amanda C. Staudt, Qinbin Li, Arlene M. Fiore, Bryan N. Duncan, Hongyu Liu, Paul Ginoux, and Valerie Thouret. Interpretation of toms observations of tropical tropospheric ozone with a global model and in situ observations. J. Geophys. Res.-Atmos., 107(D18):ACH 4–1–ACH 4–27, 2002.

[139] P. A. Mayewski, W. B. Lyons, M. J. Spencer, M. Twickler, W. Dansgaard, B. Koci, C. I. Davidson, and R. E. Honrath. Sulfate and nitrate concentrations from a south greenland ice core. Science, 232(4753):975–977, May 1986. PMID: 17759282.

[140] P. A. Mayewski, M. P. Meredith, C. P. Summerhayes, J. Turner, A. Worby, P. J. Barrett, G. Casassa, N. A. N. Bertler, T. Bracegirdle, A. C. Naveira Garabato, D. Bromwich, H. Campbell, G. S. Hamilton, W. B. Lyons, K. A. Maasch, S. Aoki, C. Xiao, and Tas van Ommen. State of the antarctic and southern ocean climate system. Rev. Geophys., 47:38 PP., January 2009.

[141] Paul A. Mayewski and Michel R. Legrand. Recent increase in nitrate concentration of antarctic snow. Nature, 346(6281):258–260, July 1990.

[142] Justin R. McCabe, Mark H. Thiemens, and Joel Savarino. A record of ozone variability in south pole antarctic snow: Role of nitrate oxygen isotopes. J. Geophys. Res.-Atmos., 112(D12), 2007.

[143] Michael McDonald, Robert L. de Zafra, and Giovanni Muscari. Millimeter wave spectroscopic measurements over the south pole 5. morphology and evolution of HNO3 vertical distribution, 1993 versus 1995. J. Geophys. Res.-Atmos., 105(D14):17739–17,750, July 2000.

[144] Michael B. McElroy and Ross J. Salawitch. Changing composition of the global stratosphere. Science, 243(4892):763–770, February 1989.

[145] C. A. McLinden, S. C. Olsen, B. Hannegan, O. Wild, M. J. Prather, and J. Sundet. Stratospheric ozone in 3-d models: A simple chemistry and the cross-tropopause flux. J. Geophys. Res.-Atmos., 105(D11):14653–14665, June 2000.

[146] ME. 2nd seoul metropolitan air quality improvement plan (2015 -2024). Ministry of Environment, 2013.

[147] G. P. Mills, W. T. Sturges, R. A. Salmon, S. J.-B. Bauguitte, K. A. Read, and B. J. Bandy. Seasonal variation of peroxyacetylnitrate (PAN) in coastal antarctica measured with a new instrument for the detection of sub-part per trillion mixing ratios of PAN. Atmos. Chem. Phys., 7(17):4589–4599, 2007.

[148] Kwang-Joo Moon, Jin-Seok Han, and Yoo-Duck Hong. Physical, chemical and optical properties of fine aerosol as a function of relative humidity at gosan, korea during ABC-EAREX 2005. In Colin D. O'Dowd and Paul E. Wagner, editors, Nucleation and Atmospheric Aerosols, pages 999–1003. Springer Netherlands, Dordrecht, 2007.

[149] Kwang-Joo Moon, Seung-Myung Park, Jong-Sung Park, In-Ho Song, Sung-Ki Jang, Jong-Chun Kim, and Seok-Jo Lee. Chemical Characteristics and Source Apportionment ofPM $_{2.5}$ in Seoul Metropolitan Area in 2010. Journal of Korean Society for Atmospheric Environment, 27(6):711–722, December 2011.

[150] Richard H. Moss, Jae A. Edmonds, Kathy A. Hibbard, Martin R. Manning, Steven K. Rose, Detlef P. van Vuuren, Timothy R. Carter, Seita Emori, Mikiko Kainuma, Tom Kram, Gerald A. Meehl, John F. B. Mitchell, Nebojsa Nakicenovic, Keywan Riahi, Steven J. Smith, Ronald J. Stouffer, Allison M. Thomson, John P. Weyant, and Thomas J. Wilbanks. The next generation of scenarios for climate change research and assessment. Nature, 463(7282):747–756, February 2010.

[151] M. Mu, J. T. Randerson, G. R. van der Werf, L. Giglio, P. Kasibhatla, D. Morton, G. J. Collatz, R. S. DeFries, E. J. Hyer, E. M. Prins, D. W. T. Griffith, D. Wunch, G. C. Toon, V. Sherlock, and P. O. Wennberg. Daily and 3-hourly variability in global fire emissions and consequences for atmospheric model predictions of carbon monoxide. J. Geophys. Res., 116(D24):D24303, 2011.

[152] F. C. Mulick. Rotational axisymmetric mean flow and damping of acoustic waves in a solid propellant. AIAA J., 3:1062–1063, 1964.

[153] F. C. Mulick. Stability of four-dimensional motions in a combustion chamber. Comb. Sci. Tech., 19:99–124, 1981.

[154] J.-F. Müller and T. Stavrakou. Inversion of CO and NOx emissions using the adjoint of the IMAGES model. Atmos. Chem. Phys., 5(5):1157–1186, May 2005.

[155] M Murozumi, Tsaihwa J Chow, and C Patterson. Chemical concentrations of pollutant lead aerosols, terrestrial dusts and sea salts in greenland and antarctic snow strata. Geochimica et Cosmochimica Acta, 33(10):1247–1294, October 1969.

[156] Lee T. Murray, Daniel J. Jacob, Jennifer A. Logan, Rynda C. Hudman, and William J. Koshak. Optimized regional and interannual variability of lightning in a global chemical transport model constrained by LIS/OTD satellite data. J. Geophys. Res. Atmos., 117(D20):n/a–n/a, 2012.

[157] NADP. National atmospheric deposition program (nrsp-3). NADP Program Office, Illinois State Water Survey, 2204 Griffith Dr., Champaign, IL 61820., 2015.

[158] Jason C. Neff, Elisabeth A. Holland, Frank J. Dentener, William H. McDowell, and Kristina M. Russell. The origin, composition and rates of organic nitrogen deposition: A missing piece of the nitrogen cycle? Biogeochemistry, 57-58(1):99–136, April 2002.

[159] Eiko Nemitz, Celia Milford, and Mark A. Sutton. A two-layer canopy compensation point model for describing bi-directional biosphere-atmosphere exchange of ammonia. Q.J.R. Meteorol. Soc., 127(573):815–833, April 2001.

[160] Eiko Nemitz, Mark A Sutton, Jan K Schjoerring, Søren Husted, and G Paul Wyers. Resistance modelling of ammonia exchange over oilseed rape. Agr Forest Meteorol, 105(4):405–425, December 2000.

[161] E. D. Nilsson and Ü. Rannik. Turbulent aerosol fluxes over the arctic ocean: 1. dry deposition over sea and pack ice. J. Geophys. Res.-Atmos., 106(D23):32125–32137, 2001.

[162] J. Nilsson. Critical loads for sulphur and nitrogen. In P. Mathy, editor, Air Pollution and Ecosystems, pages 85–91. Springer Netherlands, January 1988.

[163] T. Ohara, H. Akimoto, J. Kurokawa, N. Horii, K. Yamaji, X. Yan, and T. Hayasaka. An Asian emission inventory of anthropogenic emission sources for the period 1980–2020. Atmos. Chem. Phys., 7(16):4419–4444, August 2007.

[164] Jos G. J. Olivier, John A. Van Aardenne, Frank J. Dentener, Valerio Pagliari, Laurens N. Ganzeveld, and Jeroen A. H. W. Peters. Recent trends in global greenhouse gas emissions:regional trends 1970–2000 and spatial distributionof key sources in 2000. Environm. Sci., 2(2-3):81–99, 2005.

[165] J. S. Olson. Digital raster data on a 10 minute geographic 1080 x 2160 grid in global ecosystems database, version 1.0, disc a. edited by NOAA Natl. Geophys. Data Center, Boulder, Colorado, 1992.

[166] L. H. Pardo, M. J. Robin-Abbott, and C. T. Driscoll. Assessment of Nitrogen deposition effects and empirical critical loads of Nitrogen for ecoregions of the United States. 2011.

[167] Linda H. Pardo, Mark E. Fenn, Christine L. Goodale, Linda H. Geiser, Charles T. Driscoll, Edith B. Allen, Jill S. Baron, Roland Bobbink, William D. Bowman, Christopher M. Clark, Bridget Emmett, Frank S. Gilliam, Tara L. Greaver, Sharon J. Hall, Erik A. Lilleskov, Lingli Liu, Jason A. Lynch, Knute J. Nadelhoffer, Steven S. Perakis, Molly J. Robin-Abbott, John L. Stoddard, Kathleen C. Weathers, and Robin L. Dennis. Effects of nitrogen deposition and empirical nitrogen critical loads for ecoregions of the united states. Ecol. Appl., 21(8):3049–3082, May 2011.

[168] R. J. Park, S. K. Hong, H.-A. Kwon, S. Kim, A. Guenther, J.-H. Woo, and C. P. Loughner. An evaluation of ozone dry deposition simulations in East Asia. Atmos. Chem. Phys., 14(15):7929–7940, August 2014.

[169] Rokjin J. Park, Daniel J. Jacob, Mian Chin, and Randall V. Martin. Sources of carbonaceous aerosols over the united states and implications for natural visibility. J. Geophys. Res.-Atmos., 108(D12), 2003.

[170] Rokjin J. Park, Daniel J. Jacob, Brendan D. Field, Robert M. Yantosca, and Mian Chin. Natural and transboundary pollution influences on sulfate-nitrate-ammonium aerosols in the united states: Implications for policy. J. Geophys. Res.-Atmos., 109(D15204), August 2004.

[171] Bruce C. Parker, Lawrence E. Heiskell, William J. Thompson, and Edward J. Zeller. Non-biogenic fixed nitrogen in antarctica and some ecological implications. Nature, 271(5646):651–652, February 1978.

[172] M. Parrington, P. I. Palmer, D. K. Henze, D. W. Tarasick, E. J. Hyer, R. C. Owen, D. Helmig, C. Clerbaux, K. W. Bowman, M. N. Deeter, E. M. Barratt, P.-F. Coheur, D. Hurtmans, Z. Jiang, M. George, and J. R. Worden. The influence of boreal biomass burning emissions on the distribution of tropospheric ozone over north america and the north atlantic during 2010. Atmos. Chem. Phys., 12(4):2077–2098, February 2012.

[173] F. Paulot, D. K. Henze, and P. O. Wennberg. Impact of the isoprene photochemical cascade on tropical ozone. Atmos. Chem. Phys., 12(3):1307–1325, February 2012.

[174] F. Paulot, D. J. Jacob, R. W. Pinder, J. O. Bash, K. Travis, and D. K. Henze. Ammonia emissions in the united states, european union, and china derived by high-resolution inversion of ammonium wet deposition data: Interpretation with a new agricultural emissions inventory (MASAGE_nh3). J. Geophys. Res. Atmos., 119(7):4343–4364, April 2014.

[175] Fabien Paulot, Daniel J. Jacob, and Daven K. Henze. Sources and processes contributing to nitrogen deposition: an adjoint model analysis applied to biodiversity hotspots worldwide. Environ. Sci. Technol., 47(7):3226–3233, April 2013.

[176] M. C. Pitts, L. W. Thomason, L. R. Poole, and D. M. Winker. Characterization of polar stratospheric clouds with spaceborne lidar: CALIPSO and the 2006 antarctic season. Atmos. Chem. Phys., 7(19):5207–5228, October 2007.

[177] Jonathan E. Pleim, Jesse O. Bash, John T. Walker, and Ellen J. Cooter. Development and evaluation of an ammonia bidirectional flux parameterization for air quality models. J. Geophys. Res. Atmos., 118(9):3794–3806, May 2013.

[178] A. J. Prenni, E. J. T. Levin, K. B. Benedict, A. P. Sullivan, M. I. Schurman, K. A. Gebhart, D. E. Day, C. M. Carrico, W. C. Malm, B. A. Schichtel, J. L. Collett Jr., and S. M. Kreidenweis. Gas-phase reactive nitrogen near grand teton national park: Impacts of transport, anthropogenic emissions, and biomass burning. Atmos. Environ., 89:749–756, June 2014.

[179] H. O. T. Pye, H. Liao, S. Wu, L. J. Mickley, D. J. Jacob, D. K. Henze, and J. H. Seinfeld. Effect of changes in climate and emissions on future sulfate-nitrate-ammonium aerosol levels in the United States. J. Geophys. Res.-Atmos., 114(D1):D01205, January 2009.

[180] Andrew M. Rankin and Eric W. Wolff. A year-long record of size-segregated aerosol composition at halley, antarctica. J. Geophys. Res.-Atmos., 108(D24), 2003.

[181] Dave S. Reay, Frank Dentener, Pete Smith, John Grace, and Richard A. Feely. Global nitrogen deposition and carbon sinks. Nature Geosci., 1(7):430–437, July 2008.

[182] R. S. Richards and A. M. Brown. Coupling between acoustic velocity oscillations and solid propellant combustion. J. Prop. and Power, 5:828–837, 1982.

[183] Catherine Ritz, Vincent Rommelaere, and Christophe Dumas. Modeling the evolution of antarctic ice sheet over the last 420,000 years: Implications for altitude changes in the vostok region. J. Geophys. Res.-Atmos., 106(D23):31943–31964, 2001.

[184] Marco A. Rodriguez, Michael G. Barna, Kristi A. Gebhart, Jennifer L. Hand, Zachariah E. Adelman, Bret A. Schichtel, Jeffrey L. Collett Jr., and William C. Malm. Modeling the fate of atmospheric reduced nitrogen during the rocky mountain atmospheric nitrogen and sulfur study (RoMANS): Performance evaluation and diagnosis using integrated processes rate analysis. Atmos. Environ., 45(1):223–234, January 2011.

[185] Regine Röthlisberger, Manuel A. Hutterli, Stefan Sommer, Eric W. Wolff, and Robert Mulvaney. Factors controlling nitrate in ice cores: Evidence from the dome c deep ice core. J. Geophys. Res.-Atmos., 105(D16):PP. 20,565–20,572, August 2000.

[186] Regine Röthlisberger, Manuel A. Hutterli, Eric W. Wolff, Robert Mulvaney, Hubertus Fischer, Matthias Bigler, Kumiko Goto-Azuma, Margareta E. Hansson, Urs Ruth, Marie-Louise Siggaard-Andersen, and Jørgen P. Steffensen. Nitrate in greenland and antarctic ice cores: a detailed description of post-depositional processes. Ann. Glaciol., 35(1):209–216, 2002.

[187] D. A. Rotman, J. R. Tannahill, D. E. Kinnison, P. S. Connell, D. Bergmann, D. Proctor, J. M. Rodriguez, S. J. Lin, R. B. Rood, M. J. Prather, P. J. Rasch, D. B. Considine, R. Ramaroson, and S. R. Kawa. Global modeling initiative assessment model: Model description, integration, and testing of the transport shell. J. Geophys. Res.-Atmos., 106(D2):PP. 1669–1691, January 2001.

[188] Morton J. Rubin. Seasonal variations of the antarctic tropopause. J. Meteor., 10(2):127–134, April 1953.

[189] Osvaldo E. Sala, F. Stuart Chapin, Iii, Juan J. Armesto, Eric Berlow, Janine Bloomfield, Rodolfo Dirzo, Elisabeth Huber-Sanwald, Laura F. Huenneke, Robert B. Jackson, Ann Kinzig, Rik Leemans, David M. Lodge, Harold A. Mooney, Martn Oesterheld, N. LeRoy Poff, Martin T. Sykes, Brian H. Walker, Marilyn Walker, and Diana H. Wall. Global biodiversity scenarios for the year 2100. Science, 287(5459):1770–1774, March 2000.

[190] R. Sander, Y. Rudich, R. von Glasow, and P. J. Crutzen. The role of BrNO3 in marine tropospheric chemistry: A model study. Geophys. Res. Lett., 26(18):2857–2860, 1999.

[191] B. Sauvage, R. V. Martin, A. van Donkelaar, X. Liu, K. Chance, L. Jaeglé, P. I. Palmer, S. Wu, and T.-M. Fu. Remote sensed and in situ constraints on processes affecting tropical tropospheric ozone. Atmos. Chem. Phys., 7(3):815–838, February 2007.

[192] J. Savarino, J. Kaiser, S. Morin, D. M. Sigman, and M. H. Thiemens. Nitrogen and oxygen isotopic constraints on the origin of atmospheric nitrate in coastal antarctica. Atmos. Chem. Phys., 7(8):1925–1945, April 2007.

[193] D. L. Savoie, J. M. Prospero, R. J. Larsen, F. Huang, M. A. Izaguirre, T. Huang, T. H. Snowdon, L. Custals, and C. G. Sanderson. Nitrogen and sulfur species in antarctic aerosols at mawson, palmer station, and marsh (king george island). J. Atmos. Chem., 17(2):95–122, 1993.

[194] Rick D. Saylor, Glenn M. Wolfe, Tilden P. Meyers, and Bruce B. Hicks. A corrected formulation of the Multilayer Model (MLM) for inferring gaseous dry deposition to vegetated surfaces. Atmos. Environ., 92:141–145, August 2014.

[195] Donna Schwede, Leiming Zhang, Robert Vet, and Gary Lear. An intercomparison of the deposition models used in the CASTNET and CAPMoN networks. Atmos. Environ., 45(6):1337–1346, February 2011.

[196] Donna B. Schwede and Gary G. Lear. A novel hybrid approach for estimating total deposition in the united states. Atmos. Environ., 92:207–220, August 2014.

[197] John H. Seinfeld and Spyros N. Pandis. Atmospheric chemistry and physics: from air pollution to climate change. Wiley, August 2006.

[198] M. W. Shephard, K. E. Cady-Pereira, M. Luo, D. K. Henze, R. W. Pinder, J. T. Walker, C. P. Rinsland, J. O. Bash, L. Zhu, V. H. Payne, and L. Clarisse. TES ammonia retrieval strategy and global observations of the spatial and seasonal variability of ammonia. Atmos. Chem. Phys., 11(20):10743–10763, October 2011.

[199] H. B. Singh, D. Herlth, R. Kolyer, L. Salas, J. D. Bradshaw, S. T. Sandholm, D. D. Davis, J. Crawford, Y. Kondo, M. Koike, R. Talbot, G. L. Gregory, G. W. Sachse, E. Browell, D. R. Blake, F. S. Rowland, R. Newell, J. Merrill, B. Heikes, S. C. Liu, P. J. Crutzen, and M. Kanakidou. Reactive nitrogen and ozone over the western pacific: Distribution, partitioning, and sources. J. Geophys. Res.-Atmos., 101(D1):1793–1808, January 1996.

[200] S. N. Smith and S. F. Mueller. Modeling natural emissions in the community multiscale air quality (CMAQ) model–i: building an emissions data base. Atmos. Chem. Phys., 10(10):4931–4952, May 2010.

[201] T. M. Smitty, R. L. Coach, and F. B. Höndra. Unsteady flow in simulated solid rocket motors. In 16st Aerospace Sciences Meeting, number 0112 in 78. AIAA, 1978.

[202] Carly J. Stevens, Nancy B. Dise, J. Owen Mountford, and David J. Gowing. Impact of nitrogen deposition on the species richness of grasslands. Science, 303(5665):1876–1879, March 2004.

[203] A. Stohl and H. Sodemann. Characteristics of atmospheric transport into the antarctic troposphere. J. Geophys. Res.-Atmos., 115:16 PP., January 2010.

[204] T. J. Sullivan, B. J. Cosby, K. A. Tonnessen, and D. W. Clow. Surface water acidification responses and critical loads of sulfur and nitrogen deposition in loch vale watershed, colorado. Water Resour. Res., 41(1):W01021, January 2005.

[205] T.J. Sullivan and T.C. McDonnell. Mapping of nutrient-nitrogen critical loads for selected national parks in the intermountain west and great lakes regions. Natural resource technical report nps/ard/nrtr—2014/895, National Park Service, Fort Collins, Colorado, 2014.

[206] M. A. Sutton, E. Nemitz, J. W. Erisman, C. Beier, K. Butterbach Bahl, P. Cellier, W. de Vries, F. Cotrufo, U. Skiba, C. Di Marco, S. Jones, P. Laville, J. F. Soussana, B. Loubet, M. Twigg, D. Famulari, J. Whitehead, M. W. Gallagher, A. Neftel, C. R. Flechard, B. Herrmann, P. L. Calanca, J. K. Schjoerring, U. Daemmgen, L. Horvath, Y. S. Tang, B. A. Emmett, A. Tietema, J. Peñuelas, M. Kesik, N. Brueggemann, K. Pilegaard, T. Vesala, C. L. Campbell, J. E. Olesen, U. Dragosits, M. R. Theobald, P. Levy, D. C. Mobbs, R. Milne, N. Viovy, N. Vuichard, J. U. Smith, P. Smith, P. Bergamaschi, D. Fowler, and S. Reis. Challenges in quantifying biosphere–atmosphere exchange of nitrogen species. Environmental Pollution, 150(1):125–139, November 2007.

[207] Joseph D. Taum. Investigation of flow turning phenomenon. In 20th Aerospace Sciences Meeting, number 0297 in 82. AIAA, 1982.

[208] Anne M. Thompson. The oxidizing capacity of the earth's atmosphere: Probable past and future changes. Science, 256(5060):1157–1165, May 1992.

[209] Tammy M. Thompson, Marco A. Rodriguez, Michael G. Barna, Kristi A. Gebhart, Jennifer L. Hand, Derek E. Day, William C. Malm, Katherine B. Benedict, Jeffrey L. Collett, and Bret A. Schichtel. Rocky Mountain National Park reduced nitrogen source apportionment: RMNP NITROGEN SOURCE APPORTIONMENT. J. Geophys. Res. Atmos., 120(9):4370–4384, May 2015.

[210] R. Traversi, I. G. Usoskin, S. K. Solanki, S. Becagli, M. Frezzotti, M. Severi, B. Stenni, and R. Udisti. Nitrate in polar ice: A new tracer of solar variability. Sol. Phys., 280(1):237–254, July 2012.

[211] A. J. Turner, D. K. Henze, R. V. Martin, and A. Hakami. The spatial extent of source influences on modeled column concentrations of short-lived species. Geophys. Res. Lett., 39(12):L12806, June 2012.

[212] John Turner and Gareth J. Marshall. Climate Change in the Polar Regions. Cambridge University Press, May 2011.

[213] Barbara J. Turpin and Ho-Jin Lim. Species Contributions to PM2.5 Mass Concentrations: Revisiting Common Assumptions for Estimating Organic Mass. Aerosol Sci Tech, 35(1):602–610, January 2001.

[214] UBA. Manual on methodologies and criteria for mapping critical levels/loads and geographical areas where they are exceeded. federal environmental agency (umweltbundesamt), 2004.

[215] Roberto Udisti, Silvia Becagli, Silvia Benassai, Emiliano Castellano, Ilaria Fattori, Massimo Innocenti, Alessio Migliori, and Rita Traversi. Atmospheresnow interaction by a comparison between aerosol and uppermost snow-layers composition at dome c, east antarctica. Ann. Glaciol., 39(1):53–61, 2004.

[216] G. R. van der Werf, D. C. Morton, R. S. DeFries, L. Giglio, J. T. Randerson, G. J. Collatz, and P. S. Kasibhatla. Estimates of fire emissions from an active deforestation region in the southern amazon based on satellite data and biogeochemical modelling. Biogeosciences, 6(2):235–249, February 2009.

[217] G. R. van der Werf, W. Peters, T. T. van Leeuwen, and L. Giglio. What could have caused pre-industrial biomass burning emissions to exceed current rates? Clim. Past, 9(1):289–306, January 2013.

[218] G. R. van der Werf, J. T. Randerson, L. Giglio, G. J. Collatz, M. Mu, P. S. Kasibhatla, D. C. Morton, R. S. DeFries, Y. Jin, and T. T. van Leeuwen. Global fire emissions and the contribution of deforestation, savanna, forest, agricultural, and peat fires (1997–2009). Atmos. Chem. Phys. Discuss., 10(6):16153–16230, June 2010.

[219] Robert Vautard, Matthias Beekmann, and Laurent Menut. Applications of adjoint modelling in atmospheric chemistry: sensitivity and inverse modelling. Environ. Modell. Softw., 15(6–7):703–709, September 2000.

[220] Sunita Verma, O. Boucher, M. S. Reddy, H. C. Upadhyaya, P. Le Van, F. S. Binkowski, and O. P. Sharma. Modeling and analysis of aerosol processes in an interactive chemistry general circulation model. J. Geophys. Res.-Atmos., 112:29 PP., February 2007.

[221] Peter M. Vitousek, John D. Aber, Robert W. Howarth, Gene E. Likens, Pamela A. Matson, David W. Schindler, William H. Schlesinger, and David G. Tilman. Human alteration of the global nitrogen cycle: sources and consequences. Ecol. Appl., 7(3):737–750, August 1997.

[222] W. De Vries, G. W. W. Wamelink, H. van Dobben, J. Kros, G. J. Reinds, J. P. Mol-Dijkstra, S. M. Smart, C. D. Evans, E. C. Rowe, S. Belyazid, H. U. Sverdrup, A. van Hinsberg, M. Posch, J-P. Hettelingh, T. Spranger, and R. Bobbink. Use of dynamic soil–vegetation models to assess impacts of nitrogen deposition on plant species composition: an overview. Ecol. Appl., 20(1):60–79, January 2010.

[223] D. Wagenbach, M. Legrand, Hubertus Fischer, F. Pichlmayer, and E. W Wolff. Atmospheric near surface nitrate at coastal antarctic sites. J. Geophys. Res.-Atmos., 103:11007–11020, 1998.

[224] J. M. Walker, S. Philip, R. V. Martin, and J. H. Seinfeld. Simulation of nitrate, sulfate, and ammonium aerosols over the united states. Atmos. Chem. Phys., 12(22):11213–11227, November 2012.

[225] T. W. Walker, D. B. A. Jones, M. Parrington, D. K. Henze, L. T. Murray, J. W. Bottenheim, K. Anlauf, J. R. Worden, K. W. Bowman, C. Shim, K. Singh, M. Kopacz, D. W. Tarasick, J. Davies, P. von der Gathen, A. M. Thompson, and C. C. Carouge. Impacts of midlatitude precursor emissions and local photochemistry on ozone abundances in the arctic. J. Geophys. Res.-Atmos., 117:D01305, January 2012.

[226] Yuhang Wang, Yunsoo Choi, Tao Zeng, Douglas Davis, Martin Buhr, L. Gregory Huey, and William Neff. Assessing the photochemical impact of snow emissions over antarctica during ANTCI 2003. Atmos. Environ., 42(12):2849–2863, April 2008.

[227] Yuhang Wang, Daniel J. Jacob, and Jennifer A. Logan. Global simulation of tropospheric o_3-no_x-hydrocarbon chemistry 3. origin of tropospheric ozone and effects of nonmethane hydrocarbons. J. Geophys. Res., 103(D9):10757–10,767, May 1998.

[228] Yuxuan X. Wang, Michael B. McElroy, Daniel J. Jacob, and Robert M. Yantosca. A nested grid formulation for chemical transport over asia: Applications to CO. J. Geophys. Res., 109(D22):D22307, November 2004.

[229] D. W. Waugh and L. M. Polvani. Stratospheric polar vortices. Geoph. Monog. Sereies, 190:43–57, 2010.

[230] K. J. Wecht, D. J. Jacob, S. C. Wofsy, E. A. Kort, J. R. Worden, S. S. Kulawik, D. K. Henze, M. Kopacz, and V. H. Payne. Validation of TES methane with HIPPO aircraft observations: implications for inverse modeling of methane sources. Atmos. Chem. Phys., 12(4):1823–1832, February 2012.

[231] R. Weller, A. E. Jones, A. Wille, H.-W. Jacobi, H. P. McIntyre, W. T. Sturges, M. Huke, and D. Wagenbach. Seasonality of reactive nitrogen oxides (NOy) at neumayer station, antarctica. J. Geophys. Res.-Atmos., 107(D23):4673, December 2002.

[232] R. Weller, F. Traufetter, H. Fischer, H. Oerter, C. Piel, and H. Miller. Postdepositional losses of methane sulfonate, nitrate, and chloride at the european project for ice coring in antarctica deep-drilling site in dronning maud land, antarctica. J. Geophys. Res.-Atmos., 109(D7):D07301, April 2004.

[233] Rolf Weller, Dietmar Wagenbach, Michel Legrand, Christoph Elsässer, Xiangshan Tian-Kunze, and Gert König-Langlo. Continuous 25-yr aerosol records at coastal antarctica – i: inter-annual variability of ionic compounds and links to climate indices. Tellus B, 63(5):901–919, 2011.

[234] M.L. Wesely. Parameterization of surface resistances to gaseous dry deposition in regional-scale numerical models. Atmos. Environ., 23(6):1293–1304, 1989.

[235] M.L. Wesely and B.B. Hicks. Some factors that affect the deposition rates of sulfur dioxide and similar gases on vegetation. J. Air. Pollut. Control Assoc., 27(11):1110–1116, 1977.

[236] Mark W. Williams and Kathy A. Tonnessen. Critical loads for inorganic nitrogen deposition in the colorado front range, usa. Ecol. Appl., 10(6):1648–1665, December 2000.

[237] A. T. Wilson and D. A. House. Fixation of nitrogen by aurora and its contribution to the nitrogen balance of the earth. Nature, 205(4973):793–794, February 1965.

[238] E. W. Wolff, M. Bigler, M. a. J. Curran, J. E. Dibb, M. M. Frey, M. Legrand, and J. R. McConnell. The carrington event not observed in most ice core nitrate records. Geophys. Res. Lett., 39(8):L08503, April 2012.

[239] E. W. Wolff, A. E. Jones, S. J.-B. Bauguitte, and R. A. Salmon. The interpretation of spikes and trends in concentration of nitrate in polar ice cores, based on evidence from snow and atmospheric measurements. Atmos. Chem. Phys., 8(18):5627–5634, 2008.

[240] Eric W. Wolff, Anna E. Jones, Timothy J. Martin, and Thomas C. Grenfell. Modelling photochemical NOX production and nitrate loss in the upper snowpack of antarctica. Geophys. Res. Lett., 29(20):1944, October 2002.

[241] Jung-Hun Woo, Ki-Chul Choi, Hyeon Kook Kim, Bok H. Baek, Meongdo Jang, Jeong-Hee Eum, Chul Han Song, Young-Il Ma, Young Sunwoo, Lim-Seok Chang, and Seung Heon Yoo. Development of an anthropogenic emissions processing system for Asia using SMOKE. Atmos. Environ., 58:5–13, October 2012.

[242] Rosemarie Yevich and Jennifer A. Logan. An assessment of biofuel use and burning of agricultural waste in the developing world. Global Biogeochem. Cy., 17(4):1095, 2003.

[243] J. J. Yienger and H. Levy. Empirical model of global soil-biogenic nox emissions. J. Geophys. Res., 100(D6):11447–11464, 1995.

[244] Günther Zängl and Klaus P. Hoinka. The tropopause in the polar regions. J. Climate, 14(14):3117–3139, July 2001.

[245] A. A. Zardini, S. Sjogren, C. Marcolli, U. K. Krieger, M. Gysel, E. Weingartner, U. Baltensperger, and T. Peter. A combined particle trap/HTDMA hygroscopicity study of mixed inorganic/organic aerosol particles. Atmos. Chem. Phys., 8(18):5589–5601, 2008.

[246] M. Zatko, L. Geng, B. Alexander, E. Sofen, and K. Klein. The impact of snow nitrate photolysis on boundary layer chemistry and the recycling and redistribution of reactive nitrogen across Antarctica and Greenland in a global chemical transport model. Atmos. Chem. Phys., 16(5):2819–2842, March 2016.

[247] M. C. Zatko, T. C. Grenfell, B. Alexander, S. J. Doherty, J. L. Thomas, and X. Yang. The influence of snow grain size and impurities on the vertical profiles of actinic flux and associated NOx emissions on the antarctic and greenland ice sheets. Atmos. Chem. Phys., 13(7):3547–3567, April 2013.

[248] Robert A. Zeddini. Injection-induced flows in porous-walled ducts. AIAA Journal, 14:766–773, 1981.

[249] Edward J. Zeller and Bruce C. Parker. Nitrate ion in antarctic firn as a marker for solar activity. Geophys. Res. Lett., 8(8):PP. 895–898, 1981.

[250] L. Zhang, D. J. Jacob, E. M. Knipping, N. Kumar, J. W. Munger, C. C. Carouge, A. van Donkelaar, Y. X. Wang, and D. Chen. Nitrogen deposition to the United States: distribution, sources, and processes. Atmos. Chem. Phys., 12(10):4539–4554, May 2012.

[251] Lin Zhang, Daniel J. Jacob, Nicole V. Downey, Dana A. Wood, Doug Blewitt, Claire C. Carouge, Aaron van Donkelaar, Dylan B. A. Jones, Lee T. Murray, and Yuxuan Wang. Improved estimate of the policy-relevant background ozone in the United States using the GEOS-Chem global model with $1/2^\circ$ $2/3^\circ$ horizontal resolution over North America. Atmos. Environ., 45(37):6769–6776, December 2011.

[252] Lin Zhang, Daniel J. Jacob, Monika Kopacz, Daven K. Henze, Kumaresh Singh, and Daniel A. Jaffe. Intercontinental source attribution of ozone pollution at western U.S. sites using an adjoint method. Geophys. Res. Lett., 36(11), June 2009.

[253] Q. Zhang, D. G. Streets, G. R. Carmichael, K. B. He, H. Huo, A. Kannari, Z. Klimont, I. S. Park, S. Reddy, J. S. Fu, D. Chen, L. Duan, Y. Lei, L. T. Wang, and Z. L. Yao. Asian emissions in 2006 for the NASA INTEX-B mission. Atmos. Chem. Phys., 9(14):5131–5153, July 2009.

[254] Y. Zhang, L. Jaeglé, A. van Donkelaar, R. V. Martin, C. D. Holmes, H. M. Amos, Q. Wang, R. Talbot, R. Artz, S. Brooks, W. Luke, T. M. Holsen, D. Felton, E. K. Miller, K. D. Perry, D. Schmeltz, A. Steffen, R. Tordon, P. Weiss-Penzias, and R. Zsolway. Nested-grid simulation of mercury over north america. Atmos. Chem. Phys., 12(14):6095–6111, July 2012.

[255] Yang Zhang, Christian Seigneur, John H Seinfeld, Mark Jacobson, Simon L Clegg, and Francis S Binkowski. A comparative review of inorganic aerosol thermodynamic equilibrium modules: similarities, differences, and their likely causes. Atmos. Environ., 34(1):117–137, January 2000.

[256] L. Zhu, D. Henze, J. Bash, G.-R. Jeong, K. Cady-Pereira, M. Shephard, M. Luo, F. Paulot, and S. Capps. Global evaluation of ammonia bi-directional exchange. Atmos. Chem. Phys. Discuss., 15(4):4823–4877, February 2015.

[257] L. Zhu, D. K. Henze, K. E. Cady-Pereira, M. W. Shephard, M. Luo, R. W. Pinder, J. O. Bash, and G.-R. Jeong. Constraining u.s. ammonia emissions using TES remote sensing observations and the GEOS-chem adjoint model. J. Geophys. Res. Atmos., 118(8):3355–3368, April 2013.

[258] Liye Zhu, Daven K. Henze, Jesse O. Bash, Karen E. Cady-Pereira, Mark W. Shephard, Ming Luo, and Shannon L. Capps. Sources and Impacts of Atmospheric NH3: Current Understanding and Frontiers for Modeling, Measurements, and Remote Sensing in North America. Current Pollution Reports, 1(2):95–116, August 2015.